

# Daylight control modelling with a multi-screen shading device

Case study on Museum Boijmans Van Beuningen in Rotterdam



Thijs Hamilton



# Acknowledgements

---

This research could not have been made without the support of several individuals. I would like to thank Laura Franx and Jeffrey van der Laag at Deerns Nederland B.V. for offering me a working place, where I could combine my research with an actual day-to-day working situation as a junior consultant in building physics. And to all my fellow colleagues for the endless supply of coffee and the lunch walks around the Malieveld.

The equipment needed for the measurements was supplied by the Delft University of Technology thanks to Nima Forouzandeh Shahraki and for his assistance with setting up the measurements. For the support during my research and their professional advice, I thank my committee members from the Delft University of Technology: Roel Schipper, Sylvia Pont, Christian Louter and Nima Forouzandeh Shahraki and Laura at Deerns Nederland B.V.. The outcome of this thesis would not have been of the same quality without their input.

# Abstract

---

For a museum, it is important to be able to regulate the amount of daylight. Daylight influences the experience of the visitors, but it can also have a harmful effect on the displayed artwork. Within this thesis, the framework of an approach is outlined.

The museum Boijmans van Beuningen in Rotterdam is currently closed for restoration. The oldest part of this museum was built around 1930. The architect Van der Steur made an extensive study of lighting in museum rooms. For the final design of the building, this resulted in a pitched roof with glass and a layer of horizontal glass panes (*legramen*) that form the ceiling of the exhibition rooms. Below the glass panes timber blades (*schoepen*) are placed under an angle to disperse the light around the room.

The museum board wants to preserve the original vision on daylight of Van der Steur and is now considering the options for sun shading above the ceiling. This addition will allow the museum to better control the light levels in the museum and to protect the valuable artwork.

This Master thesis describes a method to assess the daylight exposure in the museum Boijmans van Beuningen, without the need for extended real-world measurements. It can be used for a combined lighting design (daylight and artificial), focusing on optimal visibility and art protection. The purpose of the method is to compare different sun shading solutions and their effects on the illuminance in an exhibition room. With this approach, a toolbox is made that can be used on other museums.

The method starts with a 3D model of one of the museum rooms, based on the design model supplied by the architect. As the museum is currently being restored, several alterations had to be made to accommodate the temporary renovation state. For the validation of the model, HDR images were made on-site. These results were compared with the calculation made with the 3D model. By iteratively adapting the characteristics of the floor, the *schoepen* and the *legramen* the best possible fit was made.

With the validated model an hourly daylight simulation was done using the EPW climate-based weather data. The resulting illuminance exceeded the desired level at several points in time in the museum. For the calculation of the effects of the sun shading, three different types of sunscreens were chosen. These were schematised as a continuous layer on top of the *legramen*. Based on the behaviour of the sun shading on three specific days, a daylight factor of 2% was found between the illuminance on the wall and the outside illuminance. With this relation and the EPW weather data, it is possible to predict the desired sun shading states for an entire year. This procedure can be used to develop a control mechanism for the opening and closing of the sun shading based on local measurements. When the sun shading state changes, the illuminance can fall below the desired level of 125 lx. In that case, additional artificial lighting is needed. The calculations show that over an entire year, the total exposure is 469.286 lx-hr, this is a reduction of 82.2 % compared to the museum without any sun shading. Allowing the art to be displayed year-round. Without such a system art can only be exposed to 23% of the unblocked exposure, which corresponds for instance with the period January 1<sup>st</sup> – June 23<sup>rd</sup>.

With the developed approach the user can gather building-specific characteristics and geometries, that include some form of 'device' that controls the top light entering a room. The size of the rooms can also be changed. If the first part of the modelling process is done, and the hourly data is collected, the model behaves within the practically accepted limits that were set. In the current version, the system reacts immediately, if the threshold is exceeded the system will react by switching the state of the multi-screen device. But this version can assess what selection of screens are effective, that will reduce the incoming light, without unnecessarily over-reducing it, and so limits the need for additional diffuse artificial lighting.

# Table of Contents

---

Acknowledgements	i	
Abstract	ii	
Table of Contents	iii	
List of Figures	v	
List of Tables	viii	
Nomenclature	ix	
<b>1</b>	<b>Introduction</b>	<b>1</b>
1.1	History Boijmans Van Beuningen museum	1
1.2	Daylight Design Philosophy Van der Steur	1
1.3	21 <sup>st</sup> -century study on daylight modelling	1
<b>2</b>	<b>Literature and Theoretical background</b>	<b>3</b>
2.1	Design philosophy Boijmans museum	3
2.1.1	Van der Steur' system 'type Boymans'	3
2.1.2	In situ testing	5
2.1.3	Schoepen	6
2.2	Light	10
2.3	Sun	13
2.4	Lighting in museums	18
2.5	Damage potential of light on art	21
2.6	Simulation in Radiance	24
<b>3</b>	<b>Methodology</b>	<b>25</b>
3.1	The museum	25
3.1.1	The current state of the museum	25
3.1.2	Design of daylight modelling approach	25
3.2	On-site measurements	27
3.2.1	Diffuse Reflection Coefficient	27
3.2.2	High Dynamic Range photography setup	27
3.3	3D modelling of the rooms	29
3.4	Sensitivity analyses	31
3.5	Design of the sun shading	33
3.5.1	Sun shading control	33
<b>4</b>	<b>Study results</b>	<b>35</b>
4.1	HDR measurements results	35
4.1.1	Analysis of HDR measurements	35
4.1.2	HDR Flowchart	36
4.1.3	Resulting HDR images	38
4.2	Validation of daylight model	39
4.2.1	Diffuse reflectance	39
4.2.2	HDR comparison	40
4.2.3	Results of validation	46
4.2.4	Sensitivity analysis	48
4.3	Adaptations of the model	51

4.3.1	Validated model compared with literature by Van der Steur	51
4.3.2	Sun shading	52
4.4	Behaviour of system with sun shading	53
4.4.1	Real sensor point correlation	53
4.4.2	Annual behaviour of system based on CBDM	57
4.4.3	Annual behaviour with real KNMI data 2022	59
4.4.4	Artificial lighting	60
4.4.5	Annual exposure	62
4.5	Toolbox	63
5	Discussion	64
6	Conclusion	69
7	Recommendations	70
	References	72
	Appendices	75
A	Situation photos BVB	75
B	HDR capture script	78
C	HDR capture data	82
D	Diffuse reflectance measurements	91
E	HDR comparisons	93
F	Sun shading simulation results	96
G	Memo to the museumboard	100

# List of Figures

---

Figure 2-1: Original schematic of different types of glass used (Hannema & van der Steur, 1933, p. 49)	4
Figure 2-2: Light measurements mock-up room between December 1930 and June 1931 (Hannema & van der Steur, 1933)	5
Figure 2-3: Original technical drawing of <i>schoepen</i> from 1934 (Source: MBVB)	6
Figure 2-4: Contour lines of light levels with a traditional top light (Hannema & van der Steur, 1933)	7
Figure 2-5: Contour lines of light levels with the new system, all with the same type of glass (Hannema & van der Steur, 1933)	7
Figure 2-6: Contour lines of light levels with new system, with different types of glass (Hannema & van der Steur, 1933)	7
Figure 2-7: Early versions of exposition halls (Hannema & van der Steur, 1933)	8
Figure 2-8: Picture of museum during construction with mock-up room on the left (Source: MBVB).	9
Figure 2-9: First floor drawing from 1934 with room 228 in lower left corner, with viewpoint of 2-8 (Source: MBVB)	9
Figure 2-10: Spectral distribution on normalized human photoreceptor absorbance of red, green, and blue cone receptors and rods for different wavelengths of light (Betts, et al., 2013).	10
Figure 2-11: Graphical illustration of illuminance, reflectance, exitance and luminance	12
Figure 2-12: Equation of Time throughout the year	13
Figure 2-13: Solar Altitude in Rotterdam on the first day of the first six months of the year.	15
Figure 2-14: Solar Azimuth in Rotterdam on the first day of the first six months of the year.	16
Figure 2-15: Sun event time in Rotterdam, corrected for Daylight Saving Time for 2024 from 31 <sup>st</sup> of March until 27 <sup>th</sup> October.	17
Figure 2-16: Subjective assessment ratings for discrimination of appearance of paintings viewed under daylight, in a simulated art gallery (Loe, Rowlands, & Watson, 1982).	18
Figure 2-17: Examples of Spectral Power Distribution of different light sources, largely depended on manufacturer specific attributes (Lai, 2022)	19
Figure 2-18: Multi-dimensional lighting parameters (Huijiao & Rui, 2022)	20
Figure 2-19: Interaction of light with a diffuse translucent material (Mead, 2010)	24
Figure 3-1: Current state of the Van der Steurgebouw after removal of asbestos (photographs by Aad Hoogendoorn)	25
Figure 3-2: IFC model supplied by Mecanoo, used as baseline for Van der Steur, with on the bottom right the wing in question	26
Figure 3-3: Process flow of programs	26
Figure 3-4: Pixel response to primary colours Red (a), Green (b) and Blue (c), as made by the Building Physics department	28
Figure 3-5: Vignetting curves Sigma Fisheye 4.5mm f2.8 EX DC HSM and Canon EOS 70D, as made by the Building Physics department	28
Figure 3-6: <i>Schoepen</i> philosophy, original cross-section drawing from 1934	29
Figure 3-7: Cross section room 228 with annotations	30
Figure 3-8: View from outside into room 228	30
Figure 3-9: Top view for outside of room 228	31
Figure 3-10: Input parameter settings used for sensitivity analysis	32
Figure 3-11: Exploded view of location of sensor points around room 228, with viewpoint HDR measurement	33
Figure 3-12: Schematical representation of multi-screen shading system	34
Figure 4-1: Room 234 - 19-09-2023 - v2 - 13:37	35
Figure 4-2: HDR (post) process flow, with used argument in brackets and a reference to Appendix B.	37
Figure 4-3: Room 228 - 26-09-2023 - up - 12:17	38
Figure 4-4: Room 228 - 26-09-2023 - up - luminance map	38
Figure 4-5: Diffuse reflectance room 228 and 234	39
Figure 4-6: Flow of validation process	41
Figure 4-7: HDR results with average values at 'exhibition areas'	42
Figure 4-8: Simulated results with average values at 'exhibition areas'	42
Figure 4-9: 'Exhibition areas' used in HDR	42
Figure 4-10: 'Exhibition areas' used in simulation	42
Figure 4-11: Original HDR with false colour for 'exhibition areas'	42
Figure 4-12: Radiance with false colour for 'exhibition areas'	42
Figure 4-13: Definition of matrix grid used for comparison HDR and Radiance, with coordinate (0,0) for bottom left corner	43

Figure 4-14: Absolute change in average simulated luminance (solid line) of left wall compared to the HDR measurements (dashed line), in the vertical direction	44
Figure 4-15: Relative change in average simulated luminance of the left wall compared to the HDR measurements, in the vertical direction	44
Figure 4-16: Absolute change in average simulated luminance (solid line) of middle wall compared to the HDR measurements (dashed line), in the vertical direction	44
Figure 4-17: Relative change in average simulated luminance of middle wall compared to the HDR measurements, in the vertical direction	44
Figure 4-18: Absolute change in average simulated luminance (solid line) of right wall compared to the HDR measurements (dashed line), in the vertical direction	44
Figure 4-19: Relative change in average simulated luminance of right wall compared to the HDR measurements, in the vertical direction	44
Figure 4-20: Absolute change in average simulated luminance (solid line) of left wall compared to the HDR measurements (dashed line), in the horizontal direction	45
Figure 4-21: Relative change in average simulated luminance of the left wall compared to the HDR measurements, in the horizontal direction	45
Figure 4-22: Absolute change in average simulated luminance (solid line) of middle wall compared to the HDR measurements (dashed line), in the horizontal direction	45
Figure 4-23: Relative change in average simulated luminance of the middle wall compared to the HDR measurements, in the horizontal direction	45
Figure 4-24: Absolute change in average simulated luminance (solid line) of right wall compared to the HDR measurements (dashed line), in the horizontal direction	45
Figure 4-25: Relative change in average simulated luminance of the right wall compared to the HDR measurements, in the horizontal direction	45
Figure 4-26: Scatterplot of relation between HDR and simulated luminance. Error intervals and coefficients of determination are also given	46
Figure 4-27: Original drawing of Van der Steur, depicting the bounces on the schoepen (Hannema & van der Steur, 1933)	47
Figure 4-28: Input settings used for parameters for all 48 runs	48
Figure 4-29: Boxplot for all 48 runs of SA	48
Figure 4-30: Morris plot of ranking based on the maximum predicted illuminance	49
Figure 4-31: Morris relation with results of the parameters investigated based on maximum illuminance	49
Figure 4-32: Morris plot of ranking based on the mean predicted illuminance	49
Figure 4-33: Morris relation with results of the parameters investigated based on mean illuminance	49
Figure 4-34: Morris plot of ranking based on the minimum predicted illuminance	49
Figure 4-35: Morris relation with results of the parameters investigated based on minimum illuminance	49
Figure 4-36: Maximum illuminance with in red comparative baseline to validated model and selecting all sets between 1000-1650 lx	50
Figure 4-37: Range of input parameters based on set domain	50
Figure 4-38: Original contour lines calculated by Van der Steur (Hannema & van der Steur, 1933)	51
Figure 4-39: Results of grid-based simulation on west wall of room 228 on 26 September at 12:00	51
Figure 4-40: Test of 'glass' sun shading compared to fabric screen	52
Figure 4-41: Pyranometer (Hukseflux)	54
Figure 4-42: Hourly illuminance inside of room 228, as maximum observed value for the 21st of June	54
Figure 4-43: Hourly illuminance inside of room 228, as maximum observed value for the 21st of September	54
Figure 4-44: Hourly illuminance inside of room 228, as maximum observed value for the 21st of December	54
Figure 4-45: Daylight factor per hour on the 21st of June, September and December	55
Figure 4-46: Python script flow for calculation sun shading	56
Figure 4-47: Shading states room 228 throughout the year	57
Figure 4-48: Shading system movements per day	58
Figure 4-49: Shading system movement during opening hours of museum	58
Figure 4-50: Maximum and minimum state of shading system per day	58
Figure 4-51: Maximum illuminance per day in room 228	58
Figure 4-52: Average illuminance per day in room 228	58
Figure 4-53: Direct Horizontal Irradiance comparison between EPW and Cabauw 2022	59

Figure 4-54: Diffuse Horizontal Irradiance comparison between EPW and Cabauw 2022	59
Figure 4-55: Global Horizontal Irradiance comparison between EPW and Cabauw 2022	60
Figure 4-56: Shading state for 2022 based on Cabauw data	60
Figure 4-57: Room 228 - 21 Dec 10:00 - No sun screens	61
Figure 4-58: Philips Maxos LED 4mx850 (Philips, 2024)	61
Figure 4-59: Room 228 - 21 Dec 10:00 - Shading state 1	61
Figure 4-60: Room 228 - 21 Dec 10:00 - Shading state 1 & 30% diffuse artificial lighting	61
Figure 4-61: Room 228 - Full blackout screen + 97% diffuse artificial lighting	61
Figure 4-62: Render of artificial lighting in room 228	61
Figure 4-63: Process flow	63
Figure A-1: Attic above room 228	75
Figure A-2: Corner of <i>legramen</i> room 228	75
Figure A-3: Walkway in attic	76
Figure A-4: Closeup of <i>legramen</i>	76
Figure A-5: View of <i>legramen</i> from room 228	77
Figure A-6: Temporary build corridor	77
Figure B-7: High Dynamic Range photograph dimensions and crop	79
Figure C-8: Room 228 - 19-09-2023 - v1 - 14:10	83
Figure C-9: Room 228 - 19-09-2023 - v1 - luminance map	83
Figure C-10: Room 234 - 19-09-2023 - v1 - 13:04	84
Figure C-11: Room 234 - 19-09-2023 - v1 - luminance map	84
Figure C-12: Room 234 - 19-09-2023 - v2 - 13:37	85
Figure C-13: Room 234 - 19-09-2023 - v2 - luminance map	85
Figure C-14: Room 228 - 26-09-2023 - normal - 12:03	86
Figure C-15: Room 228 - 26-09-2023 - normal - luminance map	86
Figure C-16: Room 228 - 26-09-2023 - up - 12:17	87
Figure C-17: Room 228 - 26-09-2023 - up - luminance map	87
Figure C-18: Room 234 - 26-09-2023 - v1 - 11:18	88
Figure C-19: Room 234 - 26-09-2023 - v1 - luminance map	88
Figure C-20: Room 234 - 26-09-2023 - v2 - 11:31	89
Figure C-21: Room 234 - 26-09-2023 - v2 - luminance map	89
Figure C-22: Room 234 - 26-09-2023 - v3 - 11:38	90
Figure C-23: Room 234 - 26-09-2023 - v3 - luminance map	90
Figure E-24: Relative difference in average luminance in the vertical direction of left wall 228	93
Figure E-25: Relative difference in average luminance in the vertical direction of middle wall 228	93
Figure E-26: Relative difference in average luminance in the vertical direction of right wall 228	94
Figure E-27: Relative difference in average luminance in the horizontal direction of left wall 228	94
Figure E-28: Relative difference in average luminance in the horizontal direction of middle wall 228	95
Figure E-29: Relative difference in average luminance in the horizontal direction of right wall 228	95
Figure F-30: Shading system movements per day using Cabauw 2022	96
Figure F-31: Shading system movement during opening hours of museum using Cabauw 2022	96
Figure F-32: Maximum and minimum state of shading system per day using Cabauw 2022	97
Figure F-33: Maximum illuminance per day in room 228 using Cabauw 2022	97
Figure F-34: Average illuminance per day in room 228 using Cabauw 2022	97
Figure F-35: Shading states room 228 throughout the year using 100 lx	98
Figure F-36: Shading system movements per day using 100 lx	98
Figure F-37: Shading system movement during opening hours of museum using 100 lx	98
Figure F-38: Maximum and minimum state of shading system per day using 100 lx	99
Figure F-39: Maximum illuminance per day in room 228 using 100 lx	99
Figure F-40: Average illuminance per day in room 228 using 100 lx	99

# List of Tables

---

Table 2-1: Visual adaptation ranges (Cuttle, 2007)	11
Table 2-2: The light responsivity of pigments and substrates (CIE 157, 2004, p. 20)	22
Table 2-3: Limiting illuminance and annual luminous exposure for different classed of light-sensitive exhibit interpreted from (CIE 157, 2004, p. 26)	23
Table 3-1: Example of exposure times of measurements, times are in seconds	28
Table 3-2: Bounds of input parameters for sensitivity analysis	31
Table 4-1: Scaling factor and error difference and final acceptance or rejection	36
Table 4-2: Diffuse reflection coefficients	39
Table 4-3: Transmission coefficients	39
Table 4-4: <i>Radiance</i> settings image simulation	40
Table 4-5: Range of input parameters based on sensitivity analysis	50
Table 4-6: <i>Radiance</i> setting used for hourly grid calculation	53
Table 4-7: <i>Radiance</i> settings used DAYSIM	55
Table 4-8: Shading state comparison with actual market available options	57
Table 4-9: Years in EPW file for Rotterdam/The Hague	59
Table D-1: Diffuse reflectance measurements	92

# Nomenclature

---

## Software

Software	Version
Rhinoceros®/Rhino	6, 7 & 8
Grasshopper®	1.0.0007
Autodesk® Revit®	2023
Ladybug®	legacy version 0.0.69
Honeybee®	legacy version 0.0.66
Speckle™	2.1.11
Python™	3.8.10
Radiance	5.4a (2021-3-28)
QDsI Dashboard	3.6.7
Colibri	2.0.0
SALib	1.4.8

## Dutch terms

Dutch terms	Explanation
<i>Legraam</i>	Horizontal window in the ceiling
<i>Schoepen</i>	Blades in the ceiling to disperse the light
Melk glas(s)	4 types of glass for the horizontal window in the ceiling with different grades of loss in transmittance
Emaillé glas(s)	
Mat glas(s)	
Spekmat glas(s)	

## Abbreviations

Abbreviations	Meanings
LDR	Low Dynamic Range
HDR	High Dynamic Range
BVB	Boijmans van Beuningen
MBVB	Museum Boijmans van Beuningen
CBDM	Climate-Based Daylight Modelling
EPW	EnergyPlus™ Weather
LSTM	Local Standard Time Meridian
UCT	Universal Coordinated Time
GMT	Greenwich Mean Time

EoT	Equation of Time
TC	Time Correction factor
LT	Local Time
LST	Local Solar Time
HRA	Hour Angle
DST	Daylight Saving Time

## Symbols

Symbols	Meanings
$E$	Illuminance
$L$	Luminance
$\delta_{\odot}$	Declination
$\phi$	Latitude
$H_{\odot}$	Angle of elevation
$\zeta$	Zenith angle
$A_{\odot}$	Azimuth
$H$	Exposure
$\lambda$	Wavelength of radiation
$c$	Velocity of light
$\nu$	Radiation frequency
$\Delta E$	Just noticeable change
$\Delta T$	Time difference
$t$	Time
$\rho$	Diffuse reflectance
$E_e$	Incident irradiance
$\mu^*$	Absolute mean value Morris
$\sigma$	Standard deviation Morris

# 1 Introduction

---

Daylight is a vital factor for museums, enhancing aesthetics, conservation, and the overall visitor experience. If the environment is too dark, the colour perception in our eyes will not render the perceived information properly and the three-dimensional shape of artworks, such as sculptures, cannot be fully appreciated, and it will not match the experience intended by the original creator. On the other hand, too much light could lead to a whole different set of problems, e.g. fading, colour shift and even deterioration. Complicating the issue further is that different materials or colour pigments react differently. Museums hold many valuable artworks from different periods. It is important to create conditions that are both pleasant for the visitors and at the same time will not negatively affect the quality and longevity of the artwork.

## 1.1 History Boijmans Van Beuningen museum

Situated in Rotterdam is the Boijmans Van Beuningen (BVB) museum. In 1820 F.J.O. Boijmans was looking for an inheritor for his art collection. He chose the municipality of Rotterdam. In cooperation with Boijmans, a property was bought; the Schielandshuis and in 1849 the museum officially opened.

After a tragic fire in 1864, the Schielandshuis was rebuilt. Because of the growing number of visitors and the lack of space for the collection, the municipality decided to build the new BVB museum in 1929. The aim of the director of the museum and the architect Adriaan van der Steur was to improve the experience for the visitors. They wanted optimal visibility of the art in relatively small galleries with ample daylight. Over the years more buildings were added to the BVB museum, with the Depot being the most recent addition (2021). Since 2019, the Van der Steurgebouw has been closed for restoration. (Boijmans Van Beuningen, 2023).

## 1.2 Daylight Design Philosophy Van der Steur

Van der Steur wanted to be able to assess the daylight entry in the new BVB museum. For this purpose, they made a mock-up room to experiment with different conditions to be able to reach the desired result. From the testing in the mock-up room, they concluded that they wanted to allow the light to enter from the top of the room. To this end, a double glass roof structure was designed. The outer roof is double-pitched. Below the pitched roof, a layer of horizontal glass panes (in Dutch: *legramen*) is fitted to construct the ceiling of an exposition room. Below that ceiling timber blades (in Dutch: *schoepen*) are placed, to disperse the light around the room. Allowing the light to reflect and cascade on the way down through the *schoepen*, resulted in a predominantly diffuse light field in the room, with little variations in illuminance ratios.

## 1.3 21<sup>st</sup>-century study on daylight modelling

In 2019 the Van der Steurgebouw was closed for restoration. Because this building is a listed monument, the restoration allows no major visible changes on the outside. The museum board of BVB wants to preserve the original vision of the designers. However, they also want to be able to control the light levels and preserve the displayed artwork better (Boijmans Van Beuningen, 2023). To limit the amount of daylight that lands on the paintings and artworks hanging in the galleries, some solutions have been suggested such as a permanently fitted screen or a mechanically operated sun shading device consisting of multiple screens, above the horizontal *legramen*. At this moment several sun shading solutions are considered for the restoration of the Van der Steurgebouw.

Originally the architect Van der Steur had to build a costly mock-up room and had to measure multiple times a day for a long continuous period of time. Nowadays a digital *Radiance* simulation can

be made. Currently, there is no such model or software that can easily calculate the expected exposure at the desired level of detail in combination with a multi-screen shading device. This thesis aims to combine different software, approaches and iterations. By performing multiple different types of calculations and combining the results, the model can describe the behaviour of the system. The model developed in this thesis will be used to assess the effects of different suggested solutions for daylight entry.

For this thesis the following research questions have been formulated;

The main research question is:

How to design a method to assess the daylight exposure in museum BVB, to be used for a combined lighting design (daylight and artificial), focussing on optimal visibility and art protection, to assess a multi-screen shading device and its effects on the illuminance?

And the sub questions are:

SQ1: How to model a characteristic museum room? Based on the available information and previous studies a characteristic museum room is chosen. The goal of this sub question is to make a 3D model of this room, including the building construction (roof, walls), the interior fixtures and the external weather conditions.

SQ2: How to validate the model to actual conditions?

A measurement method will be set up to be able to validate the model.

To validate the model, measurements will be performed in the Van der Steur building. The equipment that will be used will be provided by Deerns or the TU Delft.

Based on the real-time measurements the parametric model can be calibrated and adjusted if necessary.

SQ3: Which type of sun shading gives the most optimal lighting conditions?

The improved model will be used to simulate different proposed sun shading types and determine which solution gives the best results for visibility (illuminance ( $lx$ ), the contrast ratio of luminance (wall-art) and for protection (total exposure ( $lx*hr$ )). The properties of the types will be modelled parametrically, to be able to optimise the solution.

SQ4: How can this method be applied to similar situations?

The last step is to describe the method for future reference in similar situations.

This research will result in a 3D model that is validated using measurements inside the building. By adding the sun shading solutions to the model, the simulations in this research will answer the question of which solution performs best, without the expensive necessity to test all solutions in situ, throughout a whole year. This will give the museum board supporting information for their choice. This method will be documented to be used for similar situations in other museums.

## Reading guide

The philosophy behind the design of the exhibition halls at the Van der Steur building is further outlined in 2.1, also discussing the analyses the architect made in the early 1930s. The background used in climate based daylight modelling is given in 2.2-2.6. In 2.5 the damage potential during the display of art is given.

The methodology of this thesis is presented in chapter 3, starting with discussing of the current state of the museum during restoration in 3.1.1, the onsite HDR measurements in 3.2 and the approach to validate the daylight model in 3.3 followed by the approach to implement sun shading and estimating the benefits of the system.

In chapter 4 the results of each part of this study are given, resulting in the behaviour of the chosen system and the annual exposure in 4.4 and the total process flow of this research in 4.5.

Discussion of the results is done in chapter 5 and the conclusion is given in chapter 6. Further recommendations related to this thesis are given in 7.

# 2 Literature and Theoretical background

---

## 2.1 Design philosophy Boijmans museum

In the 1920s the municipality board of Rotterdam decided that they needed a new building to allow the museum to grow. On the 12<sup>th</sup> of April 1928, the decision was made and city architect Ad van der Steur was given the assignment to make the design. To come to a comprehensive design, he collaborated closely with the director of the museum: Dirk Hannema. A plot of land was chosen, a former part of 'Land van Hoboken', a very large estate. This resulted in a site that was free of any obstructions from any neighbouring buildings, and therefore allowing for full control of the light that entered the museum. This also limited the dangers of a potential fire and made future additions to the museum possible.

In preparation for the new museum, they went on a study trip, nationally and internationally. Because only this would allow them to step into the shoes of future visitors to experience the exhibition space. That resulted in the decision on the lighting approach that they would eventually choose. All experiences and conclusions were logged, and these formed the basis of the list of requirements. (van der Steur, Museum Boymans te Rotterdam Part I, 1935).

In the late 1920s lighting design for a purpose-built museum was still in its infancy, as previously the consensus was that only polar light (diffuse light from the north) was suitable. Many painters used this diffuse light from the north in their ateliers, as this allowed them to paint all day round in relatively constant conditions. But it is not necessarily so that the conditions that the artist was under when making the piece, are also the best to admire the art. The warmer southern light will provide more contrast and vibrance, although harsh shadows and reflections should be avoided. An easy and widely adopted method to deal with these issues is letting the light enter from the top, and diffusing the light along the way down. One method to achieve this is the use of a velum (a taut diffusing fabric) but van der Steur concluded that due to dust collecting on this fabric, the centre part would be less translucent. As these systems were faulty in the eyes of van der Steur he set out to design a completely new system (van der Steur, Museum Boymans te Rotterdam Part II, 1935).

### 2.1.1 Van der Steur' system 'type Boymans'

For the design of the new BVB museum, van der Steur considered four different types of halls, based on his study trip:

Type I	Exposition halls with exclusively top light.
Type II	Exposition halls with side light, combined with top light (cabinets).
Type III	Exposition halls with diagonal top light, combined with side light (sculptures).
Type IV	Exposition halls with normal top light (temporary exposition halls).

#### 2.1.1.1 *Type I* *Exposition halls with exclusively top light*

For this type of hall Van der Steur had encountered three main issues, for which he proposed improvements:

1. The illumination in the centre of the floor is higher than on the wall  
For a pleasant viewing experience, this should be the opposite. Therefore, the centre of the

ceiling is closed. So only light around the perimeter remains. The walls are illuminated the same, but the centre of the floor is now considerably less illuminated.

2. Reflectance of light from the floor to the walls and blinding of light from top light. These are eliminated by the use of the *schoepen*. The shape of the *schoepen* redirects the light to the walls. And for the visitor it is almost impossible to see the top windows from a normal point of view.
3. The peak brightness with a traditional top light is in the middle of the wall, just above eyelevel. And towards the corner the intensity decreases. To combat this inhomogeneity of the illumination of the wall, the *legramen* (top windows) used are altered. By changing the transmission of the different windows, more light is allowed to penetrate in the corners whereas in the middle of the wall it is more blocked, as seen in Figure 2-1. In total 4 different matt types of glass were used. The darkest *melk* glass has a loss of transmittance of 60%, followed by *emaille* glass of 50%, *mat* glass with 40%, and *spekmat* glass with 30% covering the majority of the ceiling.

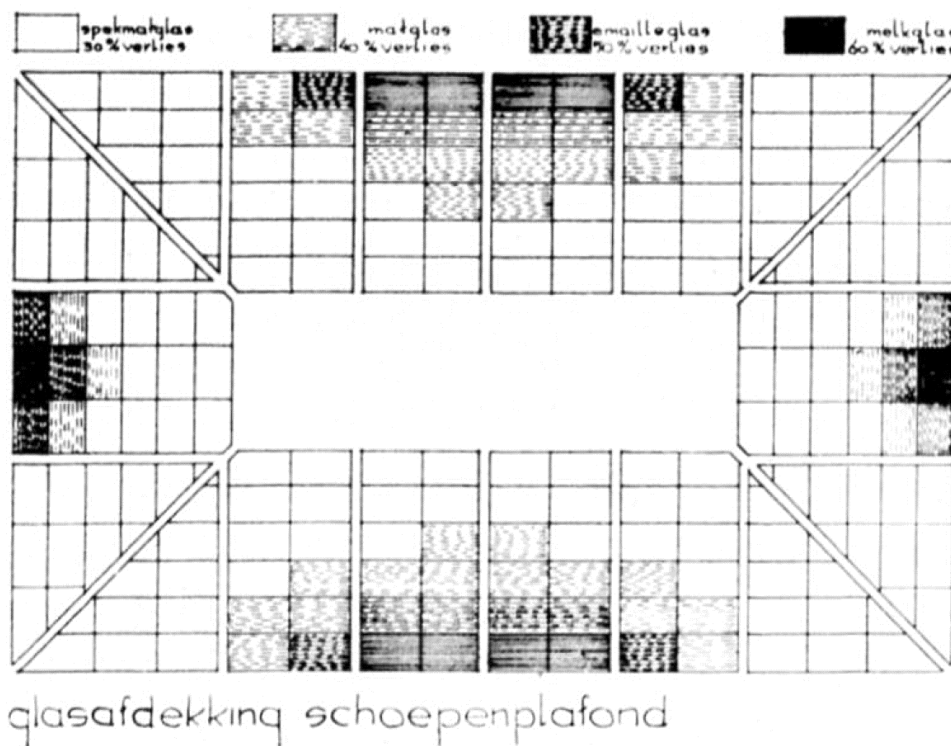


Figure 2-1: Original schematic of different types of glass used (Hannema & van der Steur, 1933, p. 49)

The impact of these changes was measured using a mock-up room, one with a traditional system and one with the newly proposed system. On bright sunny days, the illuminance was reduced. And on overcast days there was an increase in illuminance compared with the traditional system (van der Steur, Museum Boymans te Rotterdam Part II, 1935).

### 2.1.1.2 Type II Exposition halls with side light, combined with top light

For some smaller rooms, the team needed to create a more intimate ambiance. To do that they would allow for the addition of side light. However, this does introduce some of the detrimental aspects of side lighting, so multiple changes were made.

1. Intrusive reflections on the back wall. One solution would be to give the walls an angle, to reduce the size of the back wall. This would however require a lot of additional space. In the end, they did chamfer the corners of the exposition halls. By using narrow windows, the size of the reflections was reduced.

2. Directly next to the window the shadows that are cast are harsh. Therefore the space near the windows is not suitable for displaying art. Therefore the connecting corridors are placed in this area.
3. The light of the neighbouring hall seeps through the corridors. By creating curved corridors between the halls this is eliminated. As a secondary, beneficial effect, the curvature naturally guides the visitor into the next hall.
4. Light intensity on the side walls is low, and the large decorative frames of the paintings cast shadows along the walls. The light from the top is of greater intensity and therefore the shadows cast are minimal.

### 2.1.1.3 Type III *Exposition halls with diagonal top light, combined with side light (sculptures)*

These halls are intended for sculptures, typically less susceptible to light deterioration as will be discussed further in paragraph 2.5. Therefore, the acceptable light levels are higher. To minimize the casting of harsh shadows the rooms are supplemented with side light.

### 2.1.1.4 Type IV *Exposition halls with normal top light (temporary exposition halls)*

The natural character of these halls is that the collection displayed will change, from painted artworks, plastics, drawings to sculptures. Consequently, there is not a clear solution for the lighting. A general approach is taken with the traditional use of velum with opaque glass.

As an addition, the interior of the roof is fitted with lights to illuminate the building from the inside out at night. Consequently, these lights will also partly, and indirectly illuminate the top floor through the top lights, allowing for nighttime visiting of the museum.

## 2.1.2 In situ testing

Before even the first pile of the new BVB museum was driven into the ground, the design team erected a mock-up room to test their theories and optimise the appearance. From 1929 on this mock-up building was operational and consisted of 2 different types of exposition halls:

- Large, with only top light (8x12 m)
- Cabinet, with top and side light (5x6.5 m)

This building was placed on site, to mimic the actual conditions of the halls in the to be build museum. Within these halls, different configurations were tested and measured. They carried out these measurements over an extended period of time. An example of such measurements can be seen in Figure 2-2.

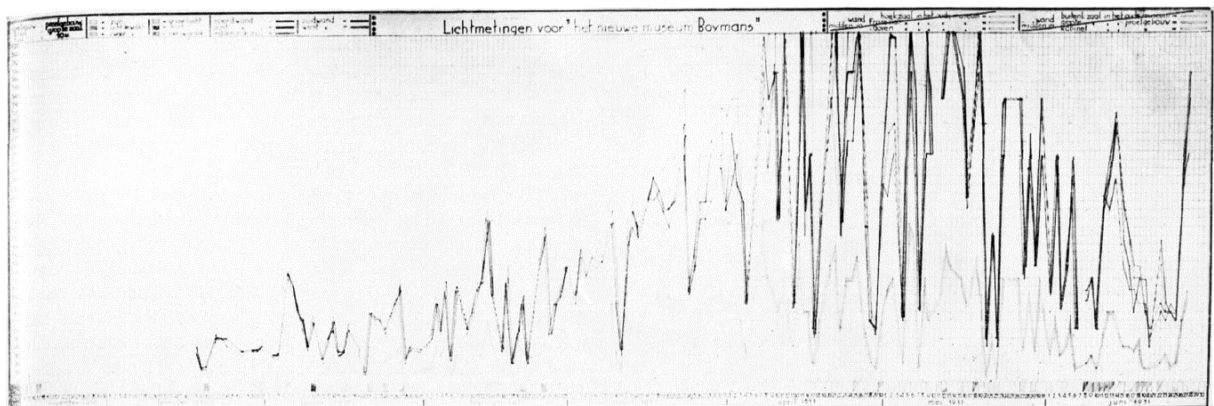


Figure 2-2: Light measurements mock-up room between December 1930 and June 1931 (Hannema & van der Steur, 1933)

Five measurements were taken, in the middle of the floor and the middle of each wall, which face the cardinal directions of North, East, South and West. Three times a day at 10, 13 and 15 o'clock the light was measured. At the same time, the weather conditions were also registered and a small square below the graph was coloured accordingly. This allowed for the (manual) identification of extremes. Similar measurements were taken at the old location of the museum. From this, some conclusions about the performance of the new system were drawn. With minimal light levels outside, the levels inside of the mock-up room were deemed favourable. And with bright sunlight the mock-up room was considerably darker compared to the old museum, meaning that the extremes in light levels throughout the year were reduced and would have a more flattened profile. Due to the addition of the *schoepen*, the difference in light levels of each wall was reduced. Even throughout the day, with the sun moving from east to west, illuminating the west, north and east walls respectively, all walls displayed the same illuminance.

### 2.1.3 Schoepen

The main objective of the *schoepen* is to redirect the incoming light away from the floor and towards the walls. The light that hits the *schoepen* will bounce and scatter, resulting in a diffuse light from above, Figure 2-3. As a basis for this, they looked at a visitor standing inside the room. They assumed an eye level of a standing person at 1.50 m, at 1 m from the middle of the room. The construction of the *schoepen* is based on the requirement that this person would not be able to see any glass directly. Another objective of van der Steur was that when the person moved towards the wall, he would never be able to see the glass under an angle less than 70°. To achieve this the distance between the *schoepen* is not constant. It changes towards the centre of the room, going from 20cm at the perimeter to 14 cm, and decreasing by 0.6 cm per *schoep*.

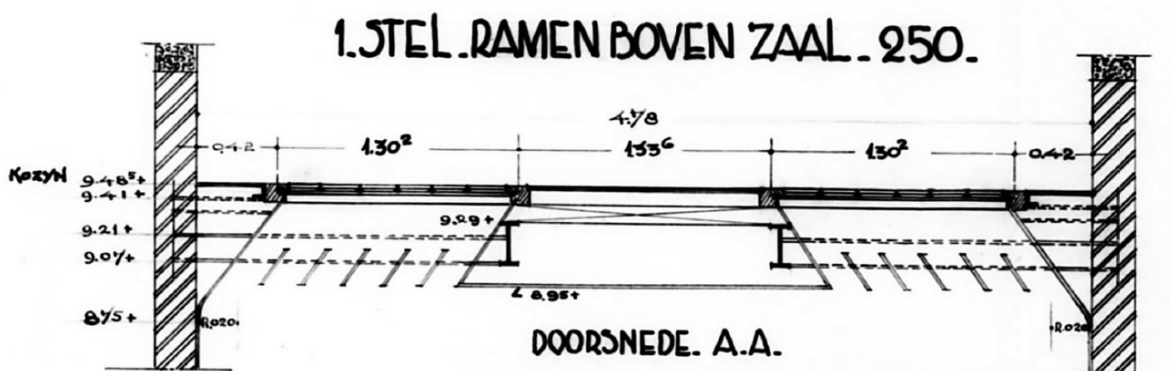


Figure 2-3: Original technical drawing of *schoepen* from 1934 (Source: MBVB)

To validate the performance of the system, the overall light cast was calculated, as a single point in the middle of the wall is insufficient to accurately describe the light distribution. To do this, iso curves were calculated and drawn. This was done by hand and must have been very labour intensive as the illumination of the wall is proportional to the amount of glass that every point on that wall is able to 'see', multiplied with the sinus of the angle of incident of the light rays from the glass, and inverse squared to the distance from the glass to the point. By summing all the values of each point on the wall a ratio of illumination was calculated. With the known illumination in the centre, the rest of the wall was computed. Later this was combined with the different types of glass as depicted in Figure 2-1 to come to a corrected situation. The results of this manual labour were presented in the periodical: *Bouwkundig Weekblad Architectura* in 1933. In this article, they compared the traditional system with a top light Figure 2-4 with the new system with one uniform type of glass Figure 2-5 and with the new system with different types of glass Figure 2-6.

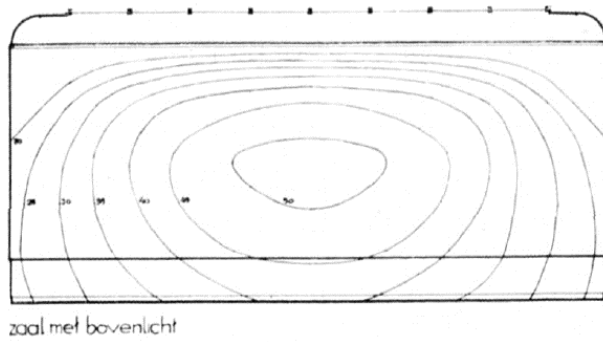


Figure 2-4: Contour lines of light levels with a traditional top light (Hannema & van der Steur, 1933)

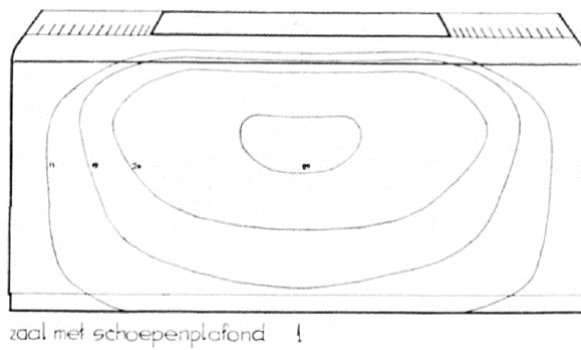


Figure 2-5: Contour lines of light levels with the new system, all with the same type of glass (Hannema & van der Steur, 1933)

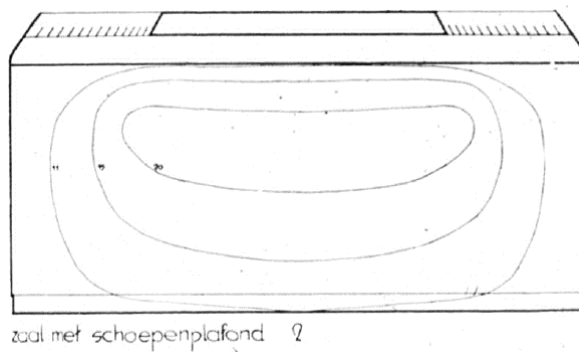


Figure 2-6: Contour lines of light levels with new system, with different types of glass (Hannema & van der Steur, 1933)

Compared to the traditional system, which has a clear drop in illuminance towards the corners, the new system can realise more illuminance in the corners. The new system with the different types of glass results in a more evenly spread illuminance map and visitors will experience fewer gradients.



Figure 2-7: Early versions of exposition halls (Hannema & van der Steur, 1933)

After the design and construction, which took over 7 years, the new “Boijmans” museum opened on 6 July of 1935. At that time in history, the museum was not yet combined with Van Beuningen.



Figure 2-8: Picture of museum during construction with mock-up room on the left (Source: MBVB).

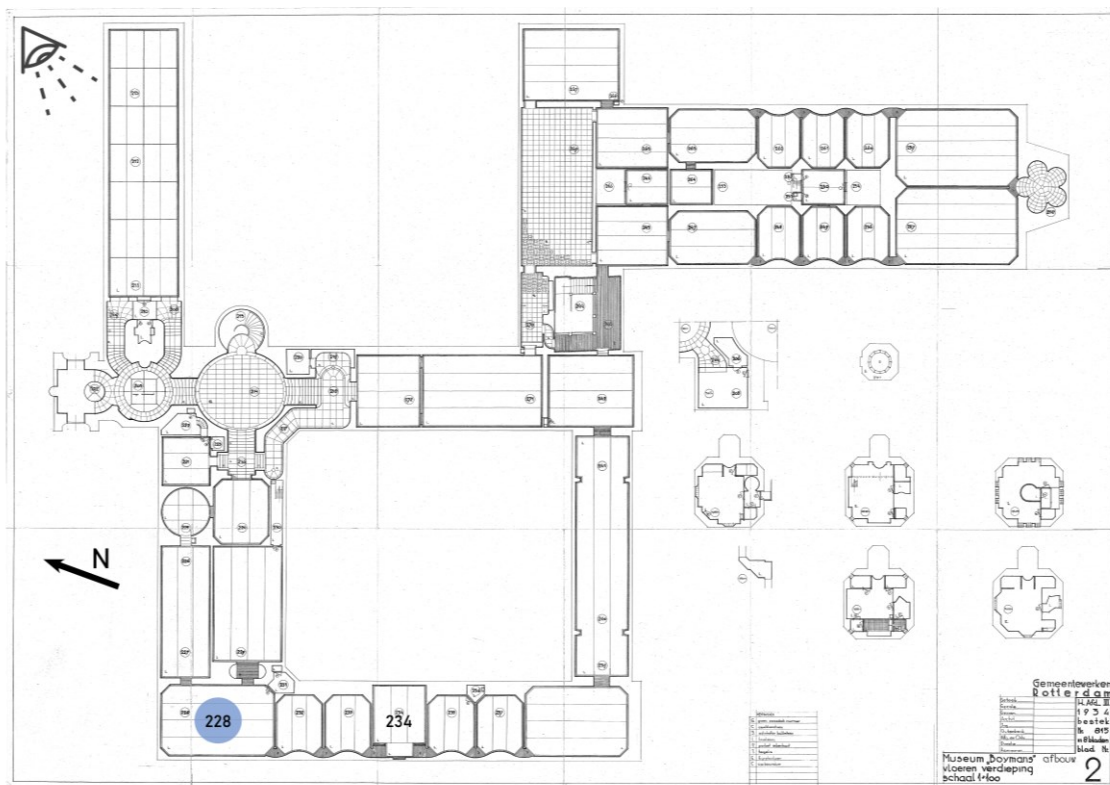


Figure 2-9: First floor drawing from 1934 with room 228 in lower left corner, with viewpoint of 2-8 (Source: MBVB)

## 2.2 Light

Almost all light that we experience during our lifetime has one origin, the sun. During the day the light rays emitted by the sun travel for 8 minutes at the speed of light to eventually illuminate our world. Also, at night the sun is able to enlighten us, with the indirect lighting from the moon. Depending on the moon phase the intensity will change. But that is not the only light source, as fire and candles were used, followed by the light bulb first patented by Thomas Edison, and later the Light Emitting Diodes (LED). These sources of artificial light allowed mankind to be productive even after the sun had long set.

In the nineteenth century, Maxwell developed his theory of electromagnetic radiation and showed that light was the visible part of a vast spectrum of electromagnetic waves. All bodies emit electromagnetic radiation, which propagates in space in the form of waves of both electric and magnetic fields (Maxwell, 1873). The ratio between the velocity of light  $c$  and the radiation frequency  $\nu$  gives the wavelength  $\lambda$  as shown in Equation 2-1.

$$\lambda = \frac{c}{\nu}$$

Equation 2-1: Wavelength formula

These wavelengths can vary over a vast range. In the late nineteenth century, scientists were able to measure these with high accuracy. Later they classified different types of radiation into wavelength bands. The visible part of the spectrum that we can see is classified as the visible spectrum. The photons of these wavelengths can stimulate the retinal photoreceptors of humans and trigger a sensory response in the visual cortex of the brain. This range is between 380 and 760 nanometres [nm]. Below 400 nm we classify the light as ultraviolet (UV) and above 760 nm infrared (IR) (Cuttle, 2007).

The photoreceptors consist of rods and cones. The rods contain the photosensitive pigment named rhodopsin. The cones have three different pigments; opsins; with each being sensitive to the primary colours: red, green, and blue. The different photoreceptors have different sensitivity, as they absorb different parts of the spectrum as seen in Figure 2-10 (Betts, et al., 2013).

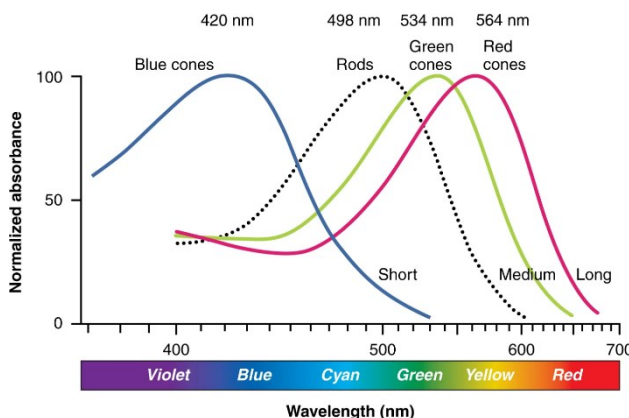


Figure 2-10: Spectral distribution on normalized human photoreceptor absorbance or red, green, and blue cone receptors and rods for different wavelengths of light (Betts, et al., 2013).

As the energy of the photon is absorbed by the receptor, an impulse is created that goes through our sensory system. At the same time, this will cause bleaching, which will reduce the absorbing power of the pigment. As light levels lower, the rate of regeneration of the pigments is larger than the effect of bleaching, resulting in an increase in sensitivity. In stable conditions, the regeneration and bleaching are in equilibrium. This allows the eyes to adapt to the different lighting conditions we face and enables the discrimination of small luminance contrasts in our field of view (Cuttle, 2007).

This adaptation does not happen instantly and can take a young person up to 40 minutes to fully adapt. The adaptation is divided into three ranges, depending on the *luminance* and *exitance* (for perfect matt materials) as seen in Table 2-1.

Adaptation range	Luminance (cd/m <sup>2</sup> )	Exitance (lm/m <sup>2</sup> )
Photopic	>3	>10
Mesopic	0.001 to 3	0.003 to 10
Scotopic	<0.001	<0.003

Table 2-1: Visual adaptation ranges (Cuttle, 2007)

As light levels reduce (Scotopic range), the cones are insufficiently stimulated to produce an impulse, all vision is handled via the rods. One downside of rods is that, as they all have the same photopigment, there is only a difference in brightness and no colours. The distribution of cones and rods throughout the retina is also different, most of the cones concentrate in the central point. The rods are grouped into the neural pathways, lowering the resolution of our vision. They are not located in the central point, therefore it is impossible to focus on a small area. In the Mesopic range, both the rods and the cones are active. As the luminance increases to over 3 cd/m<sup>2</sup> the rods are overwhelmed and ignored. The rate at which a person can adapt to these changes decreases with age.

The perception of the different colours that make up the visible part of the spectrum is that some colours will appear brighter than others. Especially in the centre of the spectrum as multiple cones contribute to the responsiveness, those colours will be brighter. The colours towards the edges of the spectrum will appear dimmer in contrast. As multiple cones are activated, multiple signals will be processed and interpreted as brighter. The density of the radiant power can be measured in watts per square meter [W/m<sup>2</sup>]. This *illuminance* of the surface is corrected for the human vision, by accounting for the retinal sensitivity. The radiant power is defined as *lumens* [lm], and the density of incident lumens is *lux* [lx]. One lux is equal to one lumen per square meter.

Part of the light that falls on a surface is reflected. The predominant *reflectance* of a surface is the ratio of reflected light to incident light and has a range of 0.0 to 1.0. For a surface to have a high reflectance it is not necessary to be shiny. But similar 'looking' surfaces can have vastly different reflectance values.

The measure of light exiting from a surface is *exitance*. This governs the reflected light, transmitted light or any light that is emitted by a self-luminous material. For an opaque and matt surface that is related to the product of the illuminance and the reflectance [lm/m<sup>2</sup>]. This measure is the same, from every viewing angle. If we dissect this for every field of view, we get *luminance*. The luminous intensity of an element is a specific direction relative to its projected area in that direction, in candelas per square meter [cd/m<sup>2</sup>] (Cuttle, 2007). For opaque matt surfaces the relation between luminance and illuminance is:

$$Luminance = Illuminance \cdot \frac{Reflectance}{\pi}$$

Equation 2-2: Luminance (Cuttle, 2007)

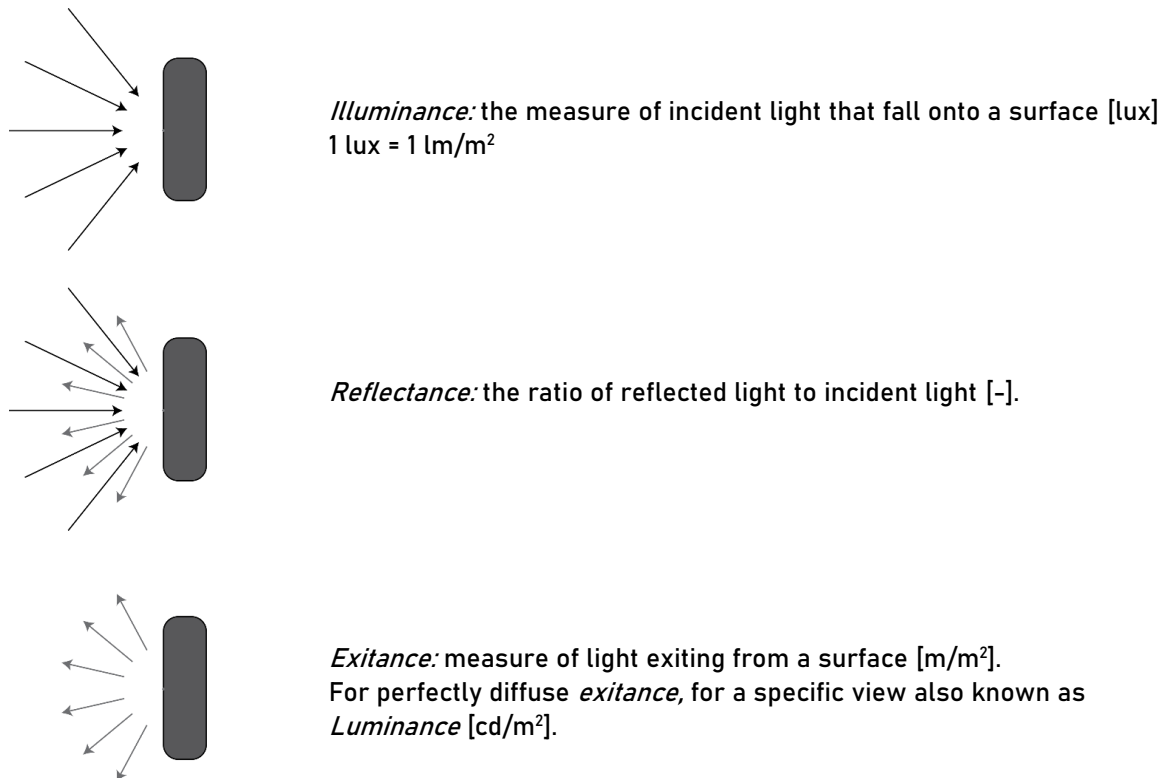


Figure 2-11: Graphical illustration of illuminance, reflectance, exitance and luminance

Any person who has spent any amount of time looking at the sky has seen that it changes colour. This is caused by the refraction of the light rays from the sun that penetrate our Earth's atmosphere. During the day this results in a blue sky. But during sunrise and sunset the angle changes and so the colours change. This also happens with a prism; light enters and is split into its separate wavelengths and colours. In a museum with daylight, this change in colour temperature will change the appearance of the colours of the artwork. The colour of light is expressed as a temperature in the unit Kelvin [K].

As light hits a surface of any colour, some of the light rays are reflected, and some are absorbed by the object. The colour that is reflected by the surface can reach the retina of our eyes. Our brains convert that information into our perceived colour. In the case of people who suffer from any form of colour blindness, in that translation, the colour is changed.

Artificial light is an additional light source that we can introduce in a room. But that has some trade-offs. The performance of these sources largely depends on the technology used to create this light. The traditional lightbulb has a colour temperature of 2800 K, and contains many yellow and red wavelengths, resulting in a 'warm' light source. Fluorescent light is considered 'cold' at 8000 K. Modern light sources such as LED allow for more finetuning of its performance and characteristics (Druzik & Michalski, 2012). One downside of light is that it could also introduce heat if the source contains any wavelength in the infra-red spectrum or ultra-violet that can damage pigments, discussed further in 0.

As light propagates as waves in our world, it interacts with the surroundings. Some energy is lost at the first bounce, and some of the wavelengths are lost. This changes the colour and the illuminance of the light. This will also influence how we perceive an object in that space. The light rays will reflect with the same angle of incident as the incoming ray, this is discussed further in 2.6. The reflected rays are also often scattered, as surfaces in the real world are not perfectly flat, creating a more dispersed light field.

## 2.3 Sun

As the earth rotates around the sun, the zenith changes throughout the year. When the solar beams reach Earth a part of the light is scattered in the atmosphere, resulting in diffuse radiation. Depending on the weather type, if the sky is clear 20-30% of the total incoming light becomes diffuse and the remaining part is considered direct radiation. With overcast skies, this is 100% diffuse light. The scattering of the light does not occur uniformly and depends on the wavelength of the different photons. This results in a blue sky during the day and arguably beautiful pastel colours at sunrise and sunset.

To calculate the position of the sun at any place on Earth at any time, we first need to take a look at the time at that position, as time is a man-made concept. At any given position there is a Local Time (LT), this Local Time depends on the time zone the location is in. As the Earth undergoes a full rotation every day, each time zone has a difference of  $15^\circ = 360^\circ/24$  hours. The local time corrected for the time zone is called the Local Standard Time Meridian:

$$LSTM = 15^\circ \Delta T_{UTC}$$

Equation 2-3: Local Standard Time Meridian

Where  $\Delta T_{UTC}$  is the difference between the Local time (LT) with the Universal Coordinated Time (UTC), which is equal to the time zone compared to Greenwich Mean Time (GMT).

To account for the eccentricity of the Earth an empirical equation is used, which is an approximation and is accurate within 0.5 minutes (Milne, 1921). This Equation of Time (EoT) is based on the day of the year.

$$EoT = 9.87 \sin 2B - 7.53 \cos B - 1.5 \sin B$$

Equation 2-4: Equation of Time

Where

$$B = \frac{360}{365}(d - 81)$$

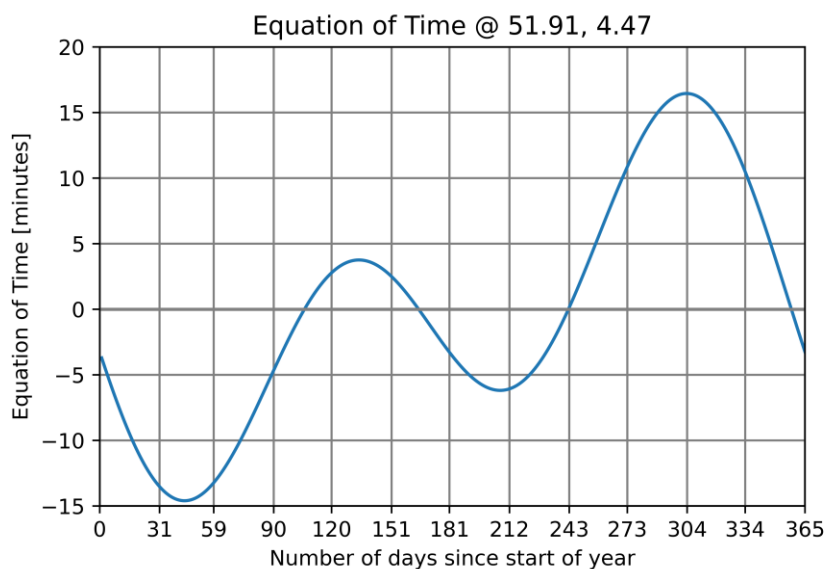


Figure 2-12: Equation of Time throughout the year

We also need to take into account the Longitude of the position, with this Time Correction Factor (TC). As the Earth rotates  $1^\circ$  every 4 minutes the following equation is used:

$$TC = 4(\text{longitude} - LSTM) + EoT$$

Equation 2-5: Time Correction Factor

From here we can calculate the Local Solar Time (LST), by adjusting the Local Time with the Time Correction Factor.

$$LST = LT + \frac{TC}{60}$$

Equation 2-6: Local Solar Time

Finally, we can construct the Hour Angle (HRA), which converts the Local Solar Time to the number of degrees that the sun moves across the sky. At solar noon, the angle is by definition  $0^\circ$ . And the Earth rotates  $15^\circ$  per hour. In the morning the angle is negative, and in the afternoon positive.

$$HRA = 15^\circ(LST - 12)$$

Equation 2-7: Hour Angle

With this time the position of the sun, relative to the location on Earth can be computed. The axis around which the Earth rotates from day to day varies throughout the year. The declination ( $\delta_\odot$ ) is tilted by  $23.45^\circ$  and oscillates around that equilibrium. As the year progresses the declination is zero at the equinoxes on March 22<sup>nd</sup> and September 22<sup>nd</sup>. At the summer solstice in the northern hemisphere, the angle is  $+23.45^\circ$  and at the winter solstice  $-23.45^\circ$ . And follows the following formula:

$$\delta_\odot(d) = -23.45^\circ * \cos\left(\frac{360}{365} * (d + 10)\right)$$

Equation 2-8: Solar declination approximation corrected for 1st January (Cooper, 1969)

As we set the location where we are as stationary, the sun moves around us. This angle changes every minute. The angle of elevation ( $H_\odot$ ) as sunrise is set at  $0^\circ$  and sunset is  $180^\circ$ . At some point in the day the sun is at its highest,  $90^\circ$  also referred to as solar noon.

$$H_\odot = \sin^{-1}[\sin \delta_\odot \sin \phi + \cos \delta_\odot \cos \phi \cos(HRA)]$$

Equation 2-9: Solar coordinates Altitude

Where  $\phi$  is the latitude at the location. A graph illustrating the altitude for the first day of the first six months is given in Figure 2-13. The remaining months are almost equal to the first six months but in reverse order.

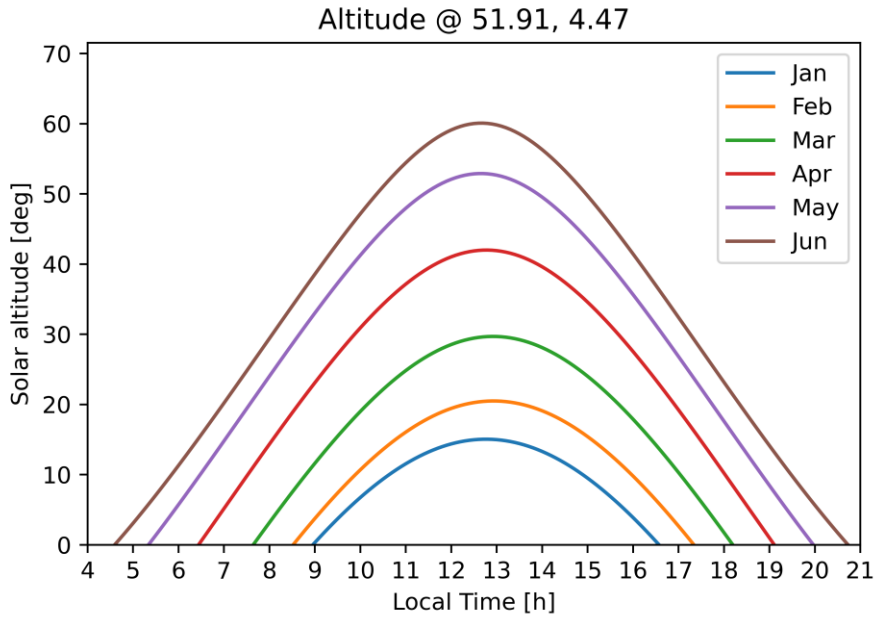


Figure 2-13: Solar Altitude in Rotterdam on the first day of the first six months of the year.

The angle between the sun and the vertical is called the zenith angle ( $\zeta$ ).

$$\zeta = 90^\circ - H_\odot$$

Equation 2-10: Zenith angle

At the same time, the sun passes from 'East' to 'West'. The angle the sun is on compared with North is defined as the azimuth ( $A_\odot$ ). With North being  $0^\circ$  and  $90^\circ$ ,  $180^\circ$  and  $270^\circ$  for East, South and West respectively. This follows the following equation:

$$A_\odot = \cos^{-1} \left[ \frac{\sin \delta_\odot \cos \phi - \cos \delta_\odot \sin \phi \cos(HRA)}{\cos H_\odot} \right]$$

Equation 2-11: Solar Azimuth

This needs to be altered to represent the system correctly, to be able to set the solar morning.

$$\begin{aligned} A_\odot &= A_\odot \text{ for } LST < 12 \text{ or } HRA < 0 \\ A_\odot &= 360^\circ - A_\odot \text{ for } LST > 12 \text{ or } HRA > 0 \end{aligned}$$

Equation 2-12: Correction for azimuth angle

The resulting graph for the first day of the first six months is given in Figure 2-14.

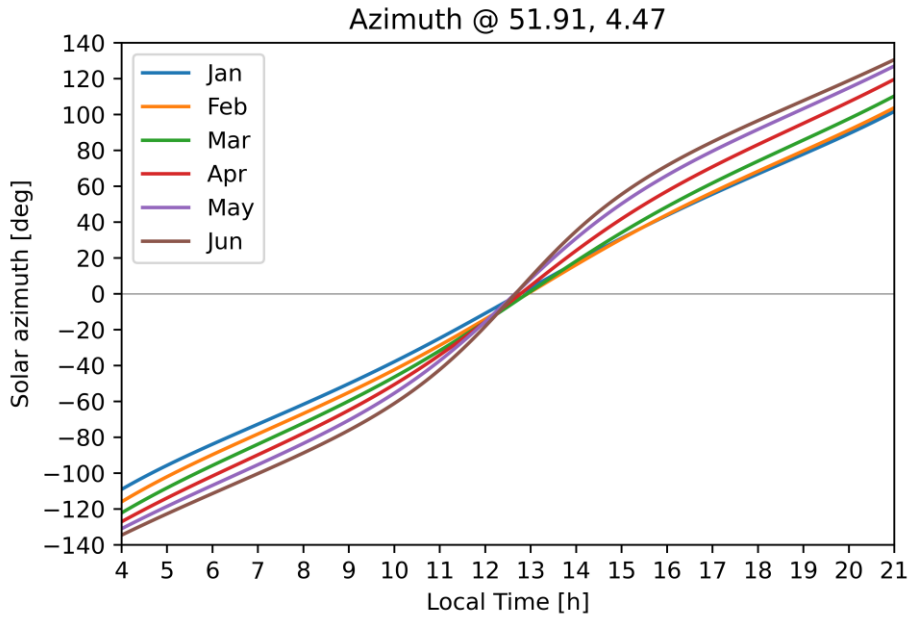


Figure 2-14: Solar Azimuth in Rotterdam on the first day of the first six months of the year.

From these 2 graphs, one could conclude that the total angle the sun travels throughout the daytime (the sun is above the horizon) changes with the seasons. As the speed at which the earth rotates is almost constant, the day length fluctuates. From these also the Solar Noon can be calculated, at which the derivative of the Altitude is 0. In Figure 2-13, the local time of the Solar Noon changes over the months.

But in many parts of the world, a man-made concept is introduced called Daylight Saving Time (DST), also referred to in Europe as 'summertime'. The objective of DST is to extend the summer evening and thus save on electricity needed to illuminate our surroundings at night. In the mornings the sun is up early, and DST makes the morning slightly darker, but that effect is only noticed by early risers. The impact of this DST could be the debate of another thesis, both economically and physiologically. Typically, this change is done on an early Sunday morning at 2 or 3 o'clock respectively. In the spring going one hour forward, and in the fall one hour back. In Europe, this takes place on the last Sunday of March and October.

To calculate sunrise an approximate correction of the zenith is set to  $90.833^\circ$  to account for the diffraction of the atmosphere that occurs at sunrise and sunset and the size of the Sun. This leads to the calculation of a new Hour Angle.

$$HRA_s = \pm \cos^{-1} \left( \frac{\cos(90.833^\circ)}{\cos(lat) \cos(\delta_\odot)} - (\tan(lat)) \tan(\delta_\odot) \right)$$

Equation 2-13: Altered Hour Angle (NOAA)

Where a positive Hour Angle corresponds to sunrise and a negative to sunset.

To calculate the time at which these events happen:

$$Sunrise = 720 - 4 * (longitude + HRA_s) - EoT$$

Equation 2-14: Sunrise time in minutes (NOAA)

Where  $\phi$  and  $\delta_\odot$  are in degrees and TC (Equation 2-5) in minutes. These minutes can be converted into hours and minutes to give the time of these events. Furthermore, these times need to be corrected for DST.

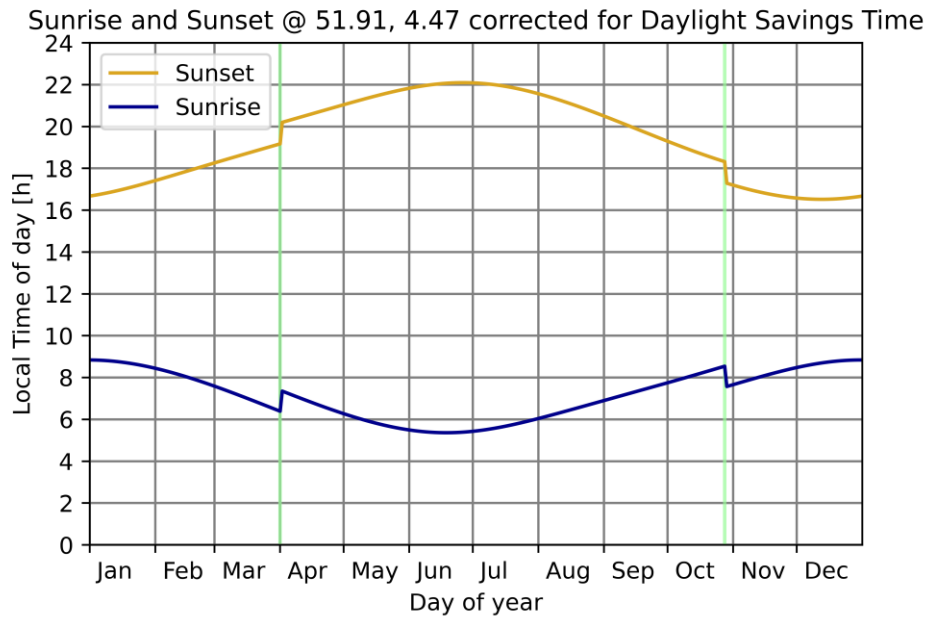


Figure 2-15: Sun event time in Rotterdam, corrected for Daylight Saving Time for 2024 from 31<sup>st</sup> of March until 27<sup>th</sup> October.

The computation of these graphs is done with Python, this and other scripts can be supplied upon request. With this script it is also possible to generate the input for buildings on other locations.

## 2.4 Lighting in museums

In museums, light is an important aspect of the experience. Too little light and our eyes are not able to make out the colours. Too much light could strain our eyes and furthermore, could irreversibly damage the art we came to admire. As common in nature, we need to strike a balance between these two extremes. By optimising the viewing conditions, the visitor can appreciate the piece of art, while the damage to it is controllable and deemed acceptable. To this extent many different researches were performed by different people.

To assess the ability of visitors to appreciate art, researchers at the Bartlett School of Architecture and Planning in London wanted to know the response of people to the lighting in a purpose-made mock-up art gallery (Loe, Rowlands, & Watson, 1982). The subjects were asked to fill out a semantic differential questionnaire, based on their assessments of appearance for five different paintings, as well as for the space. This was done under different lighting conditions, at six different illuminance levels: 10, 25, 50, 100, 200 and 400 lux. During the trial also three different fluorescent lamps were used, which are now obsolete. But as a fourth condition, they assessed daylight. By processing the results of the questionnaire via factor analysis to identify the principal dimensions by which the subjects had differentiated the conditions, two significant factors arose. The Discrimination Factor, is the ability to discriminate small details and colour, and the Quality Evaluation Factor, is the degree of pleasure from viewing the artwork. In Figure 2-16 these factors are plotted to the illuminance. At 50 lux the results are positive, indicating an overall satisfactory experience. At lower light levels the results are negative and will not yield a good viewing condition.

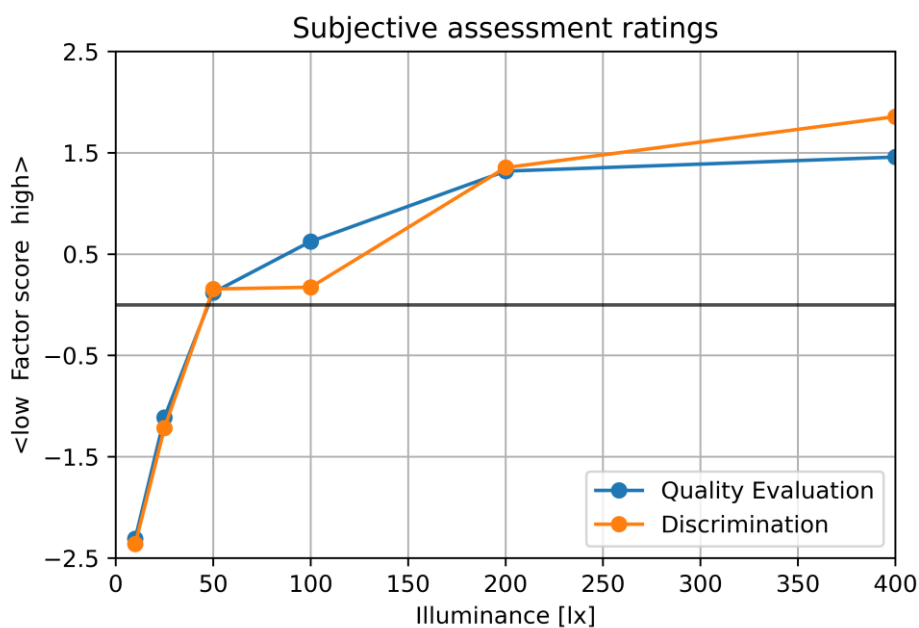


Figure 2-16: Subjective assessment ratings for discrimination of appearance of paintings viewed under daylight, in a simulated art gallery (Loe, Rowlands, & Watson, 1982).

Another aspect that influences the experience of the visitor of the museum is the way the individual art pieces are lit, with accent lighting. The lighting fixtures used for this all have their properties and shortcomings. Each light source has a certain colour temperature, and this can cause a shift in the colour of the artwork. There is a relation between the perceived illuminance and the colour temperature of the light source (Cuttle, A Proposal to Reduce the Exposure to Light of Museum Objects Without Reducing Illuminance or the Level of visual Satisfaction of Museum Visitors, 2000) & (Leccese, Salvadori, Maccheroni, & Feltrin, 2020).

The majority of the art displayed on the walls at BVB are painted artworks, with some exceptions for textiles. In the contrary to popular belief not all painted artworks should be considered flat. Depending on the style, the artist could have introduced a bumpy texture with his paint, with the intention that the raised part would catch more light, appearing lighter and other parts darker. This will result in a larger dynamic difference in the painting. To emphasise these small details, not only diffuse light is needed, as that will cast an even level of illuminance for the entire piece. With the use of cleverly chosen and positioned spotlights, the museum can emphasise different aspects. This will introduce a contrast between the artwork and the wall it is hanging on. This difference should not be too large as the eye may experience difficulties adjusting to the different parts. A ratio of 2:1 (artwork – wall) is described as a visual difference (Bokerhof, et al., 2008). In the case of sculptures, this ratio could be increased as the materials used to make sculptures are typically less sensitive to the damage associated with an increase in exposure.

The placement of the light sources, natural or artificial needs to be chosen carefully to minimise the chance of glare. This probability increases in the direction a person is looking and decreases in the peripheral vision. Depending on the specific fixtures chosen the beam of light can be controlled. Modern implementation of these lights largely relies on LED, a benefit of these is their low energy consumption and the ability to combine different types to limit the wavelengths that are emitted in the IR band. On top of that filters (Delgado, Drik, Druzik, & WestFall, 2010) can be used to further reduce that and they are significantly better than the IR emitted by incandescent light sources as seen in Figure 2-17.

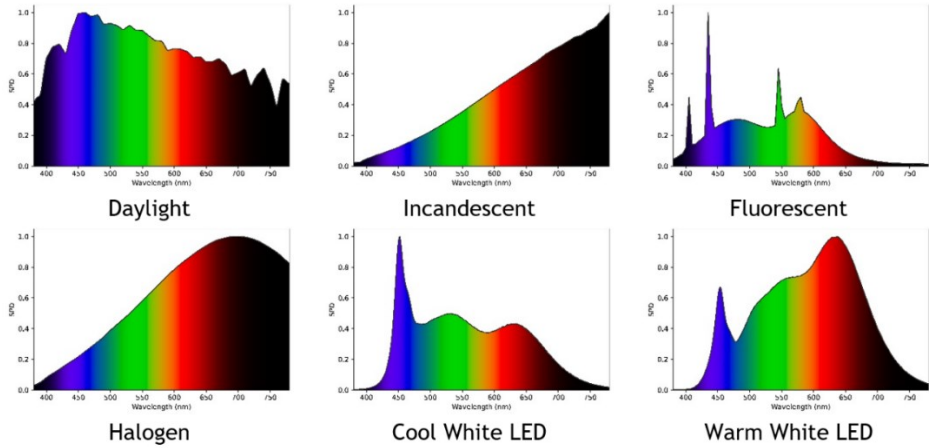


Figure 2-17: Examples of Spectral Power Distribution of different light sources, largely depended on manufacturer specific attributes (Lai, 2022)

This culminates in a multicriteria problem that the lighting designer needs to solve as illustrated in Figure 2-18.

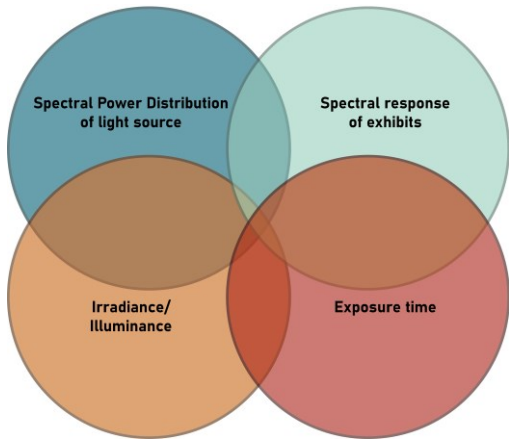


Figure 2-18: Multi-dimensional lighting parameters (Huijiao & Rui, 2022)

## 2.5 Damage potential of light on art

Based on the Reciprocity Law, we can define the exposure (H) as the integral of the irradiance ( $E_e$ ) and the time.

$$H = \int_t E_e dt \quad \text{Wh/m}^2$$

Equation 2-15: Reciprocity Law (CIE 157, 2004)

Where  $t$  is in hours and  $E_e$  is the incident irradiance on the surface ( $\text{W/m}^2$ ). With this, we get the total annual exposure of a piece of art. Meaning that if the irradiance doubles, the time it takes to receive a certain dose of exposure is halved. As artworks are classified in exposure classes, this can drastically reduce the accepted exposure and display time. The Dutch: NPR-CEN/TS 16163:2014<sup>1</sup> that governs the guidelines and procedures for appropriate lighting for indoor exhibitions follows the classification made by the CIE 157:2004<sup>2</sup>. The classification ranges from no sensitivity to low, medium and high sensitivity. These are based on the results of the ISO Blue Wool Standard (BWS). For class 2 - low sensitive materials - the upper limit of annual luminous exposure is set to  $600\,000 \text{ lx} \cdot \text{h}$  per year. As a museum is not open 24/7 the illuminance limit is 200 lx.

For the restoration of the BVB museum however, the museum board has chosen a slightly higher illuminance of 250 lx.

Natural daylight has a significant amount of radiative power in the UV and IR parts of the spectrum (Camuffo, 2019). We, humans, are not able to process these wavelengths and they also introduce a heating effect on a surface. This will increase the rate of deterioration. Some aspects are simply chemically accelerated and also stress inside of the painting can occur due to the local temperature variations. If the canvas and the paint are exposed to different temperatures cracks could form. This needs to be prevented at all costs.

If there are more pigments inside the paint, there is less binder, this will result in a higher degradation and an increased rate at which that pigment loses its ability to absorb and reflect the original wavelengths (Cuttle, Light for Art's Sake, 2007).

Not only photochemical processes can influence the art, but local conditions like the relative humidity also impact the speed at which this happens.

---

<sup>1</sup> (NPR-CEN/TS 16163, 2014)

<sup>2</sup> (CIE 157, 2004)

Responsivity category	Description	ISO BSW rating	Probable Mlx h for noticeable fade <sup>3</sup> if no UV	Examples
1: Irresponsible	<p>Most but not all mineral pigments.</p> <p>The "true fresco" palette, a coincidence with the need for stability in alkali.</p> <p>The colours of true glass enamels, ceramics (not to be confused with enamel paints).</p> <p>Many monochrome images on paper, but the tint of the paper and added tint to the carbon ink are often high responsivity, and paper itself must be cautiously considered low responsivity.</p> <p>Many high-quality modern pigments developed for exterior used, automobiles.</p>	>8		<p>Carbon, hence: true pencil, charcoal, India ink. (not iron gall ink, not the yellow in sepia).</p> <p>Ochre. Umber. Sienna. Indian red (iron oxide). Black oxide of iron.</p> <p>Ultramarine. Cobalt blue. Silver point. All the white pigments.</p>
2: Low responsivity	<p>Artist' palettes classified as "permanent" (a mix of truly permanent and low light responsivity paints, e.g. ASTM D4303 Category I; Winsor and Newton AA).</p> <p>Structural colours in insects (if UV blocked).</p> <p>A few historic plants extracts, especially indigo on wool.</p> <p>Silver/gelatin black and white prints, not RC paper, and only if all UV blocked.</p> <p>Many high-quality modern pigments developed for exterior used, automobiles.</p>	8	1100	<p>Cadmium red, orange, yellow (many belong in No responsivity but insufficient data).</p> <p>Some dyes, such as indigo and cochineal on cotton, silk, and wool, move several steps up, to 8 or better, when one tests the remnant of a partially faded sample. This is NOT true of all colours, and especially not true of those that start in the range Blue Wool 1,2. These fade uniformly fast</p>
		7	300	<p>Alizarin (madder) lake. Madder on wool. Vermillion. Chrome yellow.</p> <p>Indigo on wool.</p> <p>Water lily roots (black) on wool.</p>
3: Medium responsivity	<p>Few historic plant extracts, particularly alizarin (madder red) as a dye on wool or as a lake pigment in all media.</p> <p>The colour of most furs and feathers.</p> <p>Most colour photographic with "chrome" in the name.</p>	6	100	<p>Cochineal on silk.</p> <p>Foxglove on wool.</p> <p>Chrome tanned leather.</p>
		5	30	<p>Alizarin (madder) lake tint.</p> <p>Alizarin (madder) on wool.</p>
		4	10	<p>Lac dye on wool. Seaweed on wool.</p> <p>Ling heather tips on wool. Weld, tin mordant on wool. Vegetable tanned leather.</p>
4: High responsivity	<p>Most plant extracts, most historic bright dyes and lake pigments in all media: yellows, oranges, greens, purples, many reds, blues.</p> <p>Insect extracts, such as lac (yellow), cochineal (carmine) in all media.</p> <p>Many early synthetic colours such as the anilines, all media.</p> <p>Many cheap synthetic colorants in all media.</p> <p>Most flet tip pens including blacks.</p> <p>Most dyes used for tinting paper before 20<sup>th</sup> century.</p> <p>Most colour photographic prints with "colour" in the name.</p>	3	3	<p>Madder on silk.</p> <p>Cochineal on wool and cotton.</p> <p>Weld, alum mordant on wool.</p> <p>Indigo on paper, cotton and silk.</p>
		2	1	<p>Carmine lake. Gamboge. Quercitron lake.</p> <p>Madder on cotton. Old fustic.</p> <p>Coomassie violet on paper. Rhodamine on paper.</p> <p>Average photo colour print.</p>
		1	0.3	<p>Turmeric. Saffron. Sulphonated indigo. Many modern dyes for paper, e.g. methyl violet, victoria blue, eosine (pink), bismarck brown.</p>
5: New	Highly sensitive material or material that is rare exposed to light, (near) original state.	<1		Coloured reference material. Thermography paper. Japanese drawings.

Table 2-2: The light responsivity of pigments and substrates (CIE 157, 2004, p. 20)

<sup>3</sup> Noticeable fade is defined here as Grey Scale 4 (GS4), 30 steps is the full loss of colour

Material classification	ISO Blue Wool Standard (BWS)	Upper limit annual luminous exposure	Annual exposure time	Illuminance
1. Insensitive	-	No limit (for conservation)	No limit (for conservation)	No limit (for conservation)
2. Low sensitivity	7 & 8	600 000 lx·h per year	3 000 h per year <sup>a</sup>	200 lx
3. Medium sensitivity	4, 5 & 6	150 000 lx·h per year	3 000 h per year <sup>a</sup>	50 lx
4. High sensitivity	1, 2 & 3	15 000 lx·h per year	300 h per year <sup>b</sup>	50 lx
<sup>a</sup> Typical annual opening hours				
<sup>b</sup> Resulting annual hours using 50 lx				

Table 2-3: Limiting illuminance and annual luminous exposure for different classed of light-sensitive exhibit interpreted from (CIE 157, 2004, p. 26)

By displaying art, we must accept the fact that irreversible damage will be done to the artwork. To analyse the damaging effects of light-induced colour change, a large assessment was made focusing on the effects of the conditions in which the pigments are displayed: in open air or anoxic environments. Over 90% of the samples showed less degradation when kept at low-oxygen levels compared to air. Crossing over into anoxic conditions there was a further reduction between two and three times lower (39% of the subset) and four or more times for 47% of the subset. However, for six samples the colour change was accelerated in anoxic conditions (Beltran, Druzik, & Maekawa, 2012). Artworks consist of many different types of pigments or materials, and some react differently on the conditions. This means that it is not easy to say in general which condition will be less detrimental and so, compromises need to be made.

The CIE 157, 2004<sup>4</sup> classifies a 'just noticeable change' this is related to the change in colour that a person can distinguish. This has a value of  $\Delta E = 1.5$  in the CIELAB space. The CIE states that after 10 (just noticeable) changes the colour will appear to be washed out and consequentially the 'exhibition value' is lost. After 10 more (just noticeable) changes the piece will experience structural issues and after 10 more changes, it will start to crumble. After a total of 30 changes, the colour no longer has any remaining pigments and is deemed a 'total loss' (CIE 157, 2004). A study to quantify colour change is discussed by (Herascu, Simileanu, & Radvan, 2008). For low sensitivity pigments, a singular just noticeable change will occur after 500 years, if UV is eliminated. However, for high sensitivity pigments, adhering to the set upper annual exposure, such change will occur after just 20 years.

These factors allow a curator to define a regime where all factors are governed and stay within acceptable tolerances. Per art piece, the curator can class a piece, based on the pigments used, the medium on which the art is made, and the binder. This will lead to a maximum dose, and this can be expressed in time. For high sensitive pieces, this will result in a tightly constrained time frame at which the art is exposed, after which the piece will need to go back in, total dark, storage.

---

<sup>4</sup> (CIE 157, 2004)

## 2.6 Simulation in Radiance

Since the early days of the development of *Radiance* by (Ward Larson, et al., 1998), it has become a well-known simulation engine used by researchers for lighting predictions (Brembilla, Hopfe, & Mardaljevic, 2018). *Radiance* uses command-line scripts, which makes the effort to start with the software steep. By harnessing this work by *Honeybee*, this input is simplified. It can predict the illuminance levels within  $\pm 10\%$  (Brembilla, Drosou, & Mardaljevic, 2022). In most of the simulation types available, the sky is represented as a dome and subdivided into different patches that each have a luminance. The number of patches is set by the different simulations.

For Climate Based Daylight Modelling *Radiance* uses a backwards ray tracing approach. By starting at a point on a surface, the rays are traced throughout the space, interacting with elements inside. And inevitably if a ray manages to exit the structure and can reach the 'sky dome', it can be quantified with an illuminance value.

For the model, *Radiance* accepts many of the common 3D/CAD represented surfaces and meshes. With this, quick changes can be made without tedious command-line alterations. But computer models are a schematisation of the real world. The surfaces in the model are made up of a large collection of connecting triangles, creating an artificial flatness that should be corrected by a roughness parameter.

When light leaves its source, the luminance decays. For every doubling in distance the intensity is halved, this is known as the inverse square law. As a ray hits a surface at an angle, a part is reflected at the same angle of the incident. Some energy is absorbed by the material. In the case of translucent materials, a part is also able to be transmitted through the material. These three elements should equate to 1, as otherwise energy would have been lost.

But for not perfectly smooth surfaces the reflected light is not one perfect line. It is scattered in a radial pattern, mostly diffuse. Inside the translucent material, the incoming rays are refracted and some rays remain inside of the material for several bounces, before finally exiting the material. This can be done in a diffuse pattern or specular.

In the real world, materials are not always homogeneous and their subsurface properties are more resource intensive to predict.

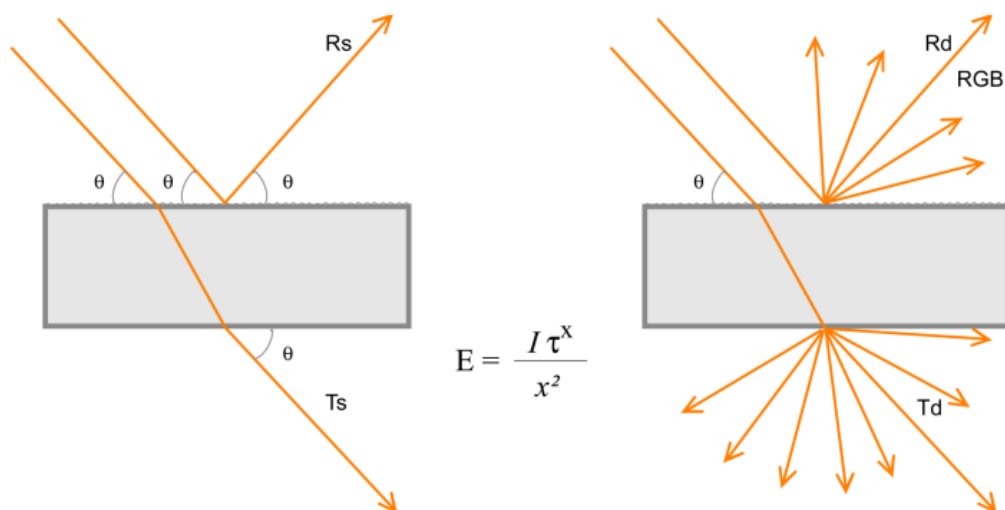


Figure 2-19: Interaction of light with a diffuse translucent material (Mead, 2010)

# 3 Methodology

---

## 3.1 The museum

For the analysis of daylight in the MBVB this study aims to compare the model/calculations with actual measurements. This chapter starts with a description of the current state of the museum, followed by the chosen approach to measure on-site. These results can then be compared with the results of the calculations on the 3D model.

### 3.1.1 The current state of the museum

The entire BVB museum complex consists of the Van der Steurgebouw (1935) by Ad van der Steur, the Tentoonstellingsgebouw (1972) by Alexander Bodon and Het Paviljoen (1991) by Hubert-Jan Henket (Boijmans Van Beuningen, 2023). The most recent addition is the Depotgebouw (2021) by MVRDV. The museum has been closed for restoration since 26 May 2019 and only the Depot is still open for visitors. The restoration started with the removal of asbestos-containing materials that were used in the original construction of the buildings because the use of this dangerous material is no longer permitted and has to be removed by a certified contractor. This does have an impact on the appearance of the interior rooms, as they had to do some major cutting to remove all the asbestos. Also, part of the restoration has to do with the air handling, which was done via big air ducts that are hidden inside of the walls Figure 3-1.



Figure 3-1: Current state of the Van der Steurgebouw after removal of asbestos (photographs by Aad Hoogendoorn<sup>5</sup>)

This means that the current state of the museum has changed considerably. With the extra holes in the walls of the exposition rooms, the removal of the floor and wooden trim around the room, the physical properties of the rooms are no longer the same as in the original exposition state. The surfaces are different, and the reflective properties have changed along with the roughness of the materials. This means that the choice of a suitable room for this research will depend on the actual conditions.

### 3.1.2 Design of daylight modelling approach

The architectural company Mecanoo was asked to carry out the restoration of the entire old part of the complex. For this they made a detailed 3D model, to accurately design the new parts and to assess the impact of the restoration process. For this study, this 3D model can be used as a starting point for the modelling of the complex and the rooms that are inside of the building, see Figure 3-2.

---

<sup>5</sup> <https://www.boijmans.nl/nieuws/asbestsanering>

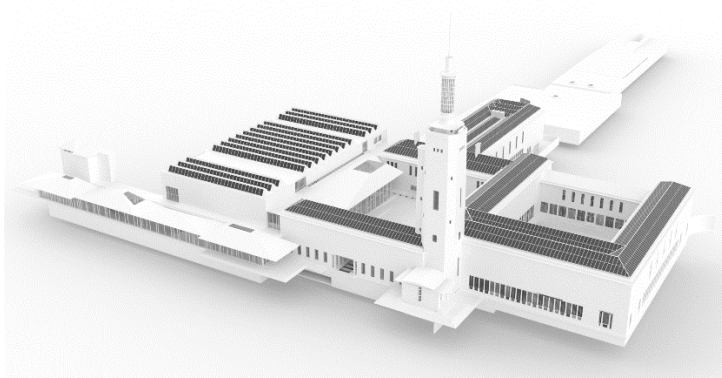


Figure 3-2: IFC model supplied by Mecanoo, used as baseline for Van der Steur, with on the bottom right the wing in question

For the Climate Based Daylight Modelling (CBDM) the content of the .IFC model (based in the Autodesk family, file extension: Industry Foundation Classes) made by Mecanoo has to be imported into *Rhino*. To achieve this a port using *Speckle* was used to transfer the meshes into *Rhino* and later into *Grasshopper*. In *Grasshopper*, using a combination of *Ladybug* and *Honeybee*, a model can be constructed where surfaces are assigned their respective properties. Combined with location-specific weather data the CBDM can be performed. These are exported directly to *Radiance* which handles the simulation of daylight in the model.

To validate the model a comparison must be made with on-site measurements. This can be done with a HDR camera as shown by (Mardaljevic, Cannon-Brookes, Blades, & Lithgow, 2021). In the process of the comparison, the parameters of the *legramen* and the *schoepen* can be varied to finally result in a close resemblance of the real-world measurements and the outcomes of the simulated model. For the comparison, a custom *Python* script is used. The validated model can be used for the calculation of the sun shading system, discussed in 3.4.

An overview of this total process is illustrated in Figure 3-3.

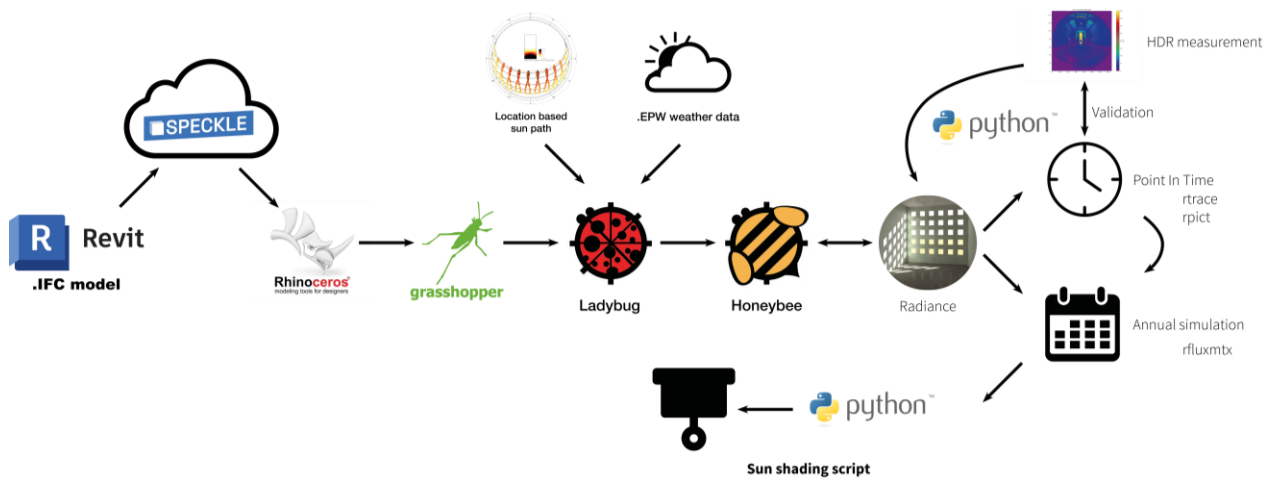


Figure 3-3: Process flow of programs

## 3.2 On-site measurements

### 3.2.1 Diffuse Reflection Coefficient

To accurately simulate the rooms for the calculation some additional parameters are needed. One of the main factors regarding modelling light levels indoors is the diffuse reflectance. To calculate this, the luminance of a surface is required as well as the illuminance that falls on the surface:

$$\rho = \pi \times \left(\frac{L}{E}\right)$$

Equation 3-1: Diffuse reflectance

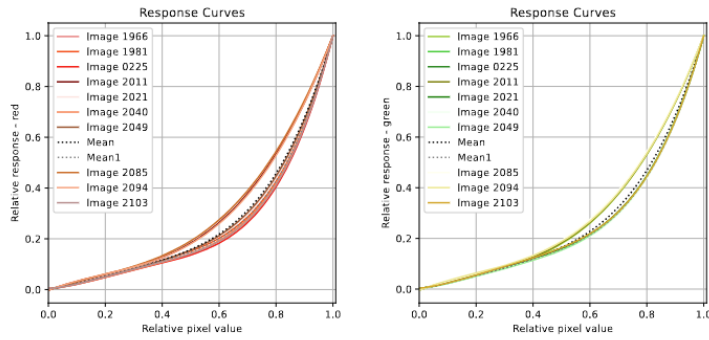
Where the output,  $\rho$  is the diffuse reflectance [-], which is by nature dimensionless and has a value between 0 and 1 with 0 being completely black and 1 highly reflective.

During the on-site measurements, the illuminance (E) and the luminance (L) will be measured. This can be done with a combination of an illuminance meter and a spot meter.

### 3.2.2 High Dynamic Range photography setup

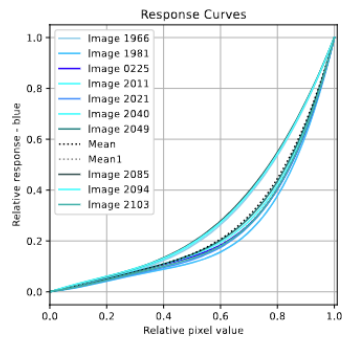
To calibrate the lighting simulations some measurements are needed. The way that the light is cast around the exposition rooms is one of the features that make this building the way that it looks. A small number of measurements at some positions around the room would not yield enough detail and introduce the variability of sunlight. Therefore, a High Dynamic Range (HDR) imaging approach is taken. By capturing the entire scene that the camera is able to capture, more data points are collected, at the same point in time. This method is described in (Pierson, Cauwerts, Bodart, & Wienold, 2021). For this method, a special camera *Canon EOS 70D, LMK mobile air*, is used, which was calibrated by TechnoTeam (TechnoTeam). This camera is calibrated for the sensitivity of different wavelengths of light for the specific image sensor. A Canon manufactured sensor follows a Bayer array, wherein for each pixel 4 subpixels are used, two green, one red and one blue receptor. The response curves of all 3 primary colours are made in accordance with (Pierson, Cauwerts, Bodart, & Wienold, 2021) by the Building Physics department of Architecture at the Delft University of Technology, see Figure 3-4. In this particular camera a Natural Density (ND) filter is placed, reducing the incoming light that hits the sensor.

This camera is paired with the *Sigma Fisheye 4.5mm F2.8 EX DC HSM*. By design, almost all camera and lens combinations will result in an image with some form of vignetting. This phenomenon is caused by the geometric mismatch between the round lens opening and the rectangular image sensor. Inside the lens, the light is concentrated with different optics and the result is that more light falls near the centre of the image, and less towards the far corners. Most pictures will have a brighter appearance in the centre and more darker corners. For normal photography, this is not an issue as the change is minimal, can be corrected during editing and could also be enhanced for artistic purposes. But during measurements, it could result in a lower measured luminance at the edges. The Sigma Fisheye lens used has a very wide Field of View (186°) and as a result the pixels near the edges of the image sensor of the camera are not exposed. The effects of vignetting of the combination of camera and lens used is shown in Figure 3-5. For every 5° angle the relative luminance of the results recorded by the camera and an external spot meter is shown, in accordance with (Pierson, Cauwerts, Bodart, & Wienold, 2021), starting at 9 o'clock. As expected there is little difference between the different angles.



(a) Red channel

(b) Green channel



(c) Blue channel

Figure 3-4: Pixel response to primary colours Red (a), Green (b) and Blue (c), as made by the Building Physics department

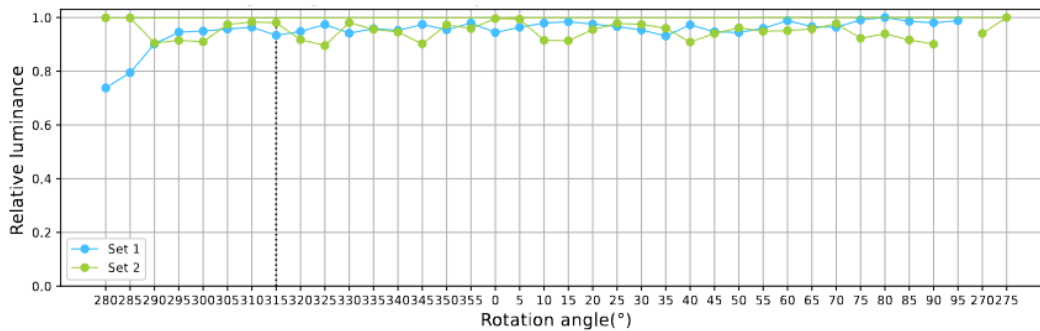


Figure 3-5: Vignetting curves Sigma Fisheye 4.5mm f2.8 EX DC HSM and Canon EOS 70D, as made by the Building Physics department

The camera can only take singular Low Dynamic Range (LDR) images. Hence multiple LDR images are taken, keeping everything constant except the shutter speed. By varying the shutter speed more or less light enters the camera. These sets of LDR images are later combined into one HDR image. To minimize any shake introduced by the operator, the camera is placed on a tripod. The exact location of the camera in the room is measured to be able to recreate the view in the software later. To further reduce shaking and to be able to accelerate the time it takes to perform a full capture, a computer program is used to control the camera. With qDslrDashboard (version 3.6.7) the camera captures 14 photographs automatically via USB. Each following photograph has an increase in exposure of 1 stop. An example of a typical increase in shutter time is given in Table 3-1.

Shot #	1	2	3	4	5	6	7	8	9	10	11	12	13	14
Exposure time in [s]	1/400	1/200	1/100	1/50	1/25	1/13	1/6	1/3	0.6	1.3	2.5	5	10	20

Table 3-1: Example of exposure times of measurements, times are in seconds

To assess if the lighting conditions lent themselves for this HDR process, an illuminance meter is placed on top of the camera by connecting the hot shoe with a small rod to the *Konica Minolta CL-200A*. If the illumination of the room changes too much during the capture, the measurement must be discarded. These bounds were set on 5% change. The illumination is only recorded just before and right after the capture. As the capture takes about 2 minutes to complete, the light levels in the room can change. During capture, care is taken to observe the illuminance meter to judge if too big of a change happened mid-capture. So even when the end measurement would be in range, that measurement will have to be discarded.

The resulting HDR images in the software yield a relative measurement, these need to be scaled according to the absolute on-site measurements. This is done by measuring the luminance with a spot luminance meter (*Konica Minolta LS-160*) on a known matt surface, the *Hagner Reflection Reference*.

All measurements are logged, the illuminance measurements, the file names of the LDR are included, the luminance as well as the time the series was taken. Only the series that meet the selection of <5% illuminance change will be compiled in 4.1.

### 3.3 3D modelling of the rooms

The architect of the BVB has made an *IFC* model of their plans for the museum. That model includes both the old buildings as well as the new additions they are designing. In the archives of the municipality of Rotterdam, there is a database with most of the original drawings, but not all drawings survived from 1929. A comparison of the model with the original drawings showed some shortcomings in the model. This may be because the old parts of the complex are of less interest to the architect. Therefore, some alterations needed to be made to accurately model the building for this research. The *IFC* model had some rooms where the *schoepen* were modelled, but those were different rooms than the rooms that were selected for this research. Also, in the *IFC* model, the distance between two panels of the *schoepen* was constant, but according to the original design drawings the distance and pitch changes.

As the original architect Van der Steur was so particular about his ceiling, for this research the *schoepen* in the model has to be adapted to the original state. The modelling of this is done in *Rhinoceros*.

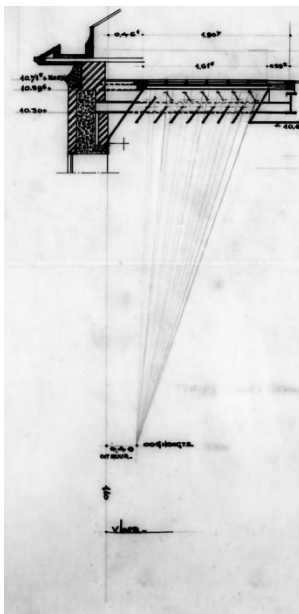


Figure 3-6: *Schoepen* philosophy, original cross-section drawing from 1934

As the architectural model does not represent the current state of the museum, further alterations are needed for the calculations. These changes are made using *Grasshopper*, as this allows to make these changes and later on, these changes can simply be disabled to go to the 'exposition state', while the model itself remains the same.

In Figure 3-7 to Figure 3-9 some examples of the 3D model are given. The roof construction (green) contains wired glass and a layer of Lexan™ but for better visibility, this is not shown in these figures.

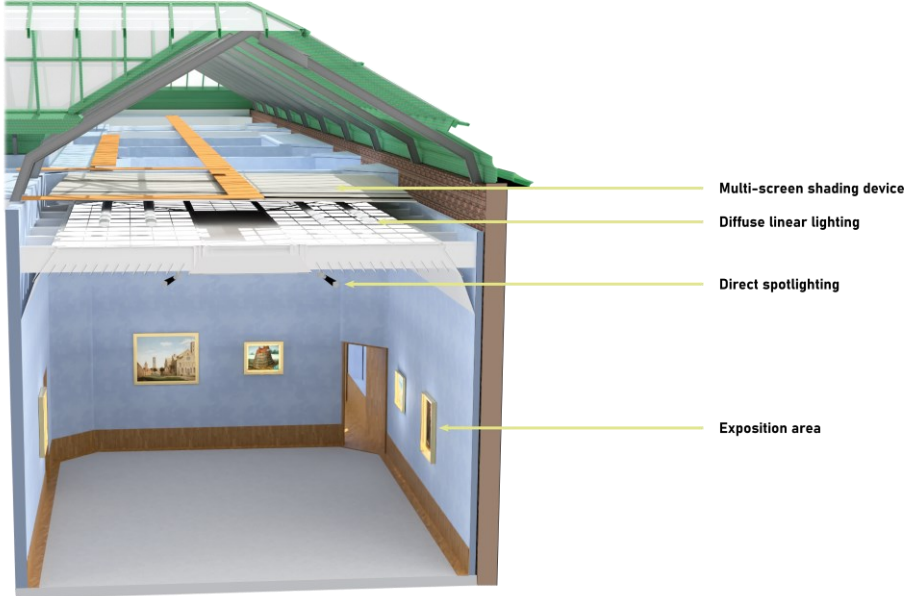


Figure 3-7: Cross section room 228 with annotations

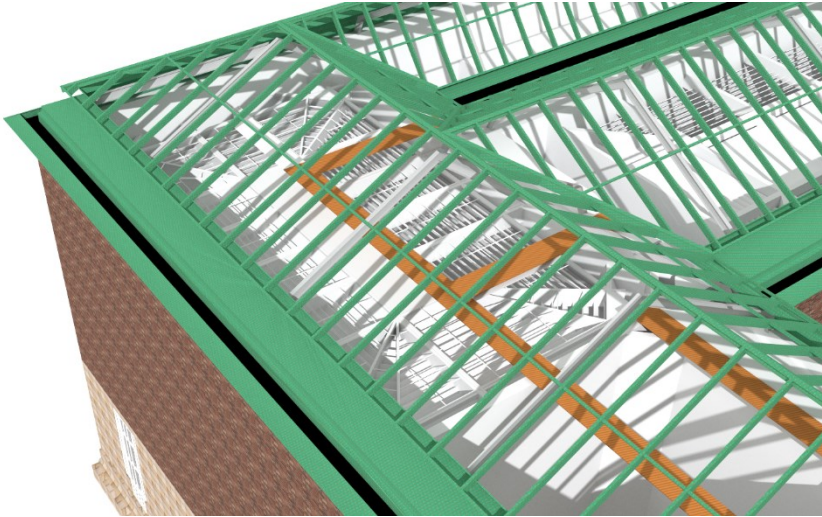


Figure 3-8: View from outside into room 228

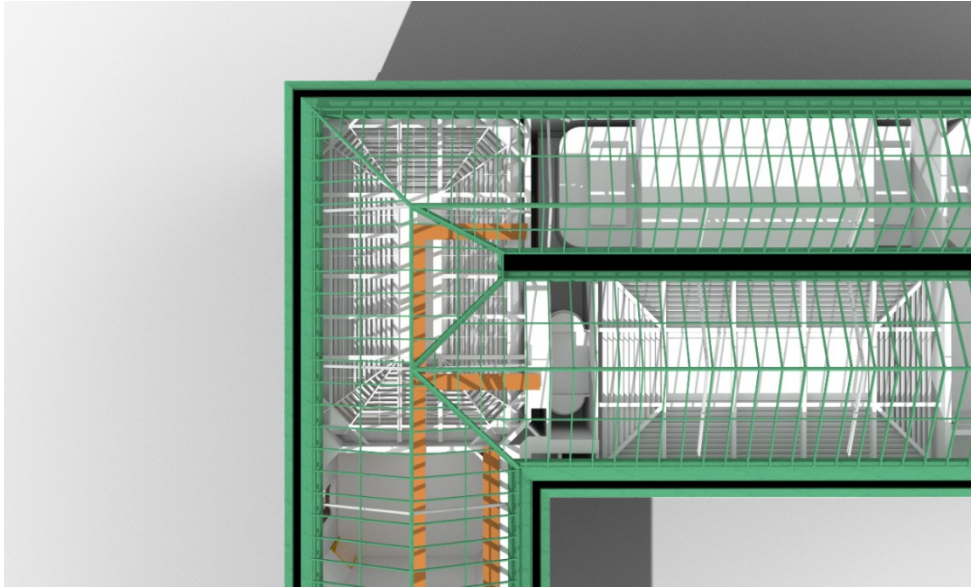


Figure 3-9: Top view for outside of room 228

### 3.4 Sensitivity analyses

To examine the impact of changes to the room, a sensitivity analysis (SA) is carried out. This is done with the Method of Morris (Morris, 1991). By varying the input parameters, the method provides an insight into the importance of each of the parameters. This is done for 5 different types of surfaces:

- Schoepen
- Wall in room 228
- Floor in room 228
- Legramen
- Roof windows used in the pitched roof

For each of these parameters an expected lower and upper bound is selected. With the Morris method, each of these domains is divided into 8 equal distance values. By using 8 ( $k$ ) trajectories and 5 ( $D$ ) parameters 48 ( $n$ ) combinations are made, as per Equation 3-2. In each simulation, each possible value of a parameter has an equal chance of occurring by applying a One-At-a-Time procedure.

$$n = k(D + 1)$$

Equation 3-2: Number of Morris SA runs (Brembilla, Hopfe, & Mardaljevic, 2018)

The bounds can be seen in Table 3-2, also the type of surface is given.

Parameter	Lower bound	Upper bound	Type
Schoepen	0.5	0.95	Diffuse reflection
Wall	0.2	0.85	Diffuse reflection
Floor	0.05	0.4	Diffuse reflection
Legramen	0.3	0.5	Diffuse transmission
Roof windows	0.4	0.7	Diffuse transmission

Table 3-2: Bounds of input parameters for sensitivity analysis

Using the *Python* package *SALib v1.4.8* all the required 48 combinations are constructed (Iwanaga, Usher, & Herman, 2022). As the number of samples is low the advances by (Campolongo, Cariboni, & Saltelli, 2007) the 'local optimization' setting are used. The distribution of the used parameters is displayed in Figure 3-10.

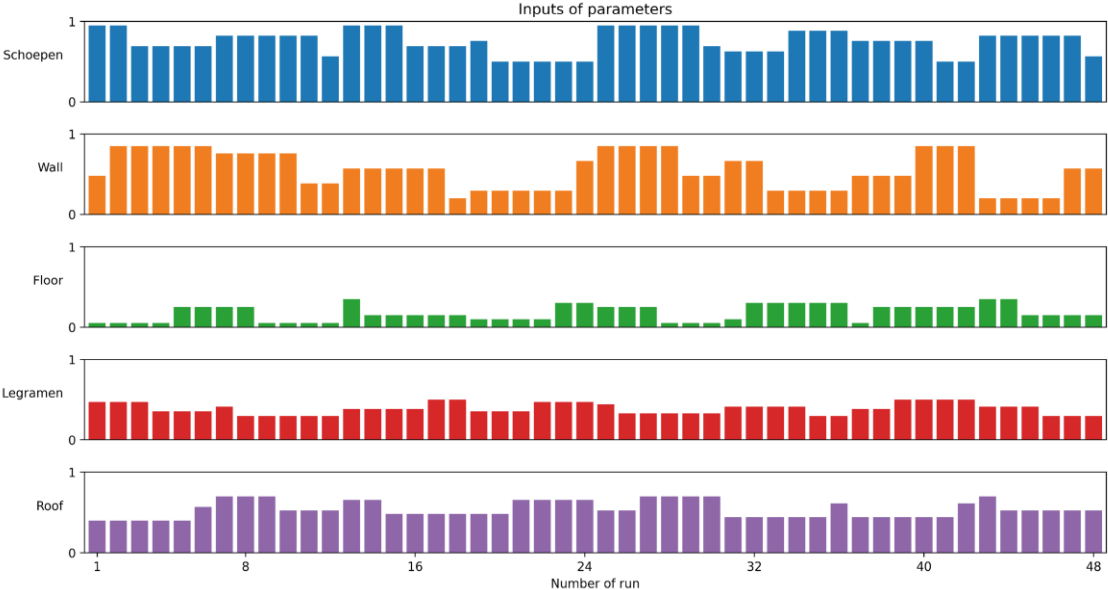


Figure 3-10: Input parameter settings used for sensitivity analysis

### 3.5 Design of the sun shading

For the control of the illuminance in the museum, the museum board is exploring the possibilities of sun shading above the horizontal *legramen*. That way the interior of the museum rooms is not changed. One requirement of the system is that the visitor is not too disturbed by the operation of changing screens. Therefore multiple sun shading screens are positioned vertically above each other. This allows for a wide variety of reduction of illuminance. This can be enhanced even more by using different types of screens as seen in Figure 3-12.

To model the effect that the sun shading will have the model is altered to include an additional horizontal surface that is positioned just above the *legramen*. This surface is a simplification of a possible screen system. Where fabric is a product that consists of individual woven strands of fibres, a sun screen is designed in such a way that there is an openness factor. Typically, the more open a screen, the higher the amount of daylight that can penetrate. Other properties listed about the appearance of the light: some screens will scatter the light in a more specular fashion and others will result in a more diffuse light field<sup>6</sup>. In this study, the particular effects of these properties are not investigated, as the light that falls on the screen (just above the *legramen*) through the outside wire glass directly followed by LEXAN™ layer of 10mm thickness. This results in a mostly diffuse light field in the attic. This diffuse light will be reduced by the sunscreen, and the properties of the *legramen* will further disperse the incoming light.

A grid simulation is performed for room 228. All hours are calculated that the sun is above the horizon at the location. These grids consist of multiple squares along the walls of hall 228 (1.6m above the ground, 0.4m high) with a sensor point in the middle of each position. The number of points varies per wall as this number is based on the length of the wall, and each point is roughly 1 meter apart as seen in Figure 3-11. With this approach, a strip is formed and one of these positions will have the highest illuminance. This maximum value is used to control the sun shading later. By choosing three dates, both the summer and winter extremes in solar positions are included as well as the late summer situation: the 21<sup>st</sup> of June (summer solstice), the 21<sup>st</sup> of December (winter solstice) and the 21<sup>st</sup> of September (equinox, halfway between solstices).

Based on this calculation a control scheme is built for the entire year.



Figure 3-11: Exploded view of location of sensor points around room 228, with viewpoint HDR measurement

#### 3.5.1 Sun shading control

For the different screens, an additional simulation is performed, on the same days as mentioned earlier, but now with an active screen. These results are calculated for 15:00 on June 21<sup>st</sup> and December 21<sup>st</sup>. This is done to verify the performance of these screens. The impact on the illuminance inside is compared to the simulation without screens, the baseline.

<sup>6</sup> Performance characteristics and classification (NEN-EN 14501 , 2021)

With this simplification, multiple states of the system are calculated. This way the reduction of illuminance during the hours that the sun vector has a direct normal line can be estimated. For this, a separate calculation will be performed to assess the hours per day that the sun is above the room.

The results of the combination of both these calculations are used as an input of a custom *Python* script to estimate the different reductions of illuminance inside based on each 'state' of screens as depicted in Figure 3-12. Also, in this logic, 0 is referred to as no screen needed and more than 7 will result in a blackout screen requirement.

- State 1: screen 1
- State 2: screen 2
- State 3: screen 3
- State 4: screen 1 + 2
- State 5: screen 1 + 3
- State 6: screen 2 + 3
- State 7: screen 1 + 2 + 3

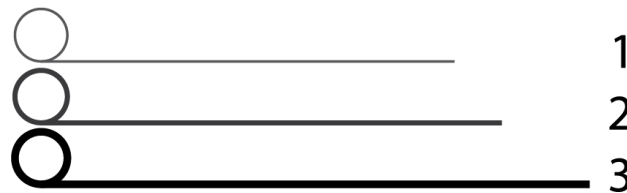


Figure 3-12: Schematical representation of multi-screen shading system

There is also the desire of the museum to have total light control. Therefore, a blackout screen will be fitted, this is not considered in the model. But it can be used if the illuminance limit is still exceeded even at state 7.

The control system starts with the illuminance at any given hour of the year. If that exceeds the limit, state 1 is checked. If that results in a value lower than the target, state 1 is used. If state 1 also exceeds the limit, state 2 is checked and so on.

The target for the sunscreen control is set according to the desired illuminance level of 250 lx (paragraph 2.5). Due to the desired contrast ratio of 2:1 (paragraph 2.4), the contribution of the daylight is limited to 125 lx, so the target is set to 125 lx. Artificial light is used as a supplement.

# 4 Study results

---

## 4.1 HDR measurements results

In the preparation of this research room 237 was mentioned as a possibility for the calculations. However, this room proved to have several large temporary openings in the walls. That made the room unsuitable for this research. The first visit to the museum on September 19<sup>th</sup> 2023 showed that there were two other possible rooms: 228 and 234. Room 228 is a large rectangular room with no vertical windows, but with some light coming in via the corridors. Room 234 is a small square room with a floor-to-roof window facing the Depotgebouw.



Figure 4-1: Room 234 - 19-09-2023 - v2 - 13:37

### 4.1.1 Analysis of HDR measurements

On the day of the first measurements, the weather was mostly cloudy and with only 1.5 hours of total sunlight, it was an intermittent day, with 1.6mm of rain. On the 26<sup>th</sup> of September, the clouds were still prevalent, but the number of sunshine hours increased to 4.7. On this day during the measurements fluctuations in illumination were observed, as fewer small clouds moved in front of the sun. Many of the measurements on the 19<sup>th</sup> were rejected on the illuminance check of 5% between the start and the end of the HDR capture.

During the measurements, a total of 30 sets of images were captured. Only 8 of them were captured with a stable illuminance ( $\leq 5\%$  between the start and end of the procedure). After computing all 8 HDR and luminance maps, 5 usable measurements were collected (deviation  $\leq 25\%$ , (Pierson, Cauwerts, Bodart, & Wienold, 2021)) 2 for room 228 and 3 for room 234.

Room #	Date	Spot meter	Illuminance	Python pixel value	Scale factor	Resulting luminance	$\Delta$	Vertical illuminance	$\Delta$
		cd/m <sup>2</sup>	lx	cd/m <sup>2</sup>	-	cd/m <sup>2</sup>	%	lx	%
234	19-09-2023	25.49	178.0	0.557	45.7	25.46	-0.08	113.3	-36.3
234	19-09-2023	8.12	61.0	0.127	63.9	8.13	+0.12	61.7	+1.22
228	19-09-2023	39.71	171.0	0.493	80.5	39.9	+0.39	166.3	-2.75
234	26-09-2023	33.78	137.0	0.306	110.4	33.8	+0.03	194.8	+42.2
234	26-09-2023	34.34	160.5	0.390	88.0	34.2	-0.40	189.3	+17.9
234	26-09-2023	41.61	183.5	0.451	92.4	41.7	+0.14	224.1	+22.1
228	26-09-2023	45.61	139.5	0.274	166.6	45.6	+0.02	293.8	+110.6
228 <sup>7</sup>	26-09-2023	40.18	276.0	0.587	68.5	40.2	-0.03	229.9	-16.7

Table 4-1: Scaling factor and error difference and final acceptance or rejection

In room 234 there is a large window directly in front of the lens. The measurements are within the 25% deviation, but the possibility exists that an error occurs because the vertical illuminance could be more related to the bright window than to the darker interior surfaces. This can cause less detail in the darker parts. In room 234 there is also a large window in the side wall, which complicates the light levels, and makes it more difficult to compare with the multiple unknown parameters in the model. This led to the conclusion that the calculations would only be made for room 228.

See the appendix C for further results of measurements.

#### 4.1.2 HDR Flowchart

The processing of the HDR measurements is done in several steps, as shown in the flowchart Figure 4-2. These steps are combined in a Python script Appendix B.

<sup>7</sup> Measurement used in rest of thesis

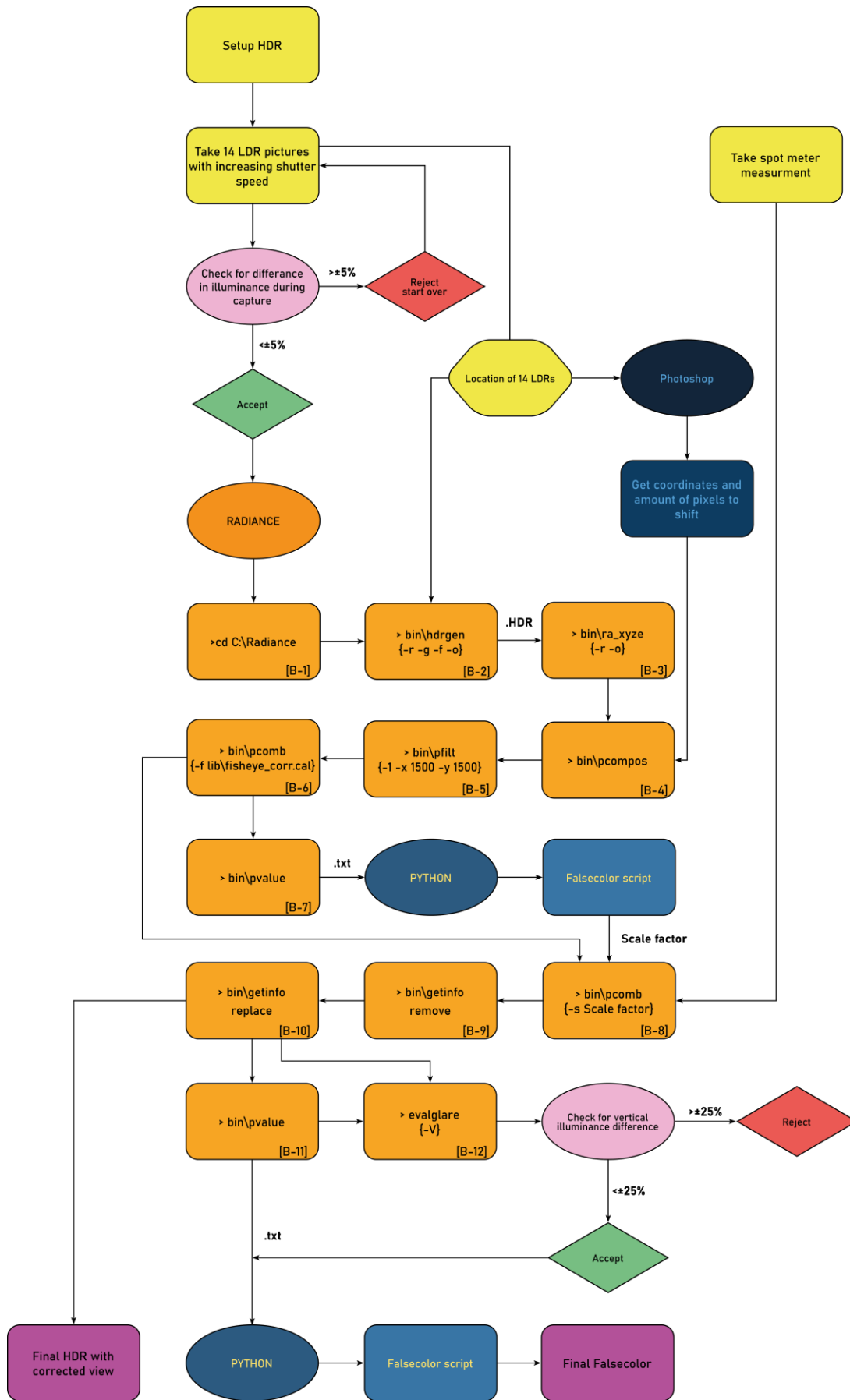


Figure 4-2: HDR (post) process flow, with used argument in brackets and a reference to Appendix B.

#### 4.1.3 Resulting HDR images

For room 228 the processing of the measurements resulted in a false colour luminance map. Clearly visible is that the daylight that is seen between the *schoepen* is not uniformly distributed, but the lighting on the walls and the floor appears to have an even gradient.

The current state of room 228 is not ideal compared to the 'exposition state', the floors were taken out and the glue that once was used to keep it there is still present. On the left side of the room, a cut in the floor was made, this is covered with underlayment. In several parts of the wall, some holes were made to help with the removal of the asbestos. The wooden trimming on the lower parts of the wall is also removed, revealing a rough brick surface. Also, a corridor is cut in the back wall, to limit the damage to the monumental pathways. In the back left a door is opened to help with the climate control system, this allows additional light to spill into the room.



Figure 4-3: Room 228 - 26-09-2023 - up - 12:17

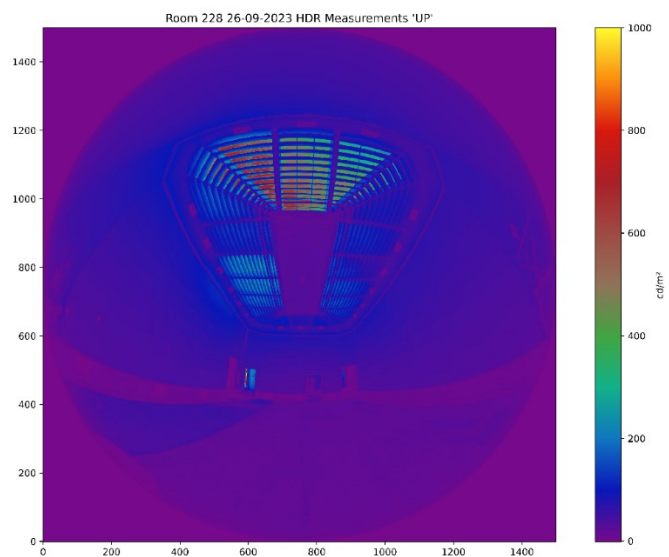


Figure 4-4: Room 228 - 26-09-2023 - up - luminance map

## 4.2 Validation of daylight model

### 4.2.1 Diffuse reflectance

Within each room several different materials are present. Therefore, for each of these materials, multiple measurements on site were taken and averaged. Full measurements can be found in the Appendix D. Within room 228 three different materials are identified: Wall, Floor and Wood Underlayment. In room 234 three different materials are labelled: Wall, Floor and Wood trim. Figure 4-5.

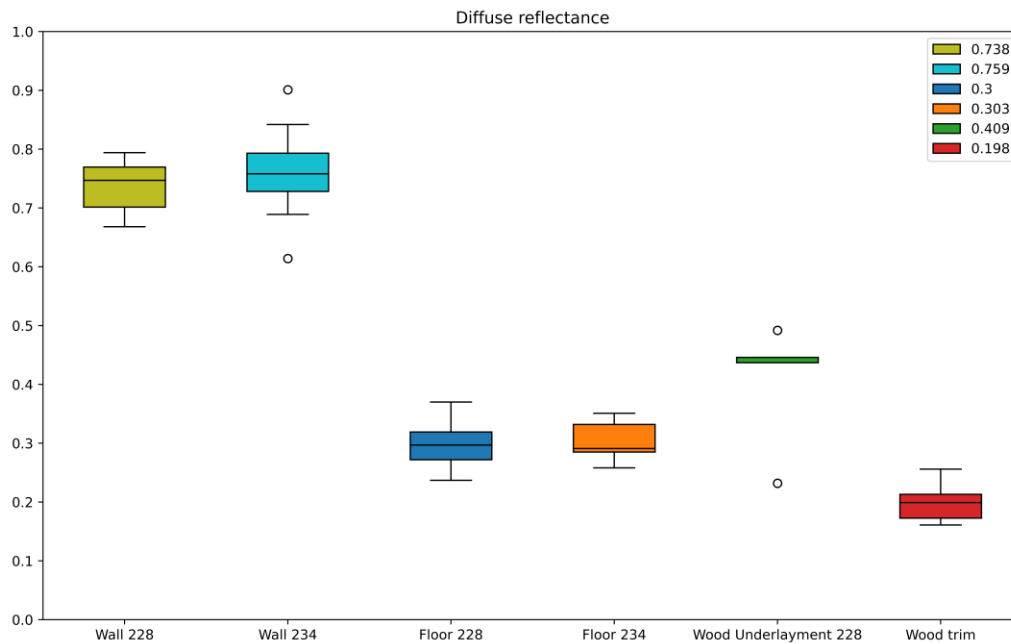


Figure 4-5: Diffuse reflectance room 228 and 234

Surface	Floor	Wall	Wood	<i>Schoepen</i> <sup>8</sup>	Roof structure
Diffuse reflection coefficient	0.4	0.759	0.198	0.75	0.7

Table 4-2: Diffuse reflection coefficients

Surface	Wired glass	Lexan™ roof	<i>Legraam</i> <sup>8</sup>
Transmission	0.85	0.72	0.42

Table 4-3: Transmission coefficients

The manufacturer of the Lexan™ legramen claims that the transmission for this thickness is 0.44. However, due to the age of the panels, their appearance has changed and they have turned yellow. Moreover, there is a lot of dirt and debris as visible in the pictures in Appendix A. Therefore the initially used transmission in the model is assumed lower. At some point in time all legramen were replaced by the currently installed legramen, all with similar transmission coefficients. The original design by Van der Steur as shown in Figure 2-1 is no longer used.

<sup>8</sup> Initial estimated values used at start

#### 4.2.2 HDR comparison

To make a comparison between the results that were acquired from the on-site HDR measurements and the calculations a translation is needed. The version of Honeybee used is only able to accept a named input for the type of view to make the image. This results in a Field of View that is 180°, the HDR set up uses a lens with a Field of View of 186°. Furthermore, the precise location of the measurements is used in the simulation. By the nature of the wide fisheye lens, the surfaces are distorted like a pincushion. Due to this geometrical distortion the absolute location of a point in the HDR measurement cannot directly be translated to the simulated version.

The 3D space is flattened to a 2D image and in the HDR procedure reduced to a size of 1500x1500 pixels. For each wall visible in the photographs a name is set as: "Left, Middle and Right". For both versions, on each wall, 4 corner coordinates of an 'exhibition area' are defined. These coordinates are expressed in both x and y and follow a counterclockwise rotation, from corner 1 (left bottom) to corner 4 (left top). For the side walls the distortion must be processed. This means that the domains need to have a changing y value in relation to x. The shapes are divided into multiple different subdomains (8 blocks in x direction, 6 blocks in y direction). This results in a grid of 48 blocks on every wall as depicted in Figure 4-9 and Figure 4-10.

The raw data from either the HDR measurements or the simulated *Radiance* results are exported as a .HDR file and contain all the necessary information. Inside the header of the *Radiance* file, an additional exposure is given. This value is needed to correctly convert the image during the *pvalue* (Appendix B) conversion from .HDR to .txt. These .txt files are loaded into *Python*. There the separate RGB values are converted into their respective illuminance values by using Equation B-1. A matrix grid is formed of 1500x1500 pixels, and all the luminance values are stored in that matrix. For each grid block in the 'exhibition areas' the average value is determined. This is done using a nested for-loop that stores this data in an 8 by 6 matrix. The flow of this process is illustrated in Figure 4-6.

The resulting images are exported as false colour and can be seen in Figure 4-7 and Figure 4-8. To show the chosen exhibition areas better, additional colour was added to differentiate them more easily from the background. They form an array of squares as seen in Figure 4-9 and Figure 4-10. Here it is visible that the domains created are not continuous in the y-axis.

In Figure 4-11 and Figure 4-12 the false colours for the exhibition areas are superimposed on top of the 3D views of the room, both for the HDR and for the simulation.

For the calculation of the image simulation, these settings were used in *Radiance*:

Rpict	-vth	-ps	-pt	-pj	-dj	-ds	-dt	-dc	-dr	-dp	-st	-ab	-ad	-as	-ar	-aa	-lr	-lw
		2	0.05	0.9	1.0	0.05	0.15	0.75	3	512	0.15	8	4096	4096	128	0.1	8	0.005

Table 4-4: *Radiance* settings image simulation

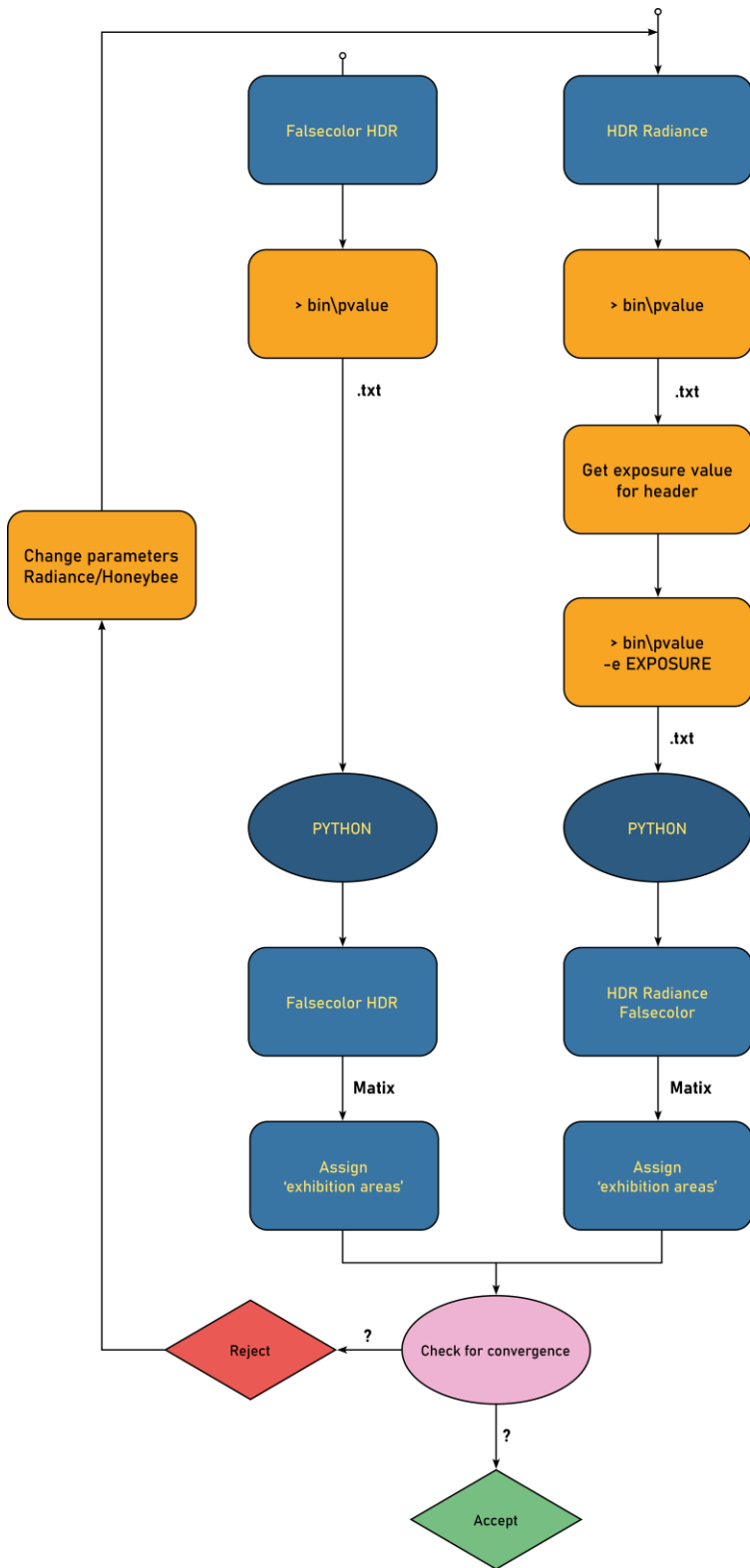


Figure 4-6: Flow of validation process

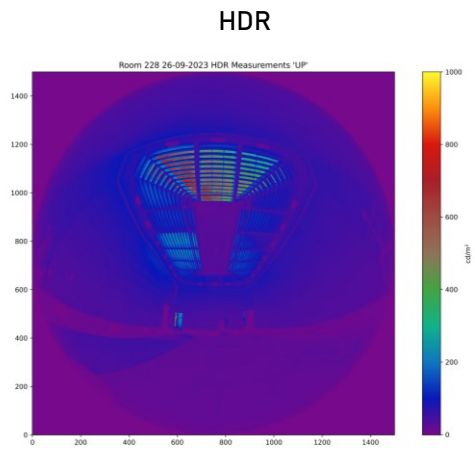


Figure 4-7: HDR results with average values at 'exhibition areas'

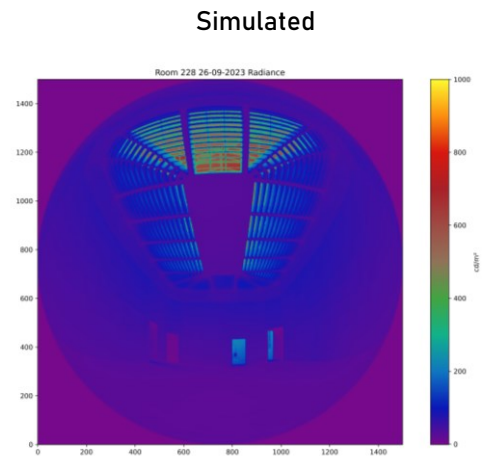


Figure 4-8: Simulated results with average values at 'exhibition areas'

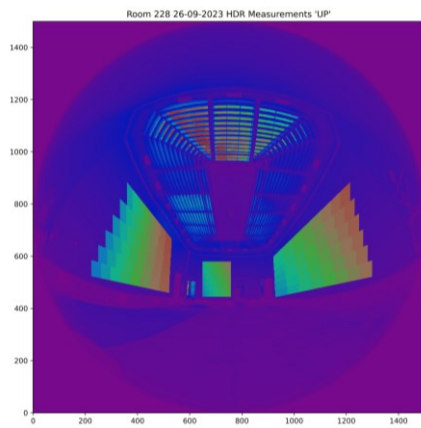


Figure 4-9: 'Exhibition areas' used in HDR

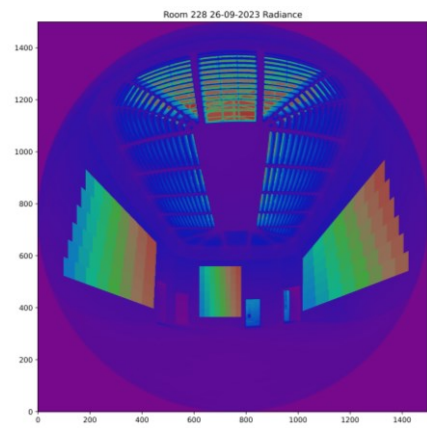


Figure 4-10: 'Exhibition areas' used in simulation



Figure 4-11: Original HDR with false colour for 'exhibition areas'

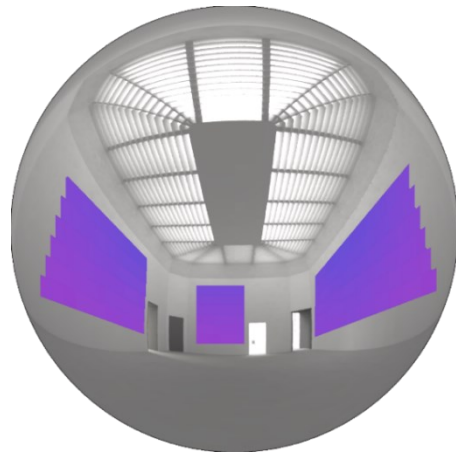


Figure 4-12: Radiance with false colour for 'exhibition areas'

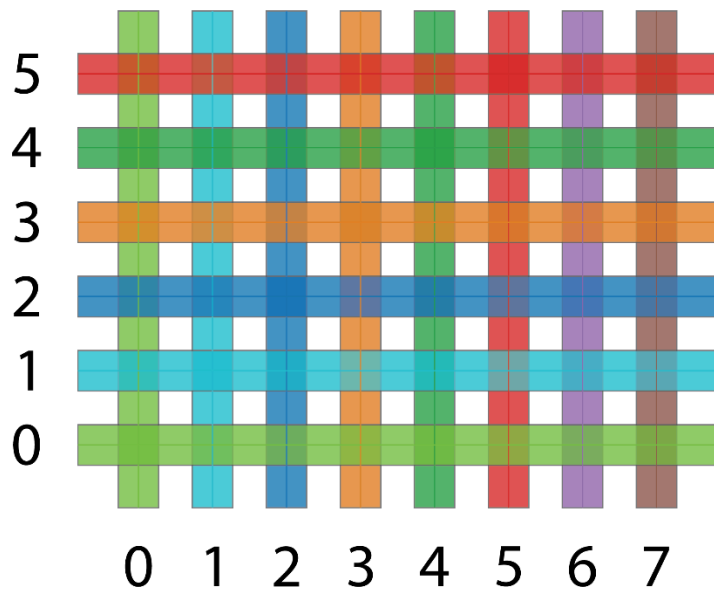


Figure 4-13: Definition of matrix grid used for comparison HDR and Radiance, with coordinate (0,0) for bottom left corner

The results of both the HDR and simulated with Radiance are compared, both in the horizontal and vertical direction. For each of the three blocks (Left, Middle and Right) there are 48 averages stored and these are represented in graphs in absolute values and in a boxplot to illustrate their spread compared to the HDR results. Each line follows the same colour and numbering as illustrated in Figure 4-13, where (0,0) is the bottom left corner.

## Vertical

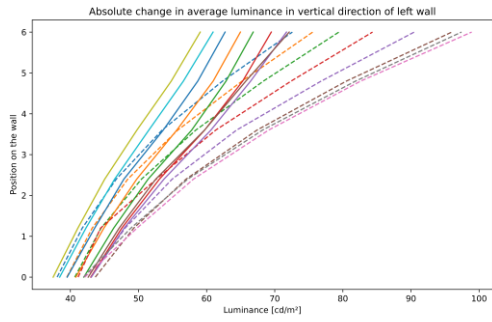


Figure 4-14: Absolute change in average simulated luminance (solid line) of left wall compared to the HDR measurements (dashed line), in the vertical direction

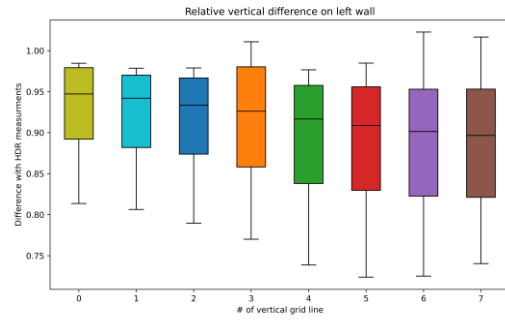


Figure 4-15: Relative change in average simulated luminance of the left wall compared to the HDR measurements, in the vertical direction

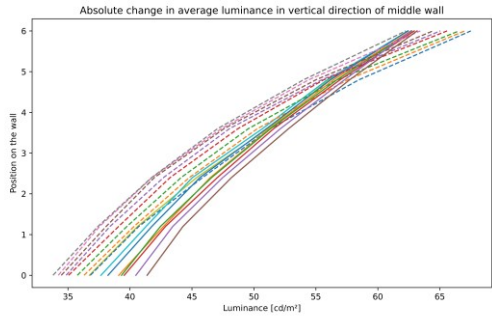


Figure 4-16: Absolute change in average simulated luminance (solid line) of middle wall compared to the HDR measurements (dashed line), in the vertical direction

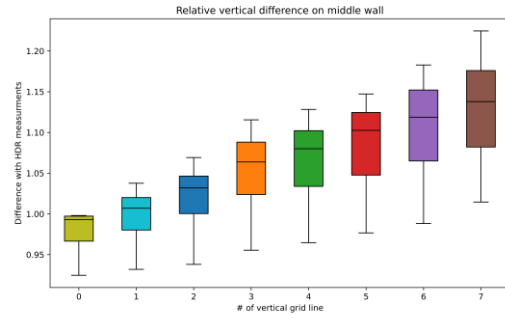


Figure 4-17: Relative change in average simulated luminance of middle wall compared to the HDR measurements, in the vertical direction

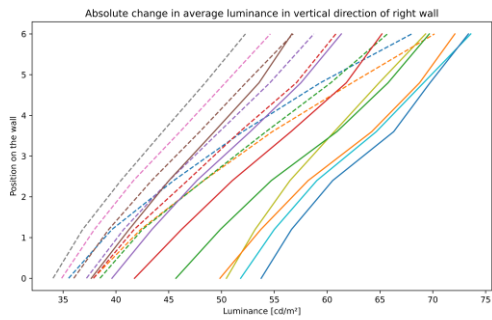


Figure 4-18: Absolute change in average simulated luminance (solid line) of right wall compared to the HDR measurements (dashed line), in the vertical direction

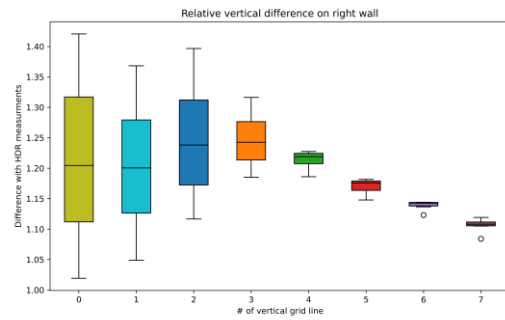


Figure 4-19: Relative change in average simulated luminance of right wall compared to the HDR measurements, in the vertical direction

## Horizontal

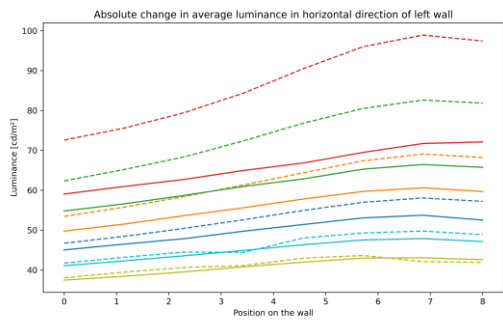


Figure 4-20: Absolute change in average simulated luminance (solid line) of left wall compared to the HDR measurements (dashed line), in the horizontal direction

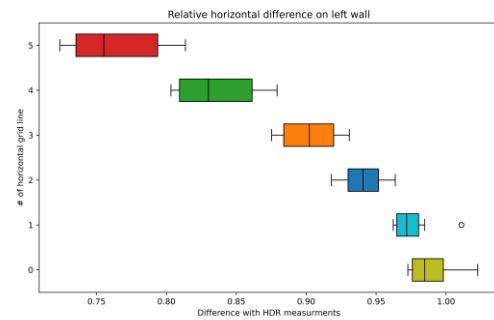


Figure 4-21: Relative change in average simulated luminance of the left wall compared to the HDR measurements, in the horizontal direction

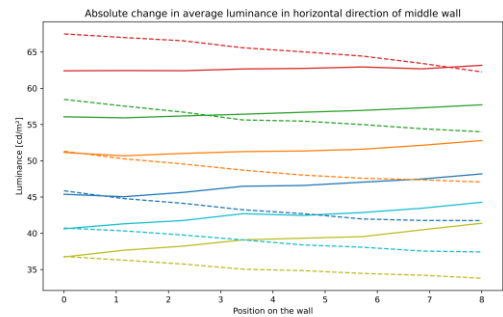


Figure 4-22: Absolute change in average simulated luminance (solid line) of middle wall compared to the HDR measurements (dashed line), in the horizontal direction

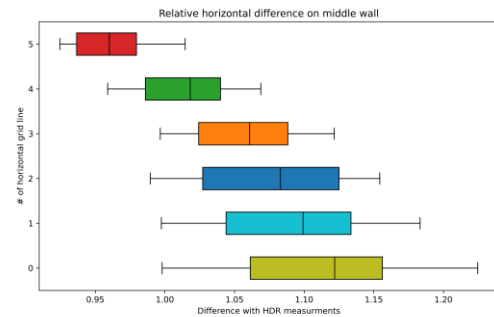


Figure 4-23: Relative change in average simulated luminance of the middle wall compared to the HDR measurements, in the horizontal direction

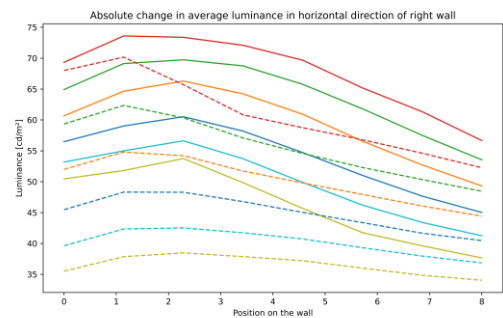


Figure 4-24: Absolute change in average simulated luminance (solid line) of right wall compared to the HDR measurements (dashed line), in the horizontal direction

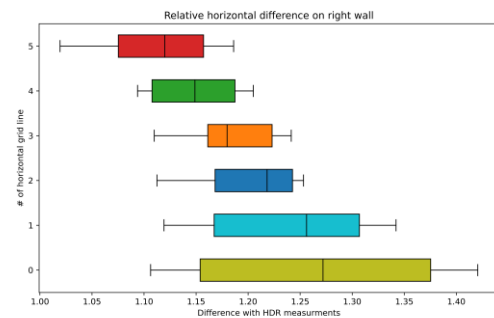


Figure 4-25: Relative change in average simulated luminance of the right wall compared to the HDR measurements, in the horizontal direction

Further relative graphs are given in Appendix E.

### 4.2.3 Results of validation

As the results of the measurements and the simulated *Radiance* results are converted into a grid, the average values for each coordinate can be compared. The left wall predominantly receives a large portion of 'direct' light through the *legramen*, as the sun on 26 September 12:00 is roughly in line with the angle of the *schoepen*. Therefore, the major factor in the distribution is related to the transmission values of the windows.

On the middle and right wall, no 'direct' light is received, but rather reflected light that has cascaded through the *schoepen*. The diffuse reflection coefficient of the *schoepen*, combined with the transmission values of the windows above contribute to the results.

The boxplots show that the relative vertical difference (Figure 4-15) of the left wall has a slight underprediction compared to the measured results, which is larger at the right end of the grid (7). The relative horizontal difference of the gridlines (Figure 4-21) shows that there is a larger underprediction in the higher lines (5), but a better match towards the lower horizontal grid lines (0). The middle wall is slightly over predicting in both directions (Figure 4-17 & Figure 4-23). The absolute horizontal (Figure 4-22) behaviour suggests that due to the open door in the back left corner during the HDR capture the direction of the decay is reversed due to light spillage.

This over-predicting trend is also visible on the right wall (Figure 4-19 & Figure 4-25). However the absolute lines (Figure 4-24) indicate a similar behaviour between the simulated results and the measured.

To estimate the measure of under- or overprediction a scatterplot of all the results is given in Figure 4-26. This shows a strong positive association between the HDR and the simulated results. For the left wall, the deviation is -3%, for the middle wall +6%, and the right wall +13%.

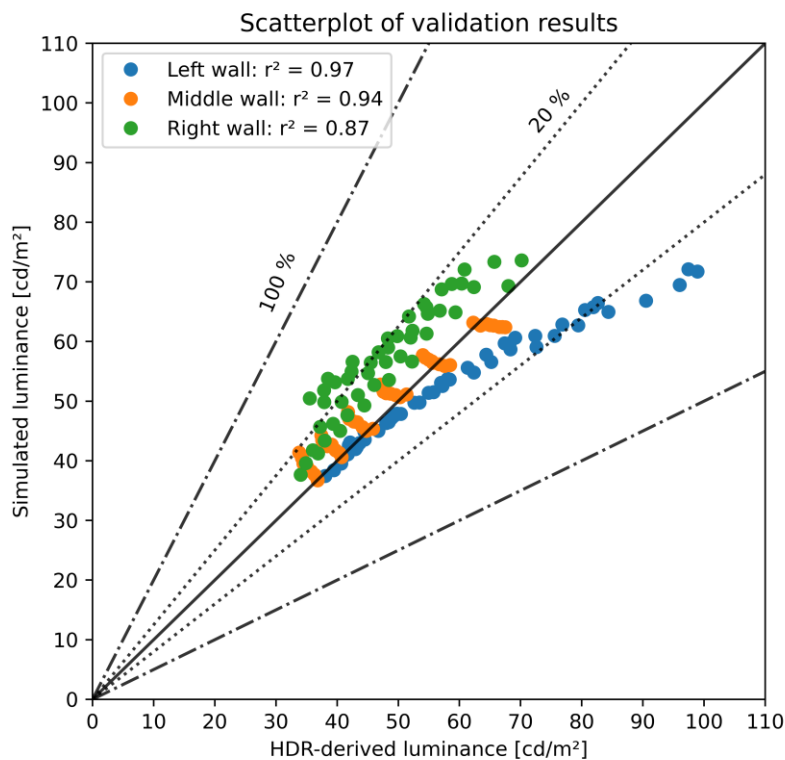


Figure 4-26: Scatterplot of relation between HDR and simulated luminance. Error intervals and coefficients of determination are also given

With the data from HDR and simulation, the model was checked for differences with the HDR measurements. An iterative process led to the values for the diffuse reflectance for the *schoepen* of 0.8 and the diffuse reflectance of the floor of 0.4. For the *legramen*, the factory specified 0.44 was used. With these variables, the best possible fit was obtained.

This results in a validated 3D model of the museum room that can now be used for other weather conditions and to assess what sun shading is needed. From the original drawings made by Van der Steur, he illustrated the possibility of a large number of bounces on the *schoepen*. This depends on the angle of the incident of the first incoming light ray. As seen in Figure 4-27 (3) the number of bounces in this layer could accumulate to 6. However, higher-order reflections will have less energy left (20% loss for diffuse reflectance of 0.8) (Yu, 2023). But as the diffuse reflection of the *schoepen* is high, this could still contribute to the overall illuminance in the room below. To accommodate for the high number of bounces on the *schoepen* the *Radiance* parameter Ambient Bounces (-ab) is set to 10, to still allow for bounces on the wall and floor below.

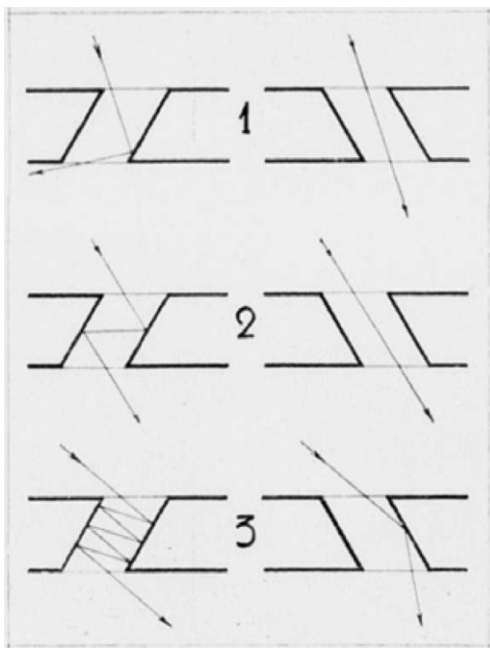


Figure 4-27: Original drawing of Van der Steur, depicting the bounces on the *schoepen* (Hannema & van der Steur, 1933)

#### 4.2.4 Sensitivity analysis

Using the Morris method a sensitivity analysis was done to determine which parameter has the most influence on the system. For each simulation, a similar approach of the later calculated sun shading is followed, as described in paragraph 3.5. All the resulting illumination values are stored per simulation run, these are plotted in Figure 4-29.

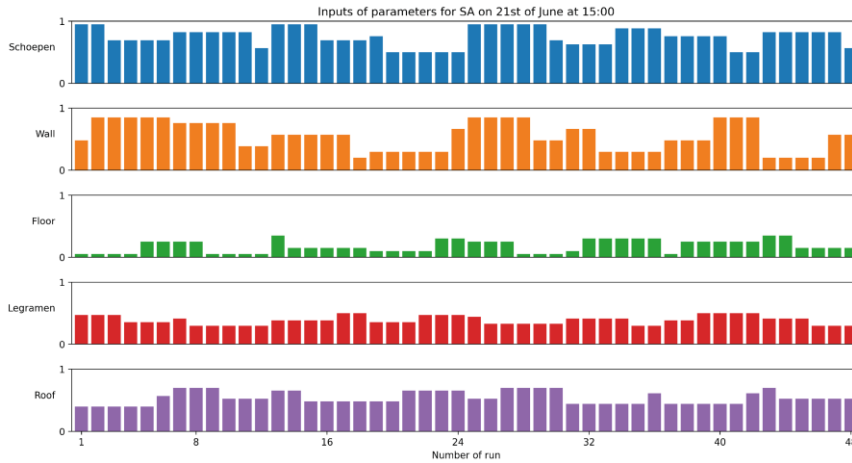


Figure 4-28: Input settings used for parameters for all 48 runs

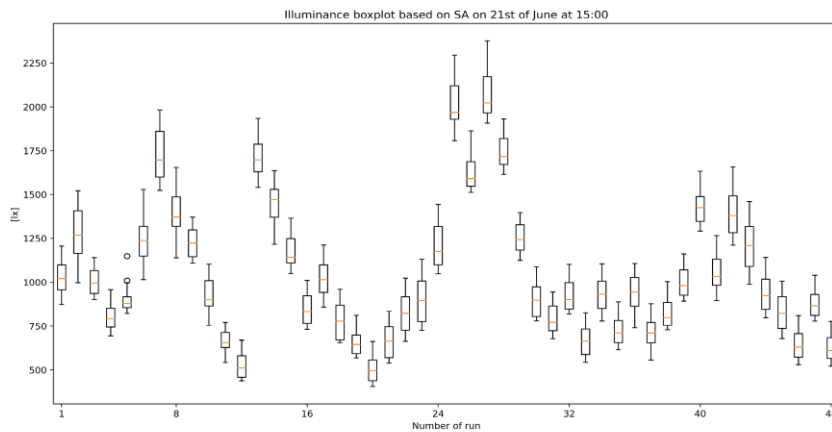


Figure 4-29: Boxplot for all 48 runs of SA

Per simulation run all values are compiled and assessed based on maximum illuminance, mean and minimum. Each resulting in a Morris ranking plot (Figure 4-30, Figure 4-32, Figure 4-34 resp.) and the Morris relation between the investigated parameters (Figure 4-31, Figure 4-33, Figure 4-35 resp.). For all types the floor is almost-monotonic and the wall is the most dominant monotonic factor. For the minimum illumination the importance of the *schoepen* increases.

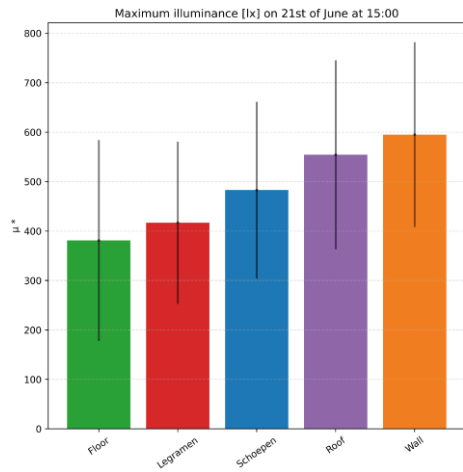


Figure 4-30: Morris plot of ranking based on the maximum predicted illuminance

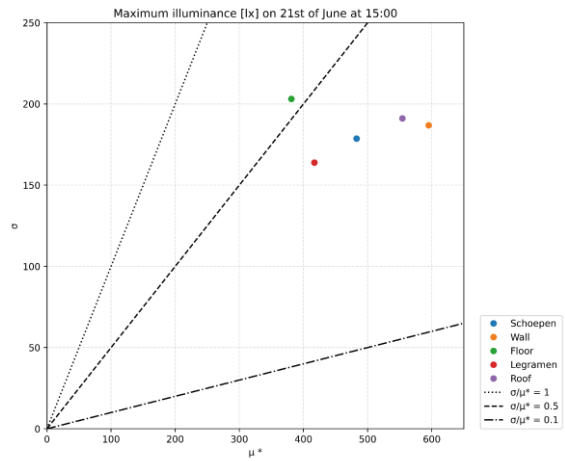


Figure 4-31: Morris relation with results of the parameters investigated based on maximum illuminance

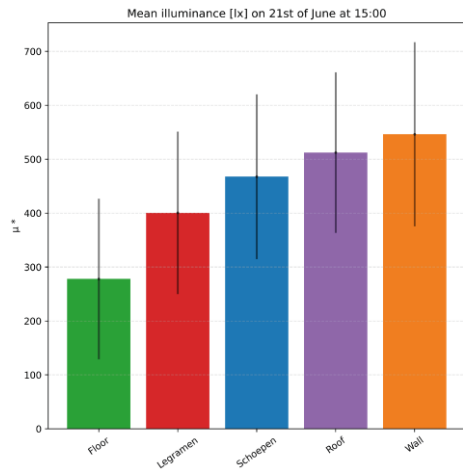


Figure 4-32: Morris plot of ranking based on the mean predicted illuminance

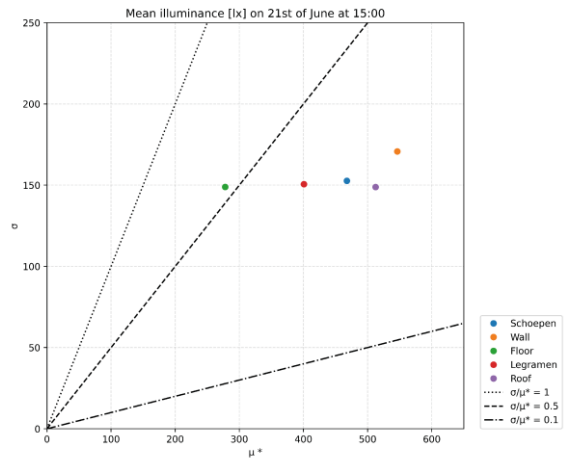


Figure 4-33: Morris relation with results of the parameters investigated based on mean illuminance

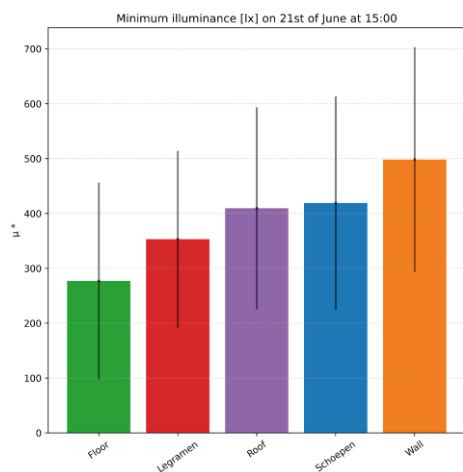


Figure 4-34: Morris plot of ranking based on the minimum predicted illuminance

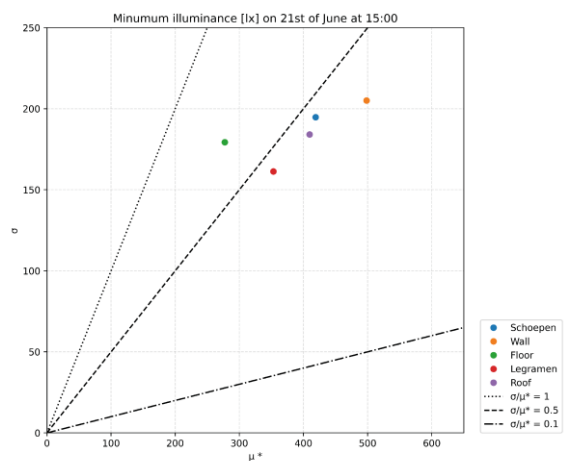


Figure 4-35: Morris relation with results of the parameters investigated based on minimum illuminance

The objective of this research is to limit the exposure of the art, therefore the maximum illuminance is investigated further. Between the simulation runs the resulting maximum illuminance fluctuates. The validated model resulted in a maximum illuminance of 1506.51 lx on the 21<sup>st</sup> of June at 15:00 as depicted by the red line in Figure 4-36. For the results between the chosen upper limit of 1650 lx and the lower limit of 1000 lx, the input parameters are plotted in Figure 4-37 to assess the usable range for each of the inputs. The range is skewed to the lower end as room 228 would need to have shading all year round as will be shown in paragraph 4.4.

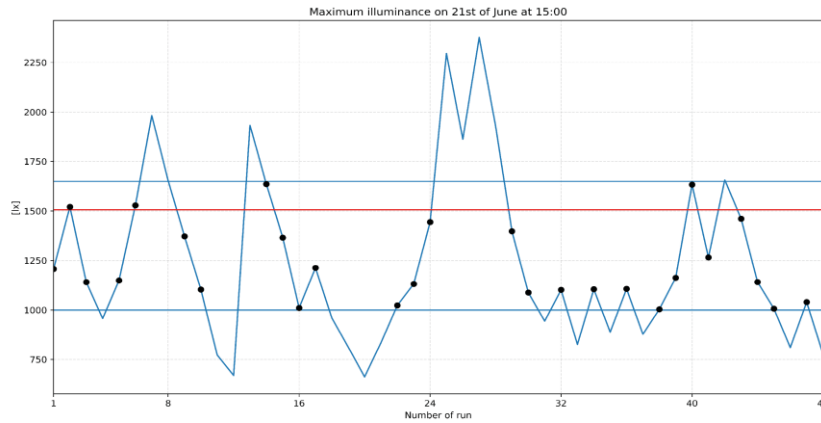


Figure 4-36: Maximum illuminance with in red comparative baseline to validated model and selecting all sets between 1000-1650 lx

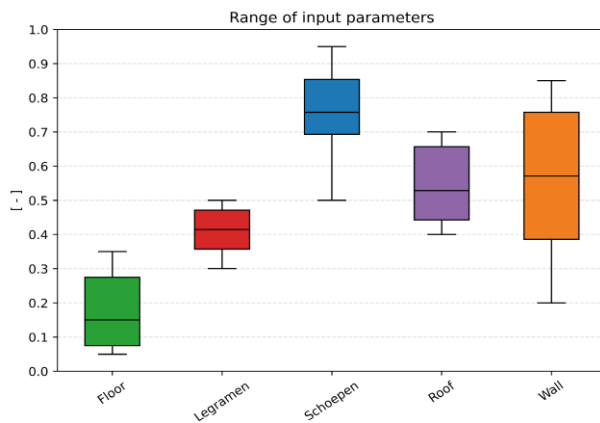


Figure 4-37: Range of input parameters based on set domain

	First Quartile	Median	Third Quartile	Used in model
Schoepen	0.69	0.76	0.85	0.8
Wall	0.39	0.57	0.76	0.759
Floor	0.08	0.15	0.28	0.4
Legramen	0.36	0.41	0.47	0.44
Roof windows	0.44	0.53	0.66	0.621

Table 4-5: Range of input parameters based on sensitivity analysis

### 4.3 Adaptations of the model

During the validation step, the rooms had to be modelled to the state they were in during the restoration of the museum. To be able to change the temporary building state to the exposition state, the temporary corridors are made using a *Mesh Difference* operation in *Grasshopper*. This adaptation can be switched on or off as needed. For the following calculations, these changes are switched off.

#### 4.3.1 Validated model compared with literature by Van der Steur

As mentioned in 2.1.1, Van der Steur made a manual calculation of the light levels in the museum with his proposed system with *schoepen* and *legramen*, see Figure 4-38. The validated 3D model is now able to produce a similar image. Figure 4-39. Overall, both figures give an evenly spread light level. Observed is that the light can be redirected to the corners of the room. And considering the size of the room the change in vertical gradient along the wall is influenced in line with the original intent of Van der Steur. The distance between the blades in Figure 4-38 decreases more than the design that would later be implemented in the museum. The contour lines by Van der Steur are derived from the angle of the incident (sine) for every point on the wall that has a direct light path with the *legramen*, and is reduced with the inverse square of the distance between the point on the wall and the *legraam*. A process that is very labour-intensive to do by hand and fails to include reflections inside the room.

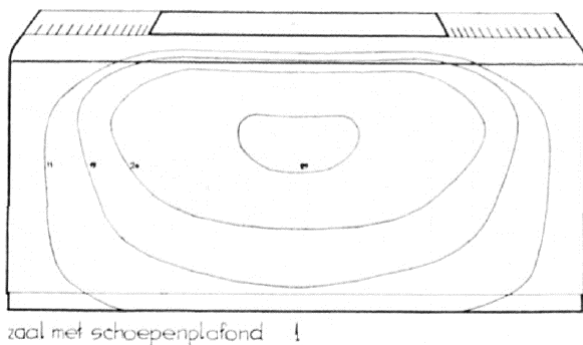


Figure 4-38: Original contour lines calculated by Van der Steur (Hannema & van der Steur, 1933)

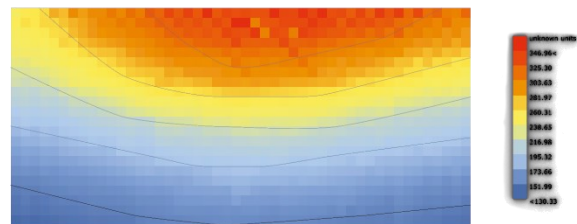


Figure 4-39: Results of grid-based simulation on west wall of room 228 on 26 September at 12:00

### 4.3.2 Sun shading

Slightly above the *legramen* the sun shading device is placed and this influences only one single hall at a time. This allows for a different lighting regime per hall.

For the sun shading a simplification is made, as actual screens are made of fabrics, which have many different properties and materials.

One of the properties of fabric is the material and the openness of the weave of the individual strands of fibre. An extensive testing regime to correctly compare different claims of manufacturers' performance, is stated in NEN 14500:2021<sup>9</sup>. And in NEN 14501:2021<sup>10</sup> the classification of these fabrics is made. Here they speak of a  $g_{tot}$ , related to the total light transmission of the system (a specific type of glass and screen, on the inside or the outside). This is the result of multiple measurements as described in NEN 14500:2021<sup>7</sup>.

As these properties don't translate themselves into the definition of material classification as used in Radiance, a simulation is needed to make the calculations. The 'sun shading' layer is altered in a glass material, with a specific light transmittance. In NEN 145001:2021 they compare each specific fabric with 4 different types of glass windows, of different build-up and also g-value. As the *legramen* are very thin, 4mm in thickness, glass type A is chosen as that is classed as a single glass of 4mm. The glass has a g-value of 0,85, and the fabrics made by Swela<sup>11</sup> in that category have a  $g_{tot}$  range between 0,17 and 0,27. From here the reduction factor of the screen is calculated by dividing the  $g_{tot}$  by the g-value of the glass. Resulting in a transmission in the range of 0,20 and 0,32, for the Swela-309 range of screens. As this is a very large reduction factor, also the other end of the spectrum is investigated. Phifer<sup>12</sup> has a broader range of screens available, with a larger openness factor. Therefore a simulation for 0.50 and 0.70 (expected upper range based on practical factors) is added.

The performance is simulated on the 21<sup>st</sup> of June and 21<sup>st</sup> of December for all 4 'glass' shading. Resulting in a reduction of exposure of the sensors in the room as further illustrated in Figure 4-40.

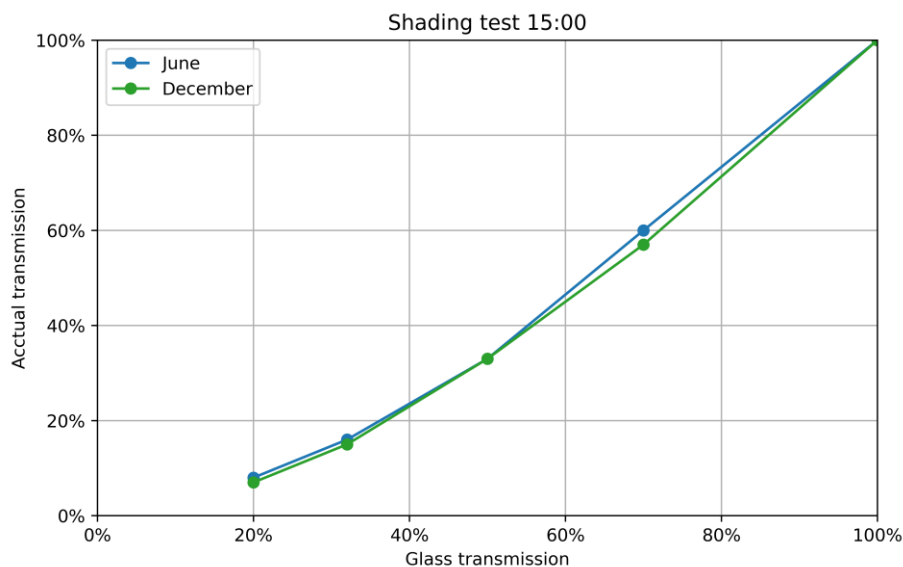


Figure 4-40: Test of 'glass' sun shading compared to fabric screen

<sup>9</sup> Test and calculation methods (NEN-EN 14500, 2021)

<sup>10</sup> Performance characteristics and classification (NEN-EN 14501, 2021)

<sup>11</sup> (Swela, 2024)

<sup>12</sup> (Phifer 2000, 2024)

For the calculation of the sun shading these settings were used in Radiance:

Rtrace	-	-	-dp	-ds	-dt	-dc	-dr	-st	-lr	-lw	-ab	-ad	-as	-ar	-aa	-af
	l	h	512	0.05	0.15	0.75	3	0.15	8	0.005	10	4096	4096	300	0.1	

Table 4-6: *Radiance* setting used for hourly grid calculation

For the calculation of the sun shading the grids used to calculate the illuminance in room 228 were changed. For this case, all 4 walls are considered and sensor points were placed in a strip, in the middle of the designated 'exhibition area' which starts at 1.6 m above the floor and has a height of 0.4 m, see Figure 3-11. These sensor points are effective in the middle of that band, at 1.8 m above the floor. These sensors are placed along the wall, this is done to get illuminance values for the whole of each strip.

As a result of this approach, one of these points will receive the largest amount of sunlight and therefore this will be the point to consider as the most harmful to the displayed artworks. The location of this point changes throughout the day and depends on the position of the sun. However, the precise location is not deemed necessary as the maximum point may not exceed the set threshold.

#### 4.4 Behaviour of system with sun shading

##### 4.4.1 Real sensor point correlation

As the system is intended to be implemented in the real world, only simulation values will not be enough. To operate the sun shading screens at the museum a sensor near the building needs to be placed. For this application a pyranometer is typically used, see Figure 4-41. This sensor consists of a dome that can detect incoming solar radiation from 180° with the horizon and 360° around. This measurement can then be used to control the system. To validate the effectiveness of the system illuminance meters will be needed inside of the exposition halls (these may also include UV radiation).

To simulate this sensor in this research, a virtual sensor point at the top of the roof is used, this has a relatively unobstructed view to the sides and no obstruction vertically. In *Radiance* a single sensor point is used with a vector pointing towards the sky. The data obtained from this is used as input for the *Phyton* script to govern the different shading states.

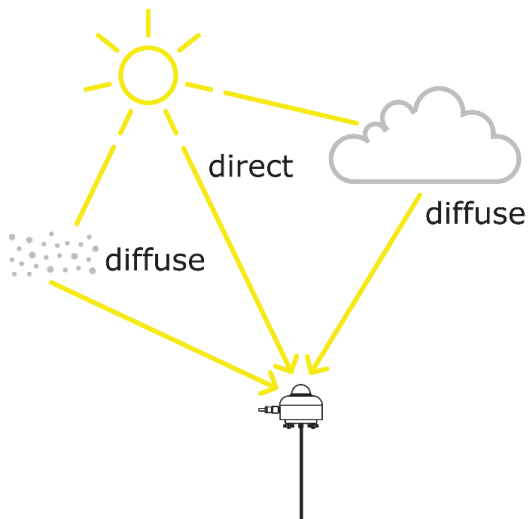


Figure 4-41: Pyranometer (Hukseflux)

A separate hourly simulation was carried out for the summer solstice, the winter solstice and the equinox (21<sup>st</sup> of June (Figure 4-42), the 21<sup>st</sup> of December (Figure 4-44) and the 21<sup>st</sup> of September (Figure 4-43)). This was done automatically with the use of Colibri to calculate the different hours consecutively.

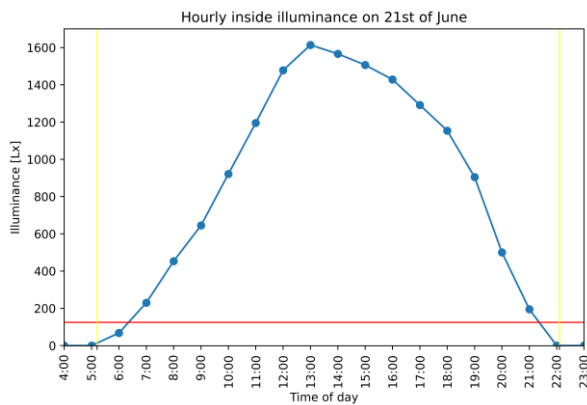


Figure 4-42: Hourly illuminance inside of room 228, as maximum observed value for the 21st of June

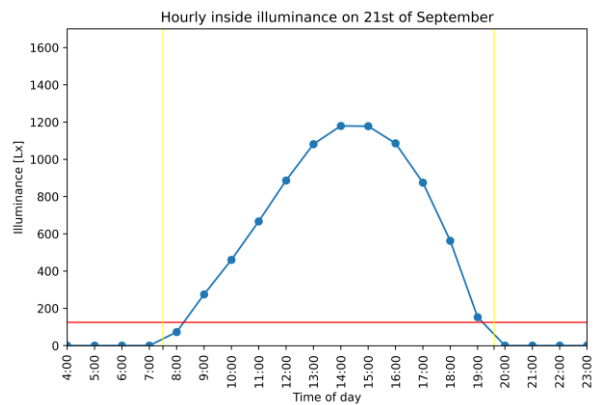


Figure 4-43: Hourly illuminance inside of room 228, as maximum observed value for the 21st of September

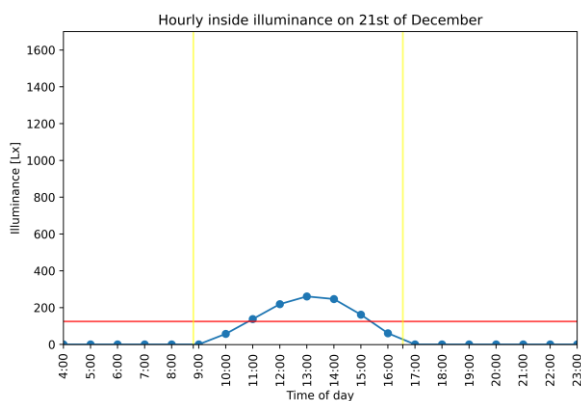


Figure 4-44: Hourly illuminance inside of room 228, as maximum observed value for the 21st of December

Using this information and the data obtained by the simulated 'pyranometer' on the roof the percentage of daylight inside (daylight factor) is calculated for these days.

For the calculation of the annual sensor, these settings were used in Radiance:

DAYSIM	-dt	-dr	-ad	-dp	-pt	-sj	-lw	-ab	-aa	-ps	-ds	-dj	-pj	-ar	-av	-dc	-st	-as	-lw
	0.15	3	4096	512	0.05	1	0.005	6	0.1	2	0.05	0.7	0.9	128	0	0.75	0.15	4096	8

Table 4-7: Radiance settings used DAYSIM

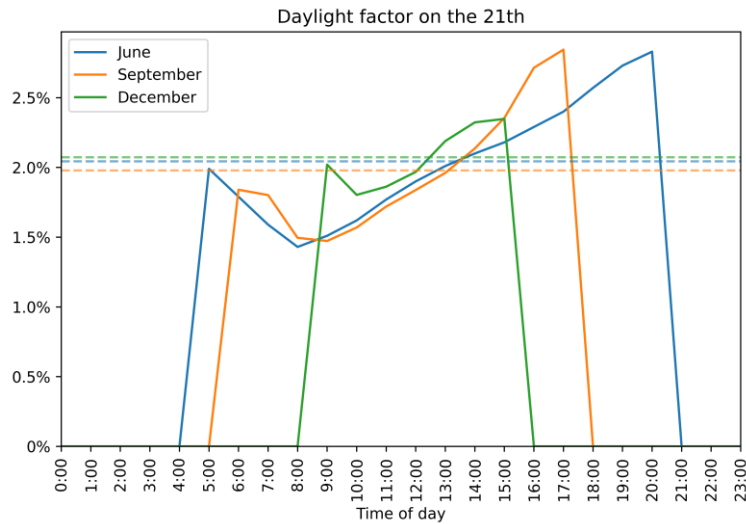


Figure 4-45: Daylight factor per hour on the 21st of June, September and December

As the sun rises in the east, the top part of the roof structure is illuminated first. Via the roof, the interior is indirectly lit. This results in the fact that the percentage of daylight that can penetrate the building at the beginning of the day is higher than would be expected, as seen in Figure 4-45. The same is seen at the end of the day. The average values for these three dates are all 2%, with minimal variation in season.

Based on these results an average daylight factor of 2% is used for further calculations for the entire year. With this assumption, the effects of the different sun shading states can be calculated. The three screens used have a transmission value of: 0.63, 0.55 and 0.44 as seen in Table 4-8. Here also a comparison is made for market available solutions for the type and performance of the screens required. Based on the illumination target set by the museum (250 lx) and the 2:1 contrast ratio (art-wall) the threshold for the sun shading system is set at 125 lx, as outlined in paragraph 2.4 and 2.5. The system will always yield an illuminance level inside that is below the 125 lx, as seen in Figure 4-51. To be able to minimise unnecessary exposure of the artwork a blackout screen will be added (not included in this calculation).

The exposure is only investigated during the opening hours of the museum. In Figure 4-47 the utilization of the system is illustrated, with the -1 values as 'night mode' and 0 as no screens required. Typically during the day the illuminance levels increase, leading to a higher state of screens. This effect will also cause the system to change to a lower state towards the end of the day. In the summer months the illuminance before opening time is already above the threshold value and it will trigger state 1 automatically.

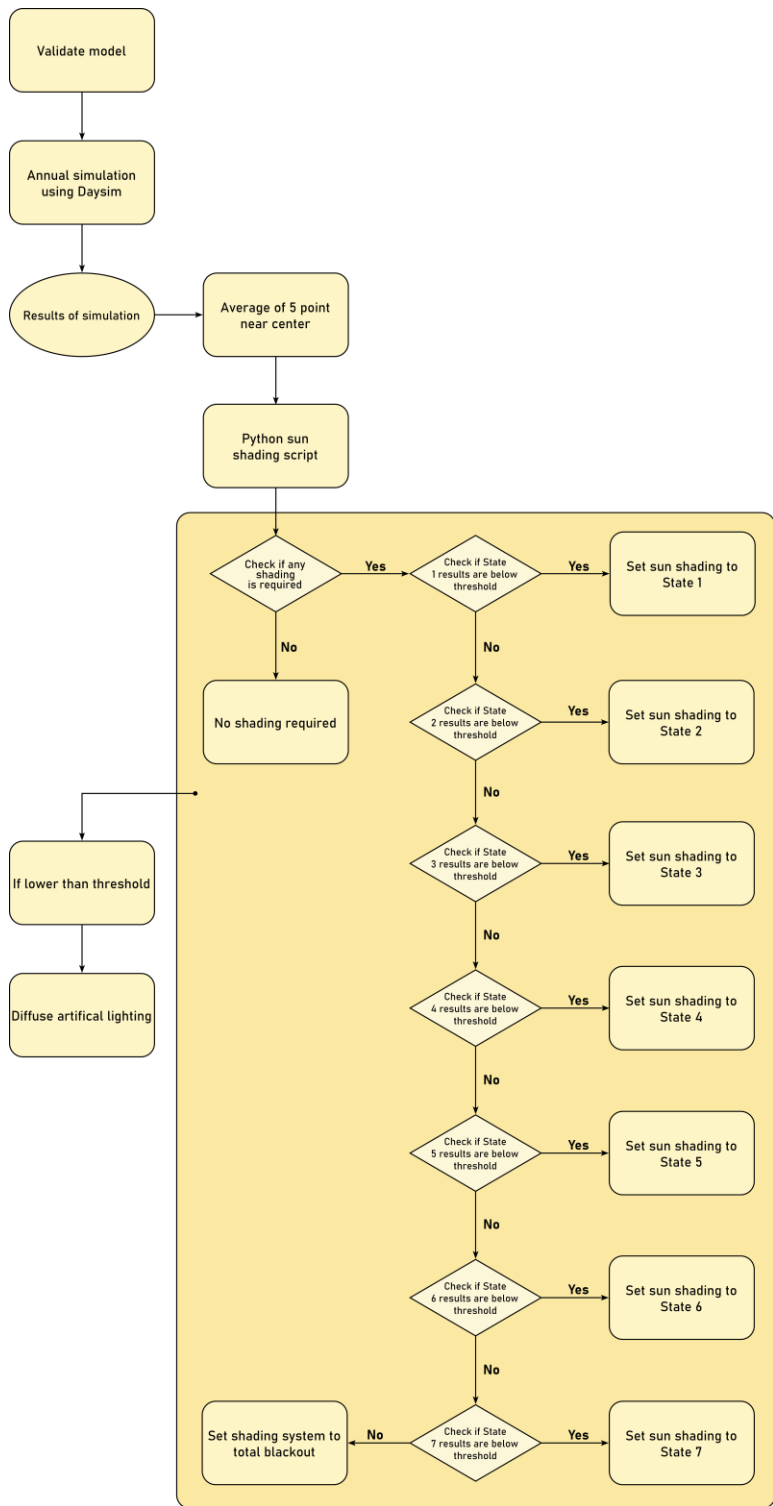


Figure 4-46: Python script flow for calculation sun shading

State	1	2	3	4	5	6	7
Screens used	1	2	3	1+2	1+3	2+3	1+2+3
Glass transmission	0.5	0.4	0.28	0.2	0.14	0.112	0.056
Screen	0.63	0.55	0.44	(0.35)	(0.28)	(0.24)	(0.15)
TABLE value glass type A <sup>13</sup>	0.535	0.468	0.374	-	-	-	-
Example	PHIFER SheerWeave® 4000 U64 Eco / Ash <sup>14</sup>	PHIFER SheerWeave® 4500 V07 Pewter <sup>15</sup>	PHIFER SheerWeave® 2000 P05 White / Platinum <sup>16</sup>	-	-	-	-

Table 4-8: Shading state comparison with actual market available options

#### 4.4.2 Annual behaviour of system based on CBDM

Based on the reduced annual exposure of the system without any implementation of sun shading a calculation is made to assess the expected performance of different types of configurations. The museum opens at 11:00 and closes at 17:00 and is also closed on Mondays. When the museum is closed, a 'night mode' will be activated, limiting the light that spills in the room, this is done using the blackout screens. During opening hours the illumination is checked inside and if it exceeds the threshold a screen is used as illustrated in Figure 4-47.

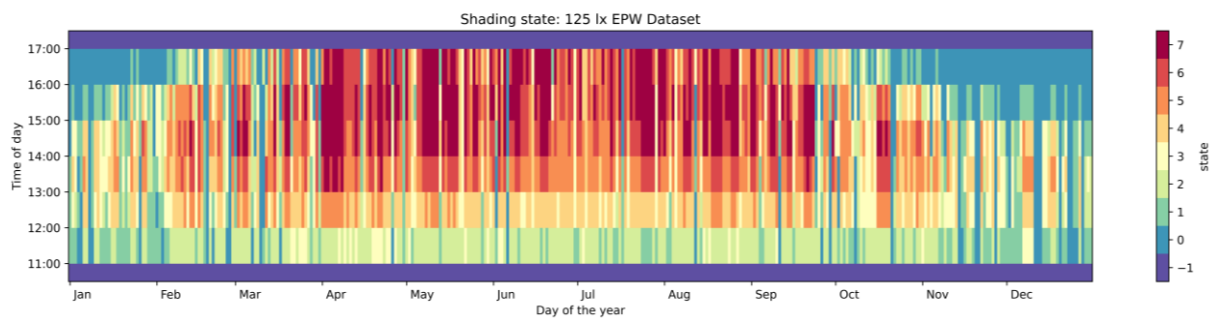


Figure 4-47: Shading states room 228 throughout the year

<sup>13</sup> Complaint with (NEN-EN 14501 , 2021)

<sup>14</sup> (Phifer 4000, 2024)

<sup>15</sup> (Phifer 4500, 2024)

<sup>16</sup> (Phifer 2000, 2024)

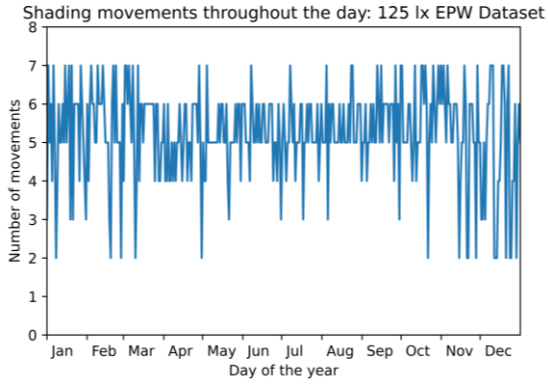


Figure 4-48: Shading system movements per day

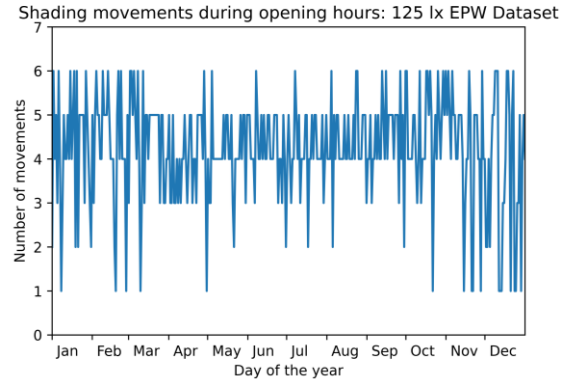


Figure 4-49: Shading system movement during opening hours of museum

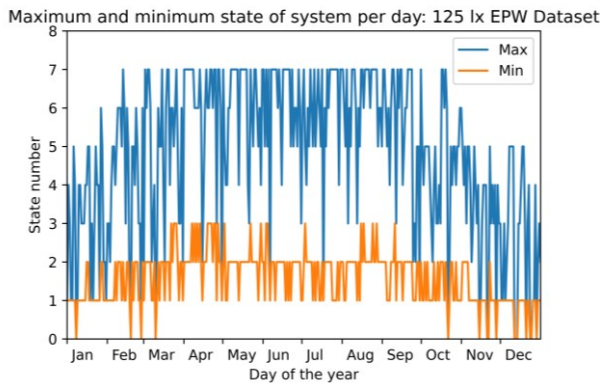


Figure 4-50: Maximum and minimum state of shading system per day

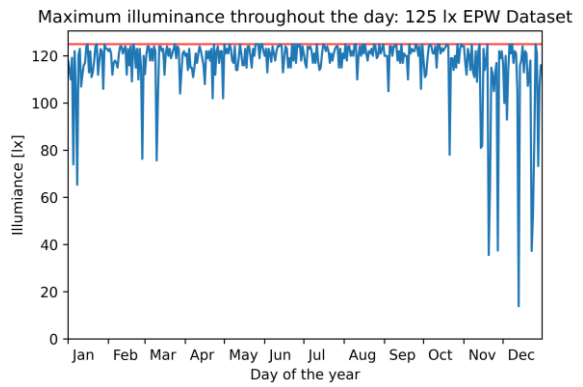


Figure 4-51: Maximum illuminance per day in room 228

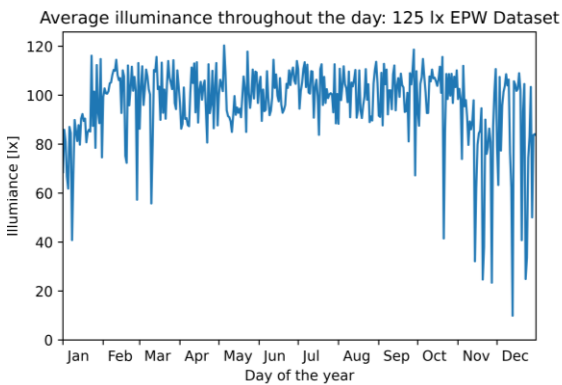


Figure 4-52: Average illuminance per day in room 228

The movements are graphed in Figure 4-48 and those that occur during openings hours in Figure 4-49. Depending on the day of the year, a different state could be used at the start of the day and result in a different maximum state as seen in Figure 4-50. In Figure 4-51 the daily maximum is given, with the average in Figure 4-52.

#### 4.4.3 Annual behaviour with real KNMI data 2022

For the annual simulation Ladybug imports the weather files from their database. Most commonly used is the EPW file, which is a file type based on Energy Plus. This is suitable for many types of simulation. However by the nature of the simulations, the dataset has been changed to work better. The stream consists of actual measured data, but the months of the year have been changed. This is done to get a climate average year. In the case of Rotterdam/The Hague, the data set is picked from a period of 52 years, ranging from 1957 to 2021 as seen in Table 4-9.

Month	Jan	Feb	Mar	Apr	May	Jun	Jul	Aug	Sep	Oct	Nov	Dec
Month of year used	1957	1999	2008	2002	1976	2000	2012	1959	2019	1999	2017	2003

Table 4-9: Years in EPW file for Rotterdam/The Hague

To compare the results, the annual simulation was computed again by using one real data set of measurements that were carried out for the duration of a full calendar year. This type of data is not available at any place close to the museum. Therefore, a dataset from Cabauw is used, this data is only used as a rough comparison. The measurements are done as part of the Baseline Surface Radiation Network (BSRN) (Knap, 2022) by the KNMI. At Cabauw a vertical construction is used to mount varying measurement devices and the location is roughly 30 km East of the museum. Because the data for 2023 was not yet complete, the run is made with the data from 2022. With this data, the original EPW file used by Honeybee is altered. The Diffuse Horizontal Irradiance, Direct Normal Irradiance are changed. The Global Horizontal Irradiance (GHI) is taken from another KNMI dataset, as the raw data from Cabauw also introduces negative values at hours that the moon is visible. The resulting GHI from both sets are compared and are similar. The Total Sky Cover is also retrieved from that set. The raw data from Cabauw is given per minute, so to be used in any of the simulations, the average hourly value is computed and used. Some data points are empty, this has to do with the cleaning of the sensor, these points are changed to zero. As those points only amount to a small portion of the full hour, minimal change is introduced.

The differences between the EPW dataset and the Cabauw 2022 data are shown below.

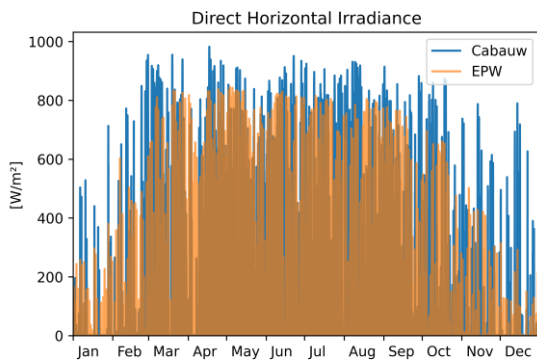


Figure 4-53: Direct Horizontal Irradiance comparison between EPW and Cabauw 2022

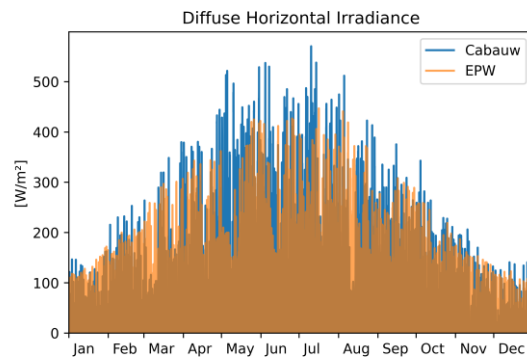


Figure 4-54: Diffuse Horizontal Irradiance comparison between EPW and Cabauw 2022

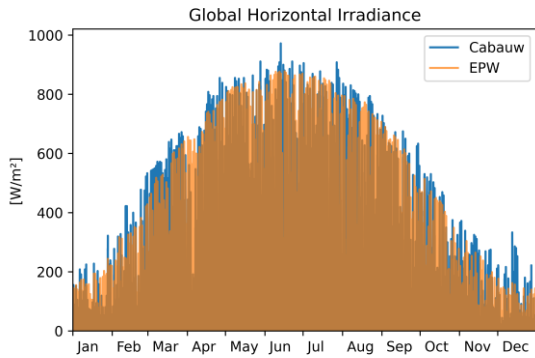


Figure 4-55: Global Horizontal Irradiance comparison between EPW and Cabauw 2022

From these graphs, above it can be concluded that for the compiled dataset that *Ladybug/Radiance* uses the Global Horizontal Irradiance is comparable as an average throughout a year. But especially in 2022 (at Cabauw) the Direct Horizontal Irradiance has a higher maximum. For the Diffuse Horizontal Irradiance, there is a trend that is slightly higher than the EPW file would suggest.

The resulting sun shading state diagram (Figure 4-56) depicts a largely similar behaviour and shows that the system is also effective in 2022. During the winter months, there seem to be some gaps in the data, resulting in a lower state than expected.

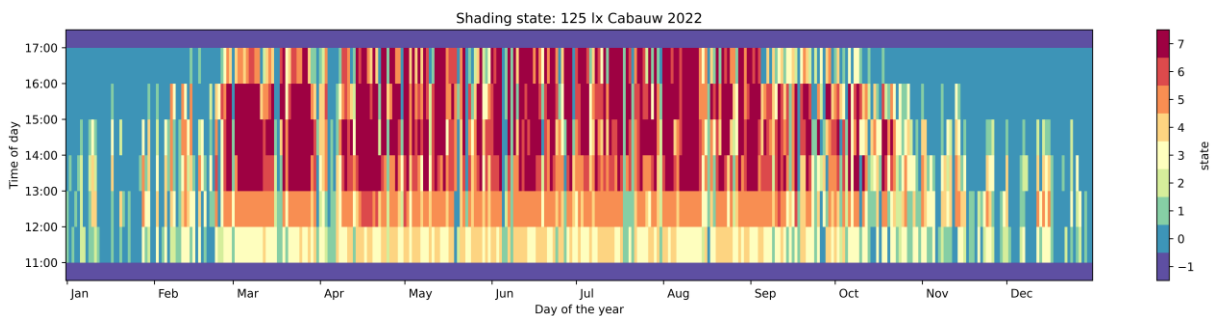


Figure 4-56: Shading state for 2022 based on Cabauw data

For the remaining plots, see Appendix F.

#### 4.4.4 Artificial lighting

As lighting conditions change and fluctuate throughout the day some additional lighting will be required to maintain a satisfactory light level. This can be done by supplementing diffuse artificial lighting above the *legramen* (Figure 3-7), for instance by using the Philips Maxos LED 4mx850 as seen in Figure 4-58.

To verify the behaviour a simulation run is done on December 21<sup>st</sup>. Without any sun shading (Figure 4-57) the light levels in the room exceed the threshold. By selecting state 1, the first screen is used resulting in a lower level (Figure 4-59). However these levels are now too low, so additional artificial lighting is required (Figure 4-60). With 30% of the total power of the 34 used lighting fixtures the illuminance in the room is increased to just above the desired 125 lx. So the calculated 30% is slightly too powerful for this point in time.

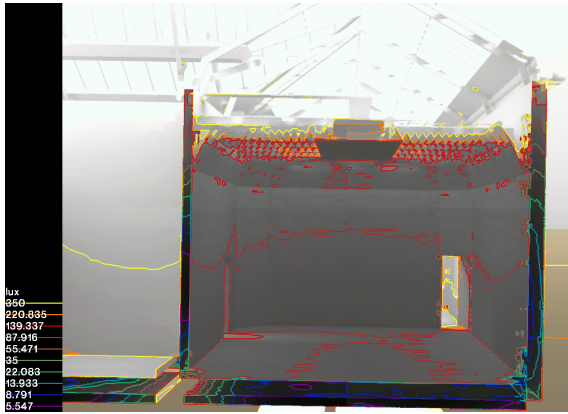


Figure 4-57: Room 228 – 21 Dec 10:00 – No sun screens



Figure 4-58: Philips Maxos LED 4mx850 (Philips, 2024)

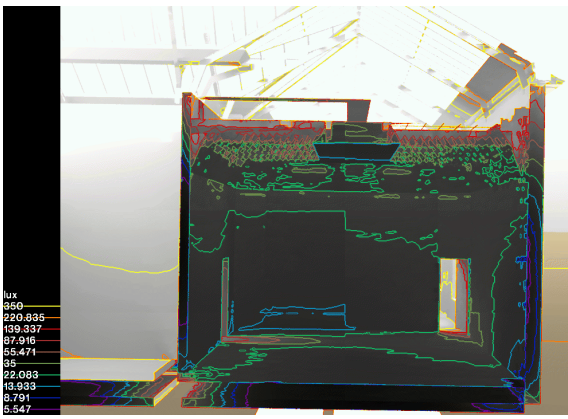


Figure 4-59: Room 228 – 21 Dec 10:00 – Shading state 1

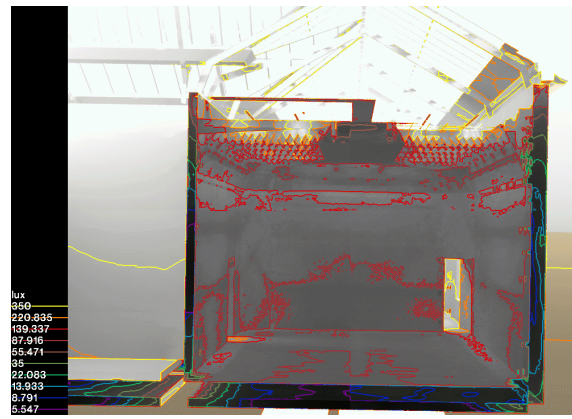


Figure 4-60: Room 228 – 21 Dec 10:00 – Shading state 1 & 30% diffuse artificial lighting

As some situations will call for a total blackout, the system is also tested to see if the available power can illuminate the room to the desired level, as seen in Figure 4-61 and a render in Figure 4-62. If there is no outside light, the artificial system can compensate to still reach the threshold illumination required.

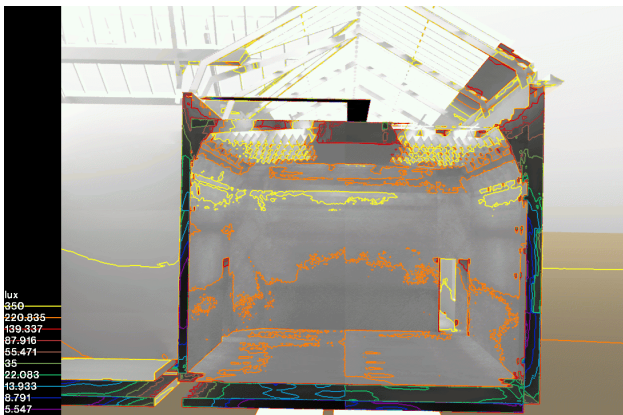


Figure 4-61: Room 228 - Full blackout screen + 97% diffuse artificial lighting

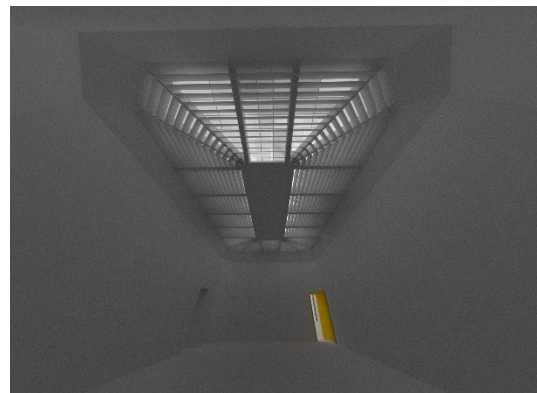


Figure 4-62: Render of artificial lighting in room 228

#### 4.4.5 Annual exposure

As the sun shading is implemented the exposure is reduced. The museum is closed on Mondays, so the amount of days is reduced to 313 days per year. Only during opening hours, the additional spotlights would be activated.

If no intervention is taken, all the light that falls on the roof finds a way to the art, also at times the museum is closed. To achieve a similar result compared to this study, the contrast ratio of 2:1 is maintained. Annually the exposure inside is 1.598.818 lx·hr, with a lighting dose of 1.040.359 lx·hr the total is 2.639.177 lx·hr.

For the proposed system the annual exposure is calculated as a flat and constant intensity of 250 lx for all opening hours, resulting in a total exposure of 469.286 lx·hr. As stated in paragraph 2.5 the museum deliberately opted for a 25% higher illuminance level, but as the opening hours are limited the annual exposure remains below the 600.000 lx·hr annual upper limit, saving an additional 22%. This decision and system could extend the lifespan of the pieces of art by the same amount. And all works could be safely displayed year-round.

Needless to emphasise, depending on the requirements of different pieces of art, for a temporary exposition e.g. the lighting regiment could easily be changed to accommodate that.

If no shading system is implemented the exposure exceeds the upper annual limit by 4.4 times. The art will need to go into dark storage for a large part of the year, to limit the exposure to the allowed dose. Without sun shading the art can only be exposed to 23% of the unblocked exposure, which corresponds for instance with the period January 1<sup>st</sup> – June 23<sup>rd</sup>.

4.5 Toolbox

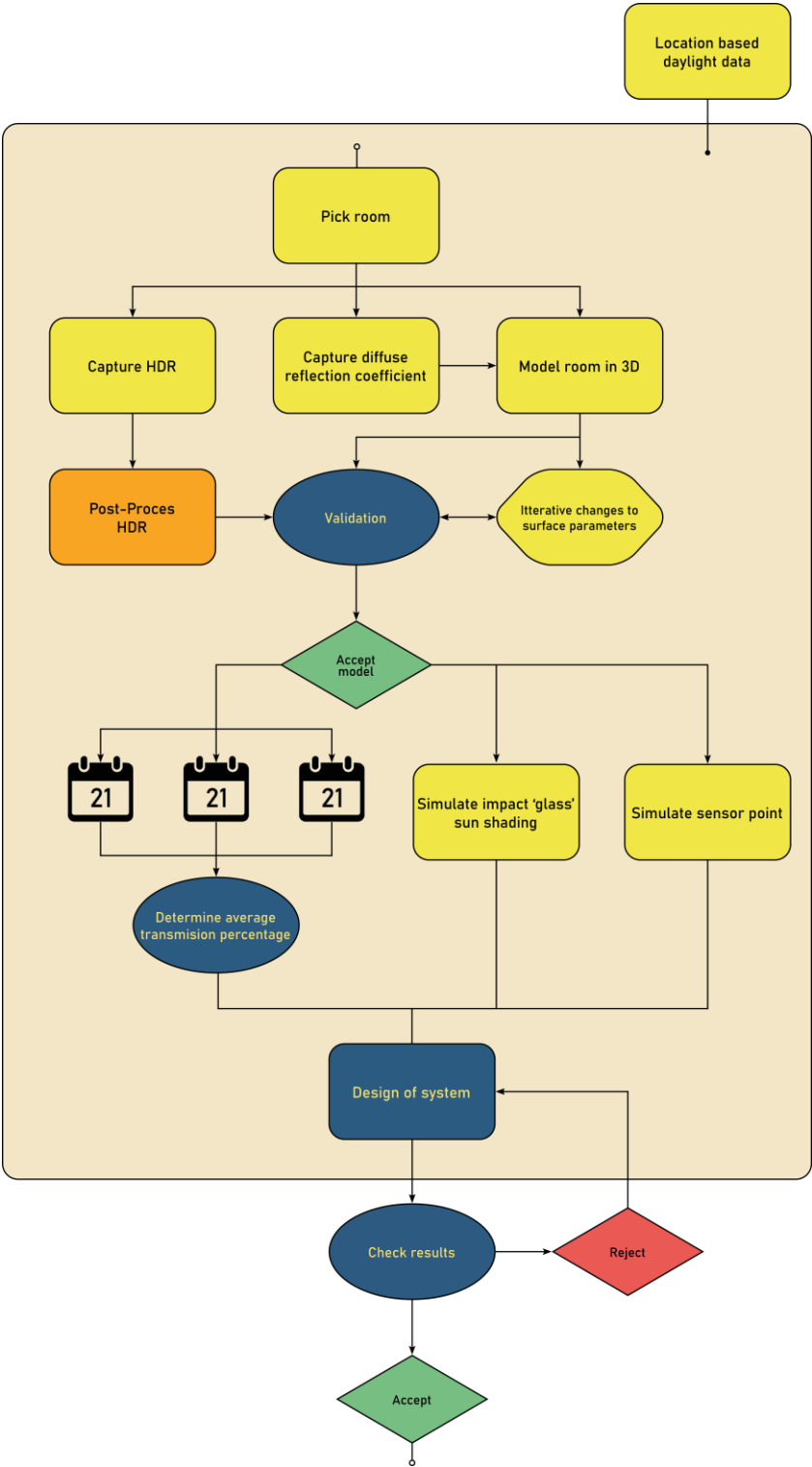


Figure 4-63: Process flow

In Figure 4-63 the developed toolbox is given. This allows for any person to adapt this approach to a different location and a different museum. All based on a multi-state shading device.

# 5 Discussion

---

The museum Boijmans van Beuningen in Rotterdam wishes to protect the displayed artworks from overexposure to light. This thesis uses a daylight modelling of a museum room with an HDR validation step. Based on this model, a multi-screen shading control system is designed. The calculation shows an 82.2% reduction of the annual exposure compared to the previous situation without any shading device.

## General remarks

### *HDR measurements*

For the validation of the model HDR images were made in the museum. Each capture consists of 14 consecutive photographs with increased exposure time, in total spanning 3 minutes. These captures are combined in a single luminance map.

In line with (Pierson, Cauwerts, Bodart, & Wienold, 2021) the illuminance at the start and the end of each measurement was recorded. If the illuminance stays within  $\pm 5\%$ , the measurement is accepted. However, the lighting conditions can fluctuate between the start and end of the capture process, and also during different individual shots. This could result in additional discrepancies.

### *Validation grid*

To compare the simulated model with the measured HDR values a mathematical approximation was made. As the Field of View of both methods are slightly different, this caused a different geometrical barrel distortion. For this calculation the legacy version of Honeybee was used, because this is better able to accept complex geometries (e.g. *schoepen*). It works with the same type of 3D model as the original model of the architect and it can include artificial lighting. This legacy version only accepts a fixed Field of View of  $180^\circ$ . The New Honeybee version would be able to accept customized Field of View, in this case ( $186^\circ$ ), but for the above-mentioned reasons the choice was made to use the legacy version.

Near the end of this research, additional information showed that the actual Field of View was  $185^\circ$  (Viula & Hordijk, 2019) instead of the used  $186^\circ$ . Theoretically, this could impact the results, but this would be marginal because the focus lies on the "exhibition areas" and not the perimeter. Therefore this was not corrected.

For the comparison of the model with the HDR images, several blocks were defined on the walls. An exact match of those blocks could not be made. The corner points of the grid location on the walls are chosen in the HDR images and then manually transposed to the Radiance output, based on visible static matching elements in the room. This could be improved by applying visible reference points (grid corners) in the room before making the HDR measurements. Even if fixed reference points had been used, the grid lines in both methods would differ slightly due to the difference in distortion. For each grid block (48) the average value is taken. This is a simplification of the actual value, but acceptable because there is a diffuse light field in the room, without specular highlights. The size of the grid elements cannot be made smaller indefinitely, because Radiance calculates the value per pixel. Besides, smaller grids would make the average value more reliable, but then some gridpoint comparisons could show larger deviations because of the barrel distortion.

### *Validation*

The validation of the model and the HDR was made by varying the characteristics of the *schoepen*, the floor and the *legramen*. It was not possible to measure all material properties on site. Because the *schoepen* and the *legramen* were not accessible for measurements, their initial properties were estimated based on literature. The diffuse reflectance of the floor was measured on-site. Because there was a lot of variation on the floor (underlayment, concrete, screed, glue) the average measured value was initially used. An iterative validation was done for these three parameters.

For three different regions, with 48 blocks, both methods have resulted in average luminance values. For the validation, these are compared, using absolute and relative values and boxplots. The parameters for *schoepen*, floor and *legramen* are adjusted iteratively based on these graphs. In total 20 iterations were made (including optimization of the *Python* script).

The model is overpredicting on the right wall by +13%, and for the middle wall by +6%. For the left wall, there is an underprediction of 3%. More iterations will yield a better convergence.

The values on the left wall show a good match, which indicates that the iterations have led to correct values for the *legramen*. This led to the original value supplied by the manufacturer of the *legramen*. The difference between the left and the right wall could be explained by the predominantly 'direct' sunlight on the left wall and the redirected light on the *schoepen* of the right wall. The HDR measurements were taken on September 26, around noon. At that time most sunlight came from the right. The values on the right wall show that the reflection of the *schoepen* in the model is too high. The values for the middle wall clearly show the influence of the light that comes through the door opening.

*Radiance* implements backwards ray tracing for its illuminance predictions. The light paths are calculated from their endpoint through the construction to the outside, to the light source. The incoming light will bounce multiple times before reaching the room below. In *Radiance* the parameter Ambient Bounces can be chosen in such a way that all rays are likely to contribute to the light levels inside. The reflection coefficient of the *schoepen* is relatively high. This means that only a little energy is lost per bounce (only 20% per bounce for a reflection coefficient of 0.8). The remaining energy is relatively high. The *schoepen* are pitched in such a way that the viewer is not able to see the *legramen*. Due to this pitch, the amount of reflections on the *schoepen* is likely to be high. Therefore the Ambient Bounces are set to 10 instead of the 'standard' 8 bounces. A downside of setting a higher number of Ambient Bounces is the added computational time required for each simulation run (+20%). A complete annual simulation would require more extensive computational time even at a lower resulting Level of Detail. Within this thesis, the focus was on accurately predicting the illuminance in the room. Therefore a more detailed simulation was done for the 3 selected days.

### *DAYSIM*

This issue is also present in the way DAYSIM calculates the impact of sun shading. The user can set different threshold values on which the system is operated. Using the different sun shading transmissions, DAYSIM starts calculating, once for the situation without any shading, and once for each different state. After these are finished, DAYSIM compares the outcomes with the threshold values and selects the most optimal state of the system for each hour. However, the of computational time needed for this type of detailed construction is large. The available documentation of DAYSIM is not readily available. And during a preliminary shoebox test, the behaviour of the system was not always predictable. To combat this issue a separate *Python* script was developed that uses the hourly illuminance outside as an input. Based on the detailed calculations for three days, a daylight factor of 2% was determined. Combining this reduction for the building (2%) with reductions for each different screen state, an expected performance is estimated for the entire year. With this classification of the system and the developed control strategy, the user can fully harness a custom solution, independent of the number of screens used and the threshold value.

### *Screen fabrics*

Firstly a fabric screen was implemented, with diffuse and specular transmission properties in *Radiance*. At testing, this resulted in non-consistent behaviour throughout the year for different transmissions. Therefore a simplification was made using a singular surface with glass properties. Using this layer the impact of the different transmissions was calculated and the combination of different screens was artificially calculated by multiplying the factors. However, the question is how multiple screens will behave, as each layer will allow for a diffuse and scattering transmission. The weave of the different classifications of screens should also be examined. It could be hypothesized that the effect of multiple screens allows for a smaller portion of light transmission than the

multiplication of the transmission factors. This will lead to a different result in the room, but as these values will be lower, the current system will predict conservatively.

The lighting in the museum can be influenced by the surroundings (Depotgebouw, Zalmhaventoren). These buildings can block the sun or can create extra reflections. The calculations are focussed on room 228, with only light entering from the top. The effects of the surroundings are minimal in this case and were not calculated. For other rooms in the museum with large windows in the facade, this will have more effect, especially when a museum is in a densely built-up area.

*Radiance* uses a dataset that is composed into a .EPW file that contains hourly data that is made up from different months over a period of 52 years. A further investigation was performed with the KNMI data for 2022 to get an impression of the situation in a recent year. The conclusion was that, even with the recent climate effects, there is very little difference with the standard set of EPW data.

UV radiation is an aspect that was not included in this research. As UV radiation can accelerate the deterioration process of the art, this aspect should not be underestimated. In this instance the sunlight first passes through multiple opaque materials each with its own wavelength-specific transmission, reducing the UV rays in such a manner that no singular 'hotspots' are present on a piece of art. In an ideal world, the museum would have a pyranometer on site, and multiple illuminance meters in each room, preferably with UV measurements to control the UV levels in the museum. Currently, the museum is looking to change the buildup of the *legramen* also to improve the thermal performance of the ceiling. This will further reduce the UV levels in the room.

## Model

### *Parameters*

Some parameters could not be measured, for instance, the diffuse reflection coefficient of the *schoepen*, because they were not accessible. The transmission coefficient of the *legramen* could also not be measured and verified with the values from the manufacturer. This is also the case for the roof construction with wired glass and Lexan™ plates. The fact that the materials in the room have aged and have been changed by the renovation state also indicates that the material properties will not be the same at every position. For the diffuse reflection coefficients of the wall and floor, some measurements were done on-site, but they cannot include all local variations. Currently, many surfaces are very rough, for example, the exposed brickwork and the glue that once held the floor in place. Typically after the reopening of the museum, these surfaces will have a smoother appearance. Combined with the perforations in the wall in some parts of the room, this will cause some difference with the actual expected results one might experience in the room when the restoration is finished.

To explore the effect of the chosen parameters, a sensitivity analysis was done. For the Morris (Brembilla, Hopfe, & Mardaljevic, Influence of input reflectance values on climate-based daylight metrics using sensitivity analysis, 2018) analysis, five parameters were varied: *schoepen*, wall, roof, *legramen* and roof. These were varied based on data from the literature. For each parameter 8 levels were considered, resulting in 48 combinations. The results of the sensitivity analysis show that the walls are the most influential factor.

The effects of the future material finish and colours are unknown at this stage of the renovation, and therefore not included in this research. These will have a major impact on the perception a visitor will have in the room. The colour on the wall will be a big contribution to this, but also the size and specifics of the displayed art will affect the experience (Yu, 2023).

### *Sensor points*

Along the walls, sensor points are simulated at 1,80 meters from the ground to calculate the illuminance. Typically the art is viewed at eye level which is standard 1,65 meters (Bokerhof, et al., 2008).

A certain practical minimal distance of the displayed art in relation to the wooden trim is maintained. Larger pieces of art will be hung higher and will receive 70% more exposure as seen in Figure 4-39. Therefore, the reference height of the sensor points is chosen at 1,80 meters.

By looking at the maximal value that is obtained for each hour, the model can predict the maximum value of illuminance that a piece of art will be exposed to. This eliminates the specific position on the wall, or on which wall entirely.

The museum board of MBVB expressed the desire for higher light levels inside of 125 lx on the walls with a contrast ratio of 2:1 (art-wall). This means that the illuminance on the art will be 250 lx. This is higher than the (NPR-CEN/TS 16163, 2014) regulations state. For this research, the limits of the museum board were taken. This is acceptable as the museum has fewer opening hours than the norm is referring to. The implementation of a control system is needed as otherwise the upper annual limit of 600.000 lx-hr is exceeded by 4.4 times.

## Results

### *Calculation*

Looking at the 2 solstices (21<sup>st</sup> of June and 21<sup>st</sup> of December) and the equinox in between (21<sup>st</sup> of September), the extremes of the behaviour of the room are analysed. This data is correlated with a fictive sensor point that is placed on the roof. This point is comparable with an actual pyranometer that can be installed locally at the museum. This will provide a simulated and practical input to optimize the sun shading calculation.

With the room-specific behaviour known, and the annual data gathered from the sensor an estimate of the reduction in illuminance throughout the structure is made, ending at a point on the wall. With

that, the calculation for the sun shading is run. This resulted in 3 different types of screens. By using different types a wider range of 'reduction' is created. The way the script is made, the user can easily change the types of screens or pick a different number of screens in the system. This data is eventually used to predict the behaviour of the system for the simulated year.

# 6 Conclusion

---

The main research question of this thesis is:

*How to design a method to assess the daylight exposure in museum BVB, to be used for a combined lighting design (daylight and artificial), focussing on optimal visibility and on art protection, in order to assess a multi-screen shading device and its effects on the illuminance?*

Based on the case study for museum BVB and the different steps of the four sub-questions a method has been developed. This resulted in a toolbox that can be used for other existing museum rooms with predominant top light.

By in-depth analysis of a specific room in a museum, the user can measure the real-world luminance in the room utilizing HDR capture. By constructing a model that is of high detail, the predicted light paths are more true to life. With the collected data a comparison can be made between the measured and the simulated results. During this process, the model is iteratively changed to fit the measured HDR results, as not always all surfaces can be measured to the fullest extent. As not all data points are of interest a region can be assigned focussing on the parts of the room, where art is likely to be displayed.

By doing so the Level of Detail can be increased as only limited Points In Time are assessed, reducing the required computational time. In the early stages, the user can closely monitor the behaviour of the specific room and used apparatus to control the incoming light. As that aspect is highly dependent on the specific building that is being analysed, the amount of detail will be case-specific.

For the influence on the displayed art, a horizontal strip around the room is considered, on a height the art will be hung. By calculating a building-specific daylight factor a relative resource light simulation can be made to calculate the hourly illuminance outside, without the need of considering the behaviour of the system inside for each step.

With that data, the user can design a multi-screen shading device that will fit their specific requirements and can be altered to the desired behaviour of the system. The number of screens used and their threshold values can be fully custom. With post-processing of this data, the user can verify the working and suggest changes to the system. During the workflow, the user can add additional data to the simulation if their specific location would require that.

In the specific case study at Boijmans Van Beuningen, a lot of attention was given to the specific behaviour related to the intricately constructed *schoepen* by Van der Steur.

The validation of the model results and the HDR measurements resulted in the best possible values for the parameters with a slight overprediction of the illuminance on the 'exhibition areas'. The museum board is aiming for a total illuminance of 250 lx with a ratio of contrast of 2:1 (art work - wall). And with the resulting building-specific daylight factor of 2% a control scheme for the multi-screen shading device is constructed. Adhering to the set limit by the board, the total annual exposure calculated was 469.286 lx-hr, which is a reduction of 82,2% compared to no sun shading system. Practically this allows the art to be safely displayed year round. Without sun shading the art can only be exposed to 23% of the unblocked exposure, which corresponds for instance with the period January 1<sup>st</sup> – June 23<sup>rd</sup>.

# 7 Recommendations

---

From the findings in this thesis, some recommendations for further research are listed to improve upon:

One major assumption that is made during the calculation of the impact of the different sunscreens is that the fabric of the screens is simplified to a glass surface with a varying transmission. For each singular screen that could be accurate. However, the combination of different screens, resulting in the higher states of the system the interaction between consecutive screens could lead to a different behaviour. Where glass only allows for transmission, a fabric will cause the light to be transmitted in both diffuse and specular ways. For each type and specification on a screen, those specific contributions could differ. To further investigate the actual resulting reduction of these higher-order states a physical measurement is advised.

In this model, the impact of different colours is not accounted for. The overall contribution of the specific diffuse reflection coefficient of the wall has the highest influence in the illuminance according to the sensitivity analysis. The colour of the wall will also directly impact the reflectance. Especially as the colour of the wall is an aspect that is relatively easy and most likely to change at some point in the future (change of collection that is displayed). This colour will also cast its colour on the items placed in that room (Yu, 2023), shifting the perceived colour pallet of the artwork. By using screens, especially in a multi-screen configuration the fabric used could also introduce a change in the colour of the light that enters the room. Depending on the contents of the room the light field could also change (Kartashova, 2018). For very complex cases, the spatial differentiation of the diffuse reflection coefficient of the displayed artwork could also be investigated (Forouzandeh Shahraki, Brembilla, & Jakubiec, 2022).

During the validation step between the model and the HDR measurements on-site, more improvements could be made. By placing small markers on the wall during the capture the user is later able to align the measured data more accurately to the simulated twin. Therefore the locations of each point need to be recorded and used during the comparison. Also, mathematical improvements are needed in the *Python* script to be able to make sure that the grid points of the areas of interest are represented continuously in both directions, reducing the misalignment in the vertical direction. Furthermore, some improvements could result from using the same Field of View for the simulation to the lens used in the measurements. This will make the geometrical barrel distortion similar. The HDR capture process would be more reliable if the measurements were done on an evenly lit day (sunny blue sky or fully overcast) as there will not be large fluctuation during the capture. But this is not always practically possible. Therefore, a continuous logging illuminance meter can identify captures with  $\pm 5\%$  deviation, which should be rejected.

Within the developed toolbox the user can add more simulation days. The current model assumes a constant daylight factor, for the entire year. But essentially for this building, during sunrise and sunset, there is a higher factor due to the pitched roof. Also, the neighbouring surroundings could be added to the simulation as some buildings could obstruct the direct sunlight for certain hours or other buildings could introduce reflections.

The current model only uses historical weather data to calculate the illuminance on an hourly basis. But for a system that needs to function in the real world that will not work. So a pyranometer on-site needs to be used to assess the current outside conditions, combined with a sensor inside that can measure the illuminance as well as the UV levels. This could be combined with the weather forecast for that specific day to be able to predict certain conditions throughout the day. Possibly this would reduce the amount of movements of the screens, especially for intermittent cloud cover. This control system could also predict certain conditions. If the morning is sunny, but later in the afternoon thick

rain clouds will be rolling in, the system could use more daylight in the morning, resulting in similar exposure. Therefore utilizing more natural daylight and reducing the need for additional artificial lighting. By using multiple sensors the system can verify the working and correct for deviations.

# References

---

- Beltran, V. L., Druzik, J., & Maekawa, S. (2012, January). Large-scale assessment of light-induced color changes in air and anoxic environments. *Studies in Conservation*, 57. Retrieved from [www.jstor.org/stable/42751755](http://www.jstor.org/stable/42751755)
- Betts, J. G., Young, K. A., Wise, J. A., Johnson, E., Poe, B., Kruse, D. H., . . . DeSaix, P. (2013). *Anatomy and Physiology*. Houston, Texas: OpenStax. Retrieved from <https://openstax.org/books/anatomy-and-physiology/pages/1-introduction>
- Bishop, D., & Geoffrey Chase, J. (2023, May 12). Development of a Low-Cost luminance Imaging Device with Minimal Equipment Calibration Procedures for Absolute and Relative Luminance. *Lighting in Buildings*. doi:10.3390/buildings13051266
- Boijmans Van Beuningen. (2023, June). *About the museum*. Retrieved from Boijmans.nl: <https://www.boijmans.nl/en/about-the-museum>
- Bokerhof, A., Duggen, N., de Ruijter, M., Santhagens, I., Stemerding, H., Visser, R., & Wolff, H. (2008). *Verlichting in musea en expositieruimten*. Ede: ICN & NSVV.
- Brembilla, E., Drosoou, N., & Mardaljevic, J. (2022, March 4). Assessing daylight performance in use: A comparison between longterm daylight measurements and simulations. *Energy & Buildings*. doi:10.1016/j.enbuild.2022.111989
- Brembilla, E., Hopfe, C., & Mardaljevic, J. (2018). Influence of input reflectance values on climate-based daylight metrics using sensitivity analysis. *Journal of Building Performance Simulation*, pp. 333-349. doi:10.1080/19401493.2017.1364786
- Campolongo, F., Cariboni, J., & Saltelli, A. (2007, Oct). An effective screening design for sensitivity analysis of large models. *Environmental Modelling & Software*, 22(10), pp. 1507-1518. doi:10.1016/j.envsoft.2006.10.004
- Camuffo, D. (2019). *Microclimate for cultural heritage* (3 ed.). Elsevier.
- CIE 157. (2004). *Control of damage to museum objects by optical radiation*.
- CIE 157. (2014). *Control of damage to museum objects by optical radiation*.
- Cooper, P. (1969). The absorption of radiation in solar stills. *Solar Energy*, 12(3), pp. 333-346. doi:10.1016/0038-092X(69)90047-4
- Cuttle, C. (2000, June). A Proposla to Reduce the Exposure to Light of Museum Objects Without Reducing Illuminance or the Levelofvisual Satisfaction of Museum Visitors. *Journal of the American Institute of Conservation*. doi:10.1179/019713600806082720
- Cuttle, C. (2007). *Light for Art's Sake*. Oxford: Elsevier.
- Delgado, M., Drik, C., Druzik, J., & WestFall, N. (2010, August 16). Lighting the world's treasures: Approaches to safer museum lighting. *Color Research & Application*, 36(4), pp. 238-254.
- Druzik, J. R., & Michalski, S. W. (2012). *Guidelines for Selecting Solid-State Lighting for Museums*. Ottawa: Canadian Conservation Institute.
- Druzik, J., & Eshøj, B. (2017). Museum lighting: its past and future development. *Museum Microclimates*.
- Dukai, B., van Liempt, J., Peters, R., Stoter, J., Vitalis, S., & Wu, T. (2023, March). *3D BAG*. Retrieved from 3D BAG: <https://docs.3dbag.nl/en/>
- Forouzandeh Shahraki, N., Brembilla, E., & Jakubiec, J. A. (2022). Image-based Material Characterization for Daylight Simulation Using Illuminance-proxy and Artificial Neural Networks. *Proceedings of the 14th European Lighting Conference LUX EUROPA 2022*, (pp. 171-178).
- Hannema, D., & van der Steur, A. (1933, Feb 11). Een studie over moderne museumverlichting. *Bouwkundig Weekblad Architectura*, 54, pp. 45-50.
- Herascu, N., Simileanu, M., & Radvan, R. (2008). Color changes in the artwork materials. *Romanian Reports in Physics*, 60(1), pp. 95-103. Retrieved from [https://rrp.nipne.ro/2008\\_60\\_1/10-095-103.pdf](https://rrp.nipne.ro/2008_60_1/10-095-103.pdf)
- Huijiao, T., & Rui, D. (2022). Review of lighting deterioration, lighting quality, and lighting energy saving for paintings in museums. *Building and Environment*(208). doi:<https://doi.org/10.1016/j.buildenv.2021.108608>

- Hukseflux. (n.d.). The global irradiance included direct sunlight and diffuse sunlight. Retrieved from <https://www.hukseflux.com/applications/solar-energy-pv-system-performance-monitoring/what-is-a-pyranometer>
- Hunt, E. G. (2009). *Study of museum lighting and design (Unpublished thesis)*. San Marcos, Texas: Texas State University-San Marcos. Retrieved from <https://digital.library.txstate.edu/handle/10877/3203>
- Instituut Collectie Nederland. (2005, May). Het beperken van lichtschade aan museale objecten: lichtlijnen. *ICN-Informatie*.
- Iwanaga, T., Usher, W., & Herman, J. (2022, Feb 24). Toward SALib 2.0: Advancing the accessibility and interpretability of global sensitivity analyses. *Socio-Environmental Systems Modelling*, 4. doi:10.18174/sesmo.18155
- Kartashova, T. (2018). *Structures of Physical and Visual Light Fields*. Delft.
- Knap, W. (2022). Basic and other measurements of radiation at station Cabauw (2005-02 et seq). *Koninklijk Nederlands Meteorologisch Instituut*. De Bilt: PANGAEA. doi:10.1594/PANGAEA.940531
- Lai, Y.-Y. (2022, 05 16). *What do CCT, CIE, and SPD mean in LED lighting?* Retrieved from Luminus: <https://luminusdevices.zendesk.com/hc/en-us/articles/4403685063437-What-do-CCT-CIE-and-SPD-mean-in-LED-lighting>
- Leccese, F., Salvadori, G., Maccheroni, D., & Feltrin, F. (2020, March). Lighting and visual experience of artworks: Results of a study campaign at the National Museum of San Matteo in Pisa, Italy. *Journal of Cultural Heritage*. doi:10.1016/j.culher.2020.03.007
- Loe, D. L., Rowlands, E., & Watson, N. F. (1982, 12). Preferred lighting conditions for the display of oil and watercolour paintings. *Lighting Research & Technology*, 14(4), pp. 173-192. doi:10.1177/096032718201400401
- Lucchi, L. (2018, January-February). Review of preventive conservation in museum buildings. *Journal of Cultural Heritage*, 29, pp. 180-193. doi:<https://doi.org/10.1016/j.culher.2017.09.003>
- Magdy, M. (2022, December). Insights into the Effect of UV Radiation on Paintings: A Mini-Review for the Asset Preservation of Artworks. *Advanced Research in Conservation Science*, 3(2), pp. 46-54. doi:<https://dx.doi.org/10.21608/arcs.2022.167664.1031>
- Mardaljevic, J., Cannon-Brookes, S., Blades, N., & Lithgow, K. (2021, aug 25). Reconstruction of cumulative daylight illumination fields from high dynamic range imaging: Theory, deployment and in-situ validation. *Lighting Research & Technology*, 53(4), p. 2020. doi:10.1177/1477153520945755
- Maxwell, J. (1873). *A treatise on electricity and magnetism* (Vol. 1). Oxford: Clarendon Press.
- Mead, D. (2010). *'Trans' Materials - Modeling and Specifying a Next Generation*. Retrieved from Radiance-online.org: <https://www.radiance-online.org/community/workshops/2010-freiburg/PDF/DavidMead.pdf>
- Michael, P. R., Johnstron, D. E., & Moreno, W. (2020, December). A conversion guide: solar irradiance and lux illuminance. *Journal of Measurements in Engineering*, 8. doi:10.21595/jme.2020.21667
- Milne, R. M. (1921). 593. Note on the Equation of Time. *The Mathematical Gazette*, 10(155), pp. 372-375. doi:10.2307/3604631
- Morris, M. D. (1991, May). Factorial Sampling Plans for Preliminary Computational Experiments. *TECHNOMETRICS*, 33(2).
- NEN. (2010, September). Conservation of Cultural Property - Specifications for temperature and relative humidity to limit climate-induced mechanical damage in organic hygroscopic materials. *NEN-EN 15757*.
- NEN. (2012, March). Light and lighting - Measurement and presentation of photometric data of lamps and luminaires - Part 1: Measurement and file format. *NEN-EN 13032-1+A1*.
- NEN-EN 14500. (2021). *Blinds and shutters - Thermal and visual comfort - Test and calculation methods*.
- NEN-EN 14501. (2021). *Blinds and shutters - Thermal and visual comfort - Performance characteristics and classification*.
- NOAA. (n.d.). *Solar Calculator Links*. Retrieved from Global Monitoring Laboratory: <https://gml.noaa.gov/grad/solcalc/solareqns.PDF>

- NPR-CEN/TS 16163. (2014). Conservation of Cultural Heritage - Guidelines and procedures for choosing appropriate lighting for indoor exhibitions. *NPR-CEN/TS 16163*.
- Phifer 2000. (2024). *SheerWeave® 2000/2100*. Retrieved from PHIFER: [https://www.phifer.com/wp-content/uploads/2021/12/SW-2000-2100-Swatch-Card-V20\\_061223.pdf](https://www.phifer.com/wp-content/uploads/2021/12/SW-2000-2100-Swatch-Card-V20_061223.pdf)
- Phifer 4000. (2024). *SheerWeave® 4001/4400/4000/4100*. Retrieved from [https://www.phifer.com/wp-content/uploads/2021/12/SW-4001440040004100-Swatch-Card-032023\\_V23.pdf](https://www.phifer.com/wp-content/uploads/2021/12/SW-4001440040004100-Swatch-Card-032023_V23.pdf)
- Phifer 4500. (2024). *SheerWeave® 4500/4600*. Retrieved from <https://www.phifer.com/wp-content/uploads/2023/06/sw-4600-4500-swatch-card-v23-051023.pdf>
- Philips. (2024). *4MX850 581 LED40S/830 PSD DA20 WH*. Retrieved from Philips.com: [https://www.lighting.philips.nl/prof/armaturen-voor-binnenverlichting/lichtlijnsystemen/maxos-led-industry-4mx850/910629125826\\_EU/product](https://www.lighting.philips.nl/prof/armaturen-voor-binnenverlichting/lichtlijnsystemen/maxos-led-industry-4mx850/910629125826_EU/product)
- Pierson, C., Cauwerts, C., Bodart, M., & Wienold, J. (2021). Tutorial: Luminance Mpas for Daylighting Studies from High Dynamic Range Photography. *The Journal of the Illuminating Engineering Society*. doi:10.1080/15502724.2019.1684319
- qDslrDashboard. (2022). *V3.6.7*. Retrieved from <https://dslrdashboard.info/>
- Scuello, M., Abramov, I., Gordon, J., & Weintraub, S. (2004, January 29). Museum lighting: Optimizing the illuminant. *Color Research & Application*, 29(2), pp. 121-127. doi:<https://doi-org.tudelft.idm.oclc.org/10.1002/col.10231>
- Swela. (2024). *Swela Elegance*. Retrieved from Swela: [https://www.swela.com/sites/default/files/2018-02/swela-309\\_310\\_311\\_312\\_313\\_315\\_sunvas%20\\_3.pdf?\\_gl=1\\*17ta8em\\*\\_ga\\*NjUwMzcwOTAzLjE3MDc0ODY3Mzk\\*\\_up\\*MQ..\\*\\_ga\\_PWNYJPYKJ4\\*MTcwNzQ4NjczOC4xLjEuMTcwNzQ4NjgyMS4wLjAuMA..](https://www.swela.com/sites/default/files/2018-02/swela-309_310_311_312_313_315_sunvas%20_3.pdf?_gl=1*17ta8em*_ga*NjUwMzcwOTAzLjE3MDc0ODY3Mzk*_up*MQ..*_ga_PWNYJPYKJ4*MTcwNzQ4NjczOC4xLjEuMTcwNzQ4NjgyMS4wLjAuMA..)
- TechnoTeam. (n.d.). *TECHNOTEAM LMK mobile air - Portable Imaging Photometer*. Retrieved from Opteema: [https://www.opteema.com//media/lmk\\_ma\\_web\\_en\\_eng.pdf](https://www.opteema.com//media/lmk_ma_web_en_eng.pdf)
- Thomson, G. (1986). *The Museum Environment*. Oxford: Butterworth-Heinemann Ltd.
- van der Steur, A. (1935, August 12). Museum Boymans te Rotterdam Part I. *Vakblad voor de bouwbedrijven*(32).
- van der Steur, A. (1935, August 26). Museum Boymans te Rotterdam Part II. *Vakblad voor de bouwbedrijven*(34).
- Viula, R., & Hordijk, T. (2019). A METHOD FOR ESTIMATING FISHEYE LENS' FIELD-OF-VIEW ANGLE AND PROJECTION FOR HDR LUMINANCE CAPTURE. *Conference: Proceedings of the 29th Quadrennial Session of the CIE*. doi:10.25039/x46.2019.P0061
- Ward Larson, G., Ehrlich, C., Mardaljevic, J., Shakespeare, R., Phillips, E., & Apian-Bennewitz, P. (1998). *Rendering with Radiance: The Art and Science of Lighting Visualization*. San Francisco, CA/Orlando, FL: University of San Francisco: Morgan Kaufmann.
- Yu, C. (2023). *Light and Spectra in the Wild*. Delft.

# Appendices

---

## A Situation photos BVB



Figure A-1: Attic above room 228



Figure A-2: Corner of *legramen* room 228



Figure A-3: Walkway in attic



Figure A-4: Closeup of *legramen*



Figure A-5: View of *legramen* from room 228



Figure A-6: Temporary build corridor

## B HDR capture script

### High Dynamic Range Photography Luminance maps postprocessing

After acquiring the HDR images as described in 0. These separate Low Dynamic Range images need to be merged. This is done in accordance with (Pierson, Cauwerts, Bodart, & Wienold, 2021). In their article, they elaborate on the process needed to convert these separate images into one combined luminance map.

The images were captured on the 19<sup>th</sup> of September 2023 and the 26<sup>th</sup> of September 2023. Both days had an intermediate cloudy/sunny character. This did result in some captures being deemed unusable. As the nature of the assessment to accept to reject a certain measurement only relies on a luminance measurement at the start of the capture and the end, the possibility of the luminance value fluctuating during the capture is possible. The weather type made that the sun was obstructed by some clouds and a moment later the sun could have cleared the cloud and had no longer any obstruction. Therefore, during the capture, I objectively observed the luminance meter on the possible large fluctuations.

At each position, a series of 14 images were taken. If they met the set requirements, they were accepted and therefore processed. To do this *Radiance* is used, which is executed by the command line. The default installation location of *Radiance* is: C:\Radiance. To access this location in the *Command Prompt* the following command is used.

```
> cd C:\Radiance
```

[ B-1 ]

First, all the images are combined to a single HDR image, this is done by using *hdrgen*. Any part of the syntax between “{ }” requires user input.

```
> bin\hdrgen {location of each LDR image.jpg} -r {location of the response_function.rsp} -g -f  
-o {file location of output file.hdr [ B-2 ]}
```

[ B-2 ]

At the start of the command, the location of the program used is called, in this case, the *hdrgen* is in the *bin* folder inside of the *Radiance* folder. Following each location of the LDR images is listed. Using the *-r* argument is called to indicate the location of the response function on the drive. The arguments *-g* and *-f* are used to reduce ghosting and flaring in the resulting image. *-o* provided with the location of the output and the naming of the file.

Within the header of the HDR image compiled the exposure value is stored. There is a possibility of an issue with the interpretation of that value. Therefore it is recommended to remove that value from the header, but to add it to each pixel value. To do this the program *ra\_xyze* is used, with the following syntax:

```
> bin\ra_xyze -r -o {output of [ B-2 ].hdr} > {file location of output file.hdr [ B-3 ]}
```

[ B-3 ]

The argument *-r* is used to not convert the values contained in the HDR to the CIE XYZ exponent format. *-o* is used to address the original image with the original units. After the *>* the output file is provided.

As the image is captured using a very wide fisheye lens, not all pixels of the sensor are exposed to light. Therefore, their values should be considered as zero. The image from the fisheye is circular. The nature of this specific lens will physically move the lens to focus on the desired subject. By doing this, the precise size of the circular image changes from scene to scene. The program *pcompos* is

used. This requires the number of pixels on X-axis and the number of pixels on the Y-axis that the actual image occupies. This is done with *Adobe Photoshop*<sup>®</sup>, by lining up rulers and measuring the distance in pixels between them. Also, the coordinate of the bottom left corner of the fisheye is necessary. *Photoshop* uses its coordinate system from the top left corner. *Radiance* uses a more mathematical-centric approach of the bottom left. The first arguments in *pcompos* provide the diameter of the circular image. And later the number of pixels to shift the image by is given. The required pixels needed for a correct image are located to the right of the bottom left corner, as well as above the bottom left corner. These pixels need to be shifted in the other direction, therefore these coordinates are inputted as negative, see Figure B-7.

```
. > bin\pcompos -x {diameter in X direction} -y {diameter in Y direction} {output of [ B-3 ]} -
{amount of pixels to shift in X direction} -{amount of pixels to shift in Y direction} > {file location of
output file.hdr [ B-4 ]}
```

[ B-4 ]

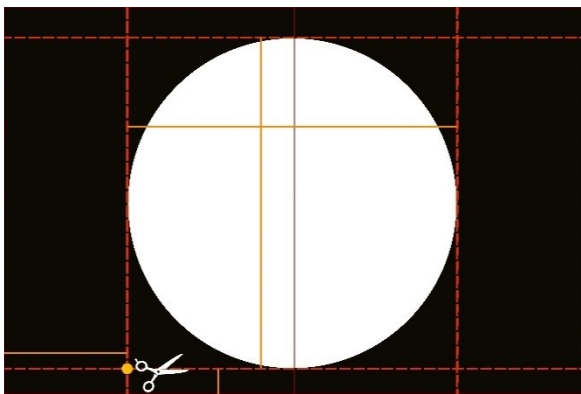


Figure B-7: High Dynamic Range photograph dimensions and crop

Due to the large number of pixels contained in the HDR image, roughly 3100 x 3100 and the computing power needed for this. The file is resized to 1500 x 1500 pixels. This is done via *pfilt*, only using one pass of the image not to introduce any additional averaging of pixel values.

```
> bin\pfilt -1 -x 1500 -y 1500 {output of [ B-4 ]} > {file location of output file.hdr [ B-5 ]}
```

[ B-5 ]

Now the HDR has a resolution of 1500 x 1500 pixels, but many pixels outside of the circular image are black and sometimes do contain a pixel value. To correct the distortion of the fisheye lens and to nullify the values that are considered out of bounds *pcomb* is used.

```
> bin\pcomb -f lib\fisheye_corr.cal {output of [ B-5 ]} > {file location of output file.hdr [ B-6 ]}
```

[ B-6 ]

After this, the pixel values are extracted and stored in a .txt file using *pvalue*.

```
> bin\pvalue {output of [ B-6 ]} > {file location of output file.txt [ B-7 ]}
```

[ B-7 ]

This text file is loaded into a *Python* script to compute a falsecolour image. Using *Photoshop* the coordinates of the calibration point as setup in Figure B-7 is determined. Using those coordinates; changing them to a bottom left system; the raw data in the text file is outputted in a coordinate with an associated R, G & B value. These values need to be converted to a luminance value. *Radiance* uses the equal-energy white point [(x,y,z) = (0.33, 0.33, 0.33)] for its calculations. The output of the camera

uses the sRGB primaries, these need to be corrected accordingly. For *falsecolour* and *evalglare Radiance* calculates the luminance with Equation B-1.

$$L = 179 \times (R \times 0.2651 + G \times 0.6701 + B \times 0.0648)$$

Equation B-1: Luminance calculation

With L as the calculated luminance of each individual pixel [ $\text{cd/m}^2$ ]; 179 is the standard luminous efficacy used in *Radiance* [ $\text{lm/W}$ ]; R, G & B are the spectrally weighted radiance of each individual pixel [ $\text{W/m}^2\text{sr}$ ].

The values of 0.2651, 0.6701, 0.0648 are derived from the CIE chromaticities for the reference/*Radiance* primaries and the equal-energy white point used with *Radiance*. This calculation is done for each pixel and appended at the end of each row. Where after the script has the luminous value for each pixel. Then we assign a colour to the luminous value in accordance with the colour scale *falsecolour* uses. This scale is nonstandard and therefore mimicked using 11 colour samples between which the colour gradient is determined linearly. After doing that the plot can be made and the luminous value of the calibration pixel is extracted. The resulting image is exported directly from *Python*.

Now we have obtained the relative luminance value of the calibration pixel for our scene. Comparing this value with the measurement we made using the spot meter, we can scale the luminance map accordingly. As the camera is fitted with an ND-2 filter, the values we can expect out of the camera would always be (if the measurement is carried out correctly) lower. If we divide the spot meter measurement with our *Python* output, we get the required scaling factor, see Equation B-2.

$$\frac{\text{Spot meter}}{\text{Python value of calibration pixel}} = \text{Scaling factor}$$

Equation B-2: Scaling factor

Returning to the *Command Prompt* we aim to scale the HDR image, for this, we use *pcomb* again. Now using the *-s* argument to tell the program what scaling factor we need. With this scaling, we directly include the effects of the installed ND filter. Also, the lens was tested for vignetting and it does not introduce these effects.

```
> bin\pcomb -s {Scaling factor from Equation B-2} {output from [ B-6 ]} > {file location of output file.hdr [ B-8 ]}
```

[ B-8 ]

After this, we need to correct the HDR image header. This stores critical information about the scene and the equipment used. First, the existing data that is in the header is erased with *getinfo*.

```
> (bin\getinfo < {output from [ B-8 ]} | {location of "Gnewin32\bin\sed.exe"} "/VIEW/d" && bin\getinfo - < {output from [ B-8 ]} > {file location of output file.hdr [ B-9 ]}
```

[ B-9 ]

As we now have stripped the header of the information needed to construct the proper view, we need to add the correct view.

```
> bin\getinfo -a "VIEW = -vta -vv 186 -vh 186" < {output from [ B-9 ]} > {file location of output file.hdr [ B-10 ]}
```

[ B-10 ]

Where the arguments *-vta* tells *Radiance* that the *view type* of lens used is classed as an angular fisheye. Allowing to set the *view horizontal* size *-vh* and *view vertical* size *-vv* to the  $186^\circ$  that the Sigma fisheye lens produces.

After this, we export the created HDR image again using *pvalue*.

```
> bin\pvalue {output from [ B-10 ]} > {file location of output file.txt}
```

[ B-11 ]

To create the final *falsecolour* image and to check the calibration pixel for the error in the created luminous value as seen in Table 4-1. Within the script the values are also clipped, this is done to get the same colour throughout different images and later the output of the simulations.

As a last step, a validity check must be made. Even if the equipment is well calibrated there is a possibility of too large deviations, making the resulting luminance map unreliable. There are two ways of checking the output for its quality: the illuminance comparison and the luminance comparison. It is preferred to use the illuminance comparison if you can expect high luminance values ( $>30.000 \text{ cd/m}^2$ ). This is the case if the sun has any meaningful influence on the scene either direct sunlight, reflections or the sky. During the capture, the vertical illuminance is measured at the start of the measurement as well as at the end. The comparison checks for the luminous balance between the captured sensor data in the HDR and the illuminance meter placed on top of the camera. The acceptable range of deviation is set at 25%, if the results fall outside of that range the luminance is over- or under-estimated. The illuminance is calculated with *evalglare* by using the argument *-V* the vertical illumine is extracted. By integration of every luminance value that is captured within the FOV. This value is compared with the average illuminance reading at the time of capture by averaging the start and end measurements. If the deviation is within  $\pm 25\%$  the luminance map is accepted, if it falls outside it is rejected.

```
> evalglare -V {output from [ B-10 ]}
```

[ B-12 ]

## C HDR capture data

Date	Time	Room	Version	spot	gem	pcompos		move x	move y	x	y	photostop		x	y	output	Pcomrb	scaling factor	header python	output	diff	evaldare			
						X	Y					move x	move y												
19-09-2023	13:04	234	v1	25_49	178.0	2577	2586	-1423	-507	931	853	22	931	647	0.557737365	45.702514496	25	25.46925	-0.081%	113.325	-64.7	Reject			
19-09-2023	13:37	234	v2	8_12	61.0	2538	2541	-1444	-540	941	860	22	941	640	0.127023478	63.925190170	25	8.129728	0.120%	61.744	0.7	1.22%	Accept		
19-09-2023	14:10	228	v1	39_71	171.0	2556	2560	-1438	-519	712	512	22	712	988	0.493321888	80.495110762	25	39.86389	0.388%	166.300	-4.7	-2.75%	Accept		
26-09-2023	11:18	234	v1	33_78	137.0	3092	3087	-1165	-260	1023	876	22	1023	624	0.306959992	110.406591875	25	33.78929	0.028%	194.841	57.8	17.92%	Accept		
26-09-2023	11:31	234	v2	34_34	160.5	3090	3088	-1168	-256	1029	874	22	1029	626	0.390320867	87.978898732	25	34.20213	-0.401%	189.267	28.8	22.14%	Accept		
26-09-2023	11:38	234	v8	41_61	183.5	3089	3088	-1170	-258	1029	874	22	1029	624	0.450553328	92.353107582	28	41.66696	0.137%	224.128	40.6	10.07%	Accept		
26-09-2023	12:03	228	Normal	45_61	139.5	3081	3085	-1171	-258	694	799	22	694	701	0.273783901	166.591241608	25	45.62011	0.022%	293.751	154.3	10.07%	Accept		
26-09-2023	12:17	228	Up	40_18	276.0	3088	3084	-1166	-262	764	566	22	764	934	0.5686354363	68.525114700	25	40.16773	-0.031%	229.856	-46.1	-16.72%	Accept		



Figure C-8: Room 228 - 19-09-2023 - v1 - 14:10

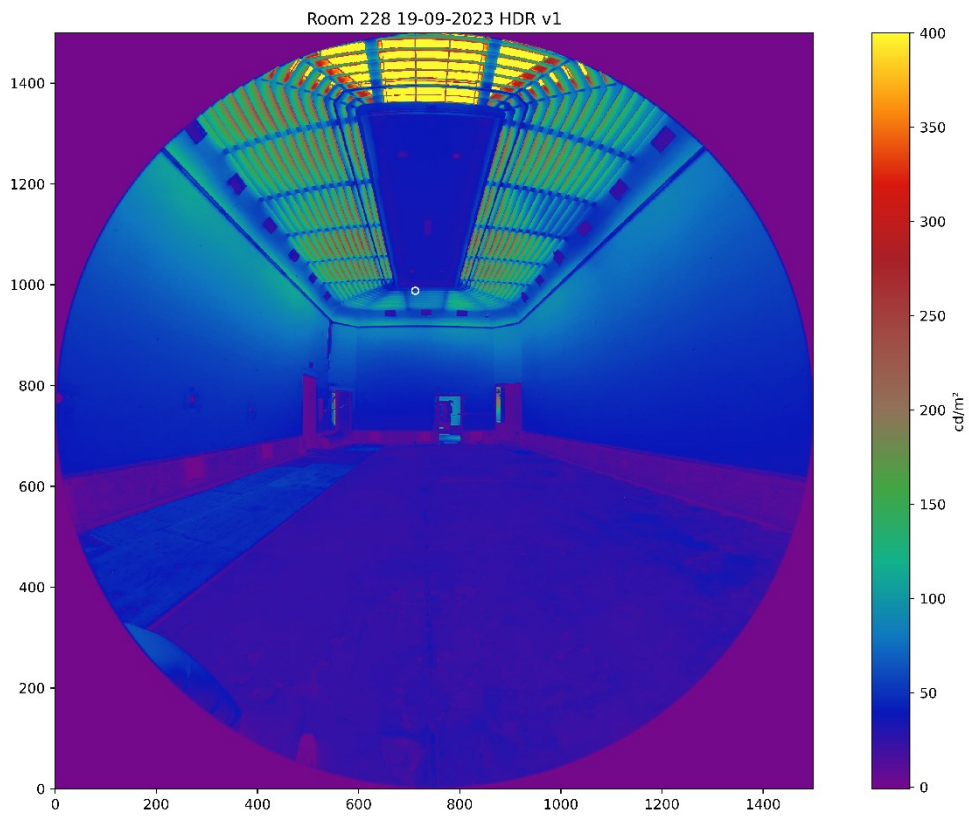


Figure C-9: Room 228 - 19-09-2023 - v1 - luminance map



Figure C-10: Room 234 - 19-09-2023 - v1 - 13:04

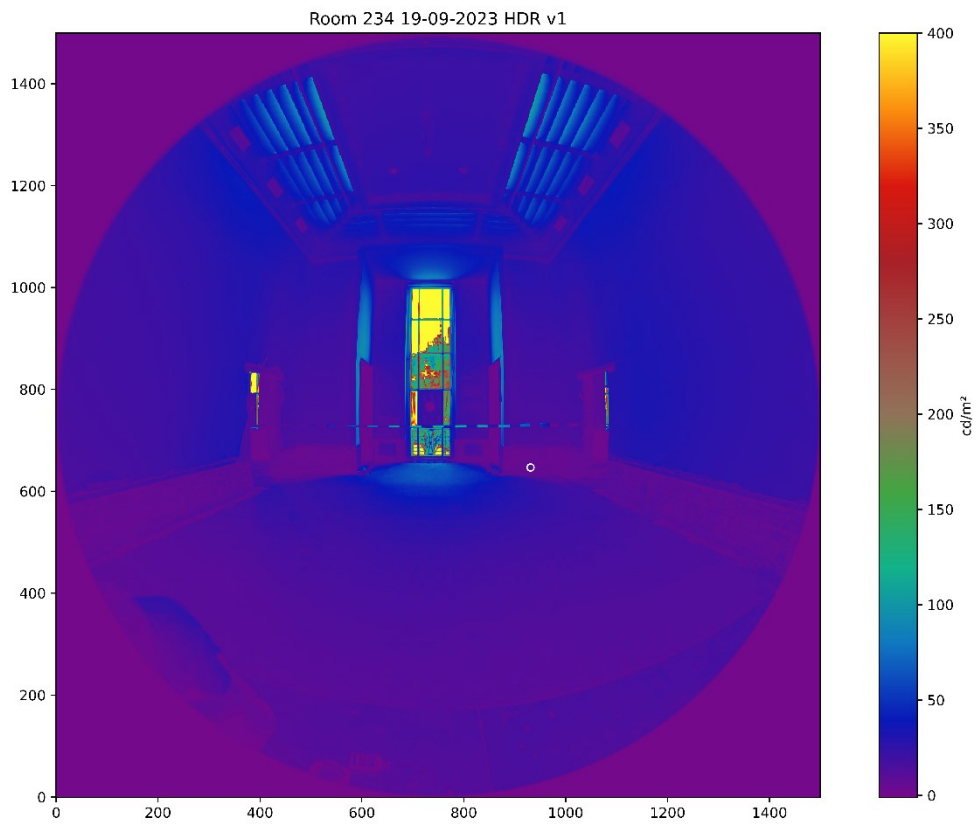


Figure C-11: Room 234 - 19-09-2023 - v1 - luminance map



Figure C-12: Room 234 - 19-09-2023 - v2 - 13:37

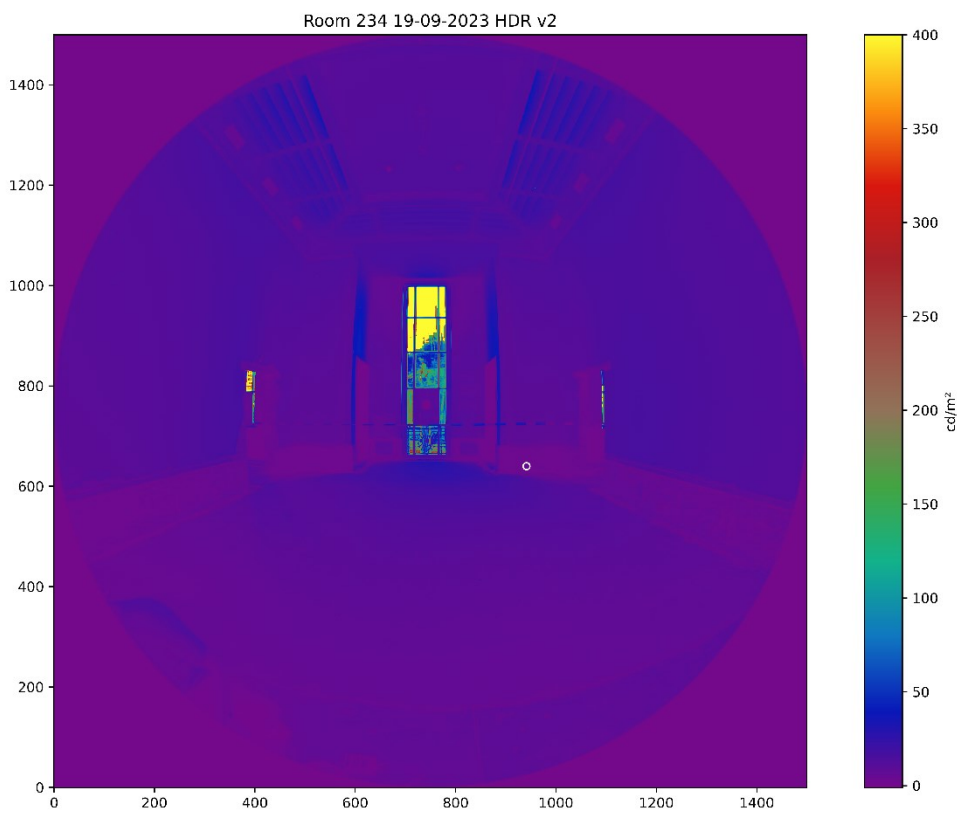


Figure C-13: Room 234 - 19-09-2023 - v2 - luminance map



Figure C-14: Room 228 - 26-09-2023 - normal - 12:03

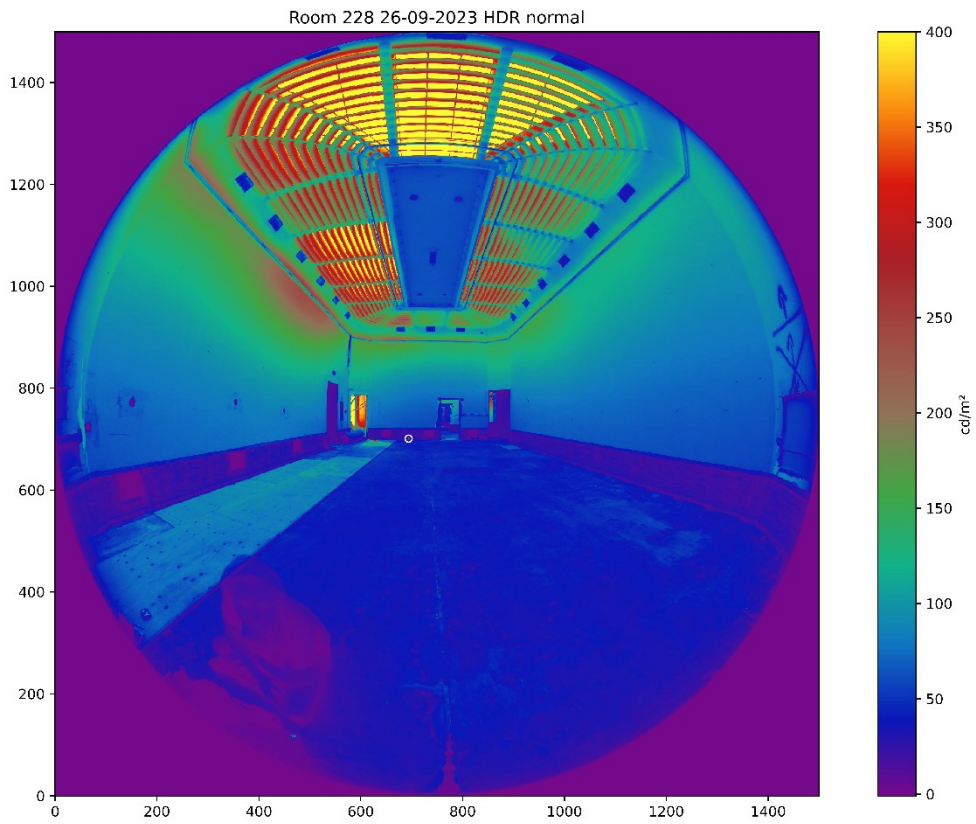


Figure C-15: Room 228 - 26-09-2023 - normal - luminance map



Figure C-16: Room 228 - 26-09-2023 - up - 12:17

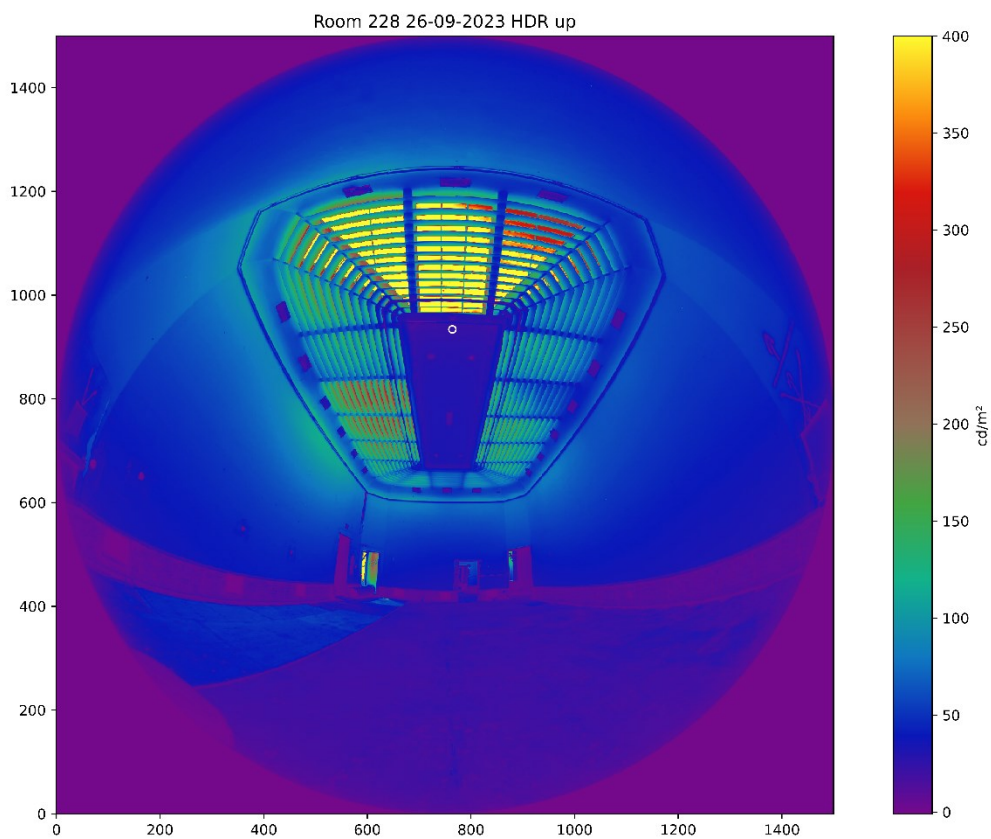


Figure C-17: Room 228 - 26-09-2023 - up - luminance map



Figure C-18: Room 234 - 26-09-2023 - v1 - 11:18

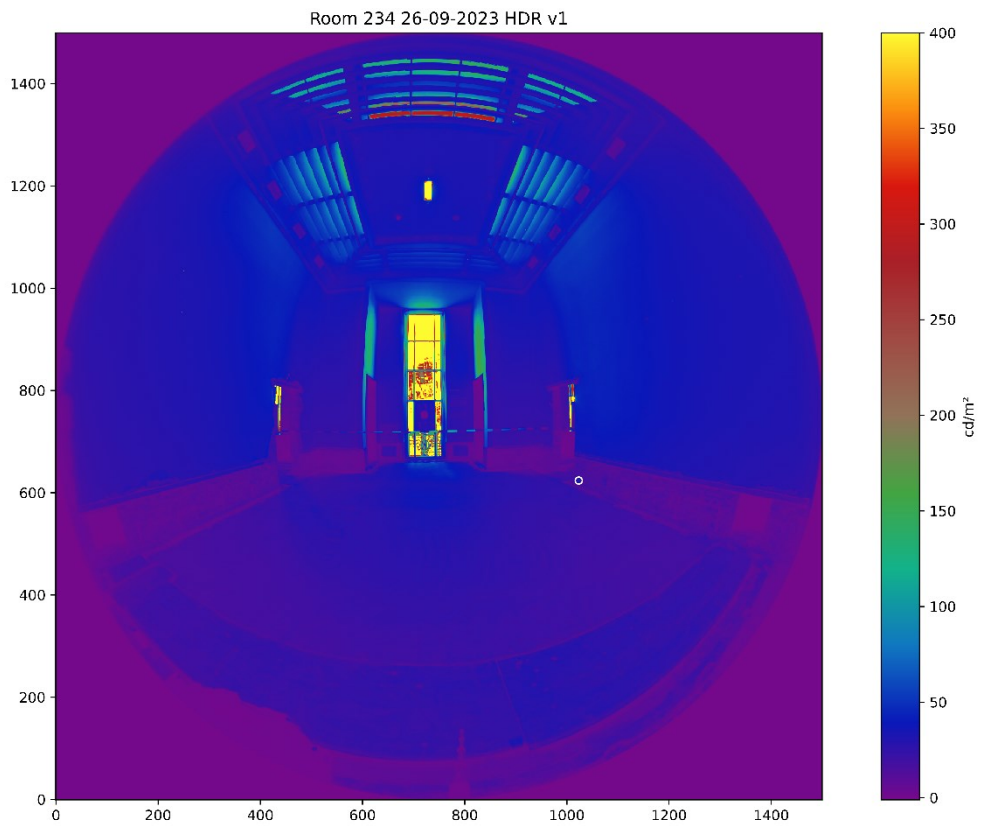


Figure C-19: Room 234 - 26-09-2023 - v1 - luminance map



Figure C-20: Room 234 - 26-09-2023 - v2 - 11:31

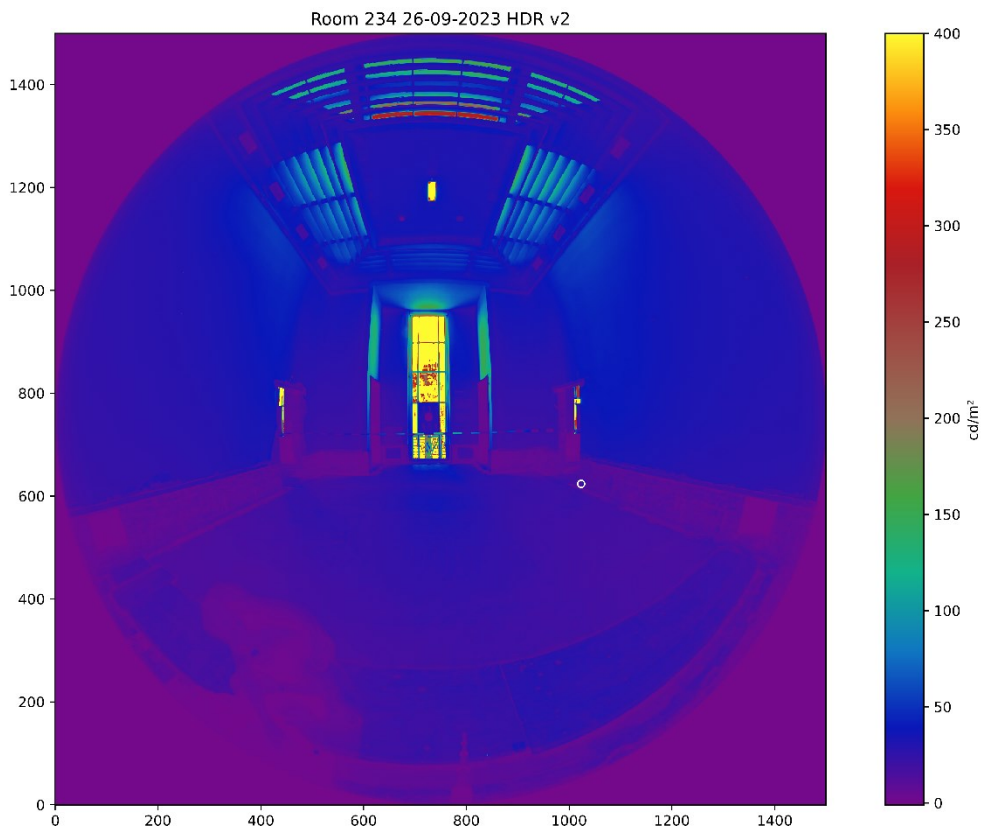


Figure C-21: Room 234 - 26-09-2023 - v2 - luminance map



Figure C-22: Room 234 - 26-09-2023 - v3 - 11:38

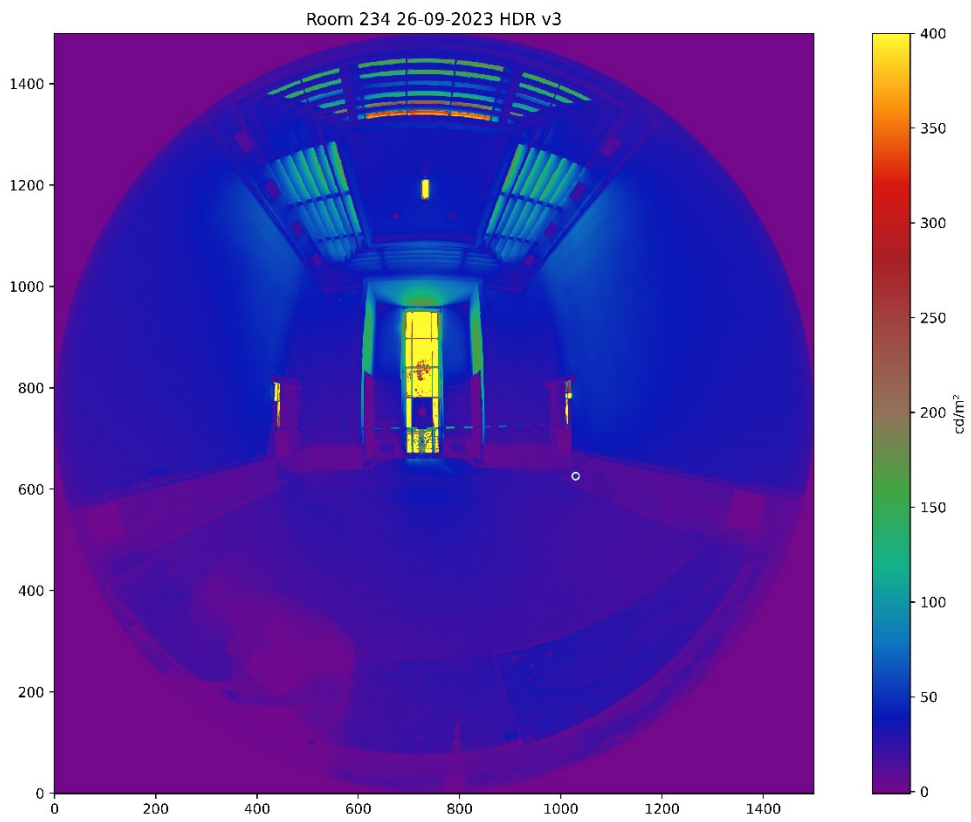


Figure C-23: Room 234 - 26-09-2023 - v3 - luminance map

## D Diffuse reflectance measurements

Room	Surface	Illuminance	Luminance	Diffuse reflectance	3.141592654
		lx	cd/m <sup>2</sup>	-	% difference with mean
228	Left	175	41.11	0.7380	-3.21%
Average	0.7617	169	41.69	0.7750	1.72%
		151	37.19	0.7737	1.56%
		146	36.02	0.7751	1.73%
		146	34.7	0.7467	-2.01%
	Front				
Average	0.7659	139	33.7	0.7617	-0.56%
		146	35.54	0.7647	-0.15%
		154	38.07	0.7766	1.38%
		155	37.53	0.7607	-0.69%
	Richt	197	43.56	0.6947	-0.59%
Average	0.6988	210	44.66	0.6681	-4.59%
		212	46.02	0.6820	-2.47%
		213	47.23	0.6966	-0.31%
		199	47.67	0.7526	7.15%
	Behind	220	48.47	0.6921	-5.67%
Average	0.7314	227	50.98	0.7055	-3.66%
		228	52.32	0.7209	-1.45%
		206	52.08	0.7942	7.92%
		214	50.68	0.7440	1.70%
	Floor	256	25.96	0.3186	6.02%
Average	0.2994	274	25.34	0.2905	-3.04%
		251	24.58	0.3077	2.69%
		245	26.85	0.3443	13.04%
		245	23.14	0.2967	-0.90%
		243	21.03	0.2719	-10.12%
		242	18.22	0.2365	-26.58%
		248	20.35	0.2578	-16.14%
		300	35.38	0.3705	19.19%
	Wood OBS	397	29.3	0.2319	-76.26%
Average	0.4087	276	38.38	0.4369	6.45%
		257	35.74	0.4369	6.46%
		263	37.36	0.4463	8.42%
		310	48.5	0.4915	16.85%
234	Left	355	69.35	0.6137	-15.45%
Average	0.7085	284	70.39	0.7787	9.00%
		292	67.71	0.7285	2.74%
		333	77.12	0.7276	2.61%
		388	85.75	0.6943	-2.05%

	Front left				
Average	0.7531	300	73.01	0.7646	1.50%
		270	68.58	0.7980	5.62%
		285	69.81	0.7695	2.13%
		335	73.51	0.6894	-9.24%
		361	85.5	0.7441	-1.21%
	Front right				
Average	0.8222	296	79.14	0.8400	2.11%
		250	67.04	0.8424	2.40%
		245	57.29	0.7346	-11.92%
		244	61.58	0.7929	-3.70%
		274	78.6	0.9012	8.76%
	Right	954	209.1	0.6886	-10.87%
Average	0.7634	681	166.8	0.7695	0.79%
		490	124.6	0.7989	4.44%
		411	105.7	0.8079	5.51%
		545	130.5	0.7523	-1.49%
	Behind	622	153.5	0.7753	3.57%
Average	0.7476	585	137.6	0.7389	-1.17%
		299	67.96	0.7141	-4.70%
		240	57.42	0.7516	0.53%
		367	88.57	0.7582	1.39%
	Floor				
Average	0.3035	518	57.9	0.3512	13.57%
		1332	140.7	0.3318	8.54%
		886	82.11	0.2911	-4.25%
		472	42.81	0.2849	-6.52%
		356	29.29	0.2585	-17.42%
234	Wood trim	77	3.95	0.1612	-23.02%
Average	0.1983	73	4.28	0.1842	-7.64%
		50	3.17	0.1992	0.46%
		57	2.92	0.1609	-23.19%
		268	17.92	0.2101	5.62%
		69	5.62	0.2559	22.52%
		72	4.96	0.2164	8.39%
	PIR	235	45.65	0.6103	-10.43%
Average	0.6739	202	42.31	0.6580	-2.42%
		212	56.67	0.8398	19.75%
		253	50.6	0.6283	-7.26%
		252	50.8	0.6333	-6.42%

Table D-1: Diffuse reflectance measurements

## E HDR comparisons

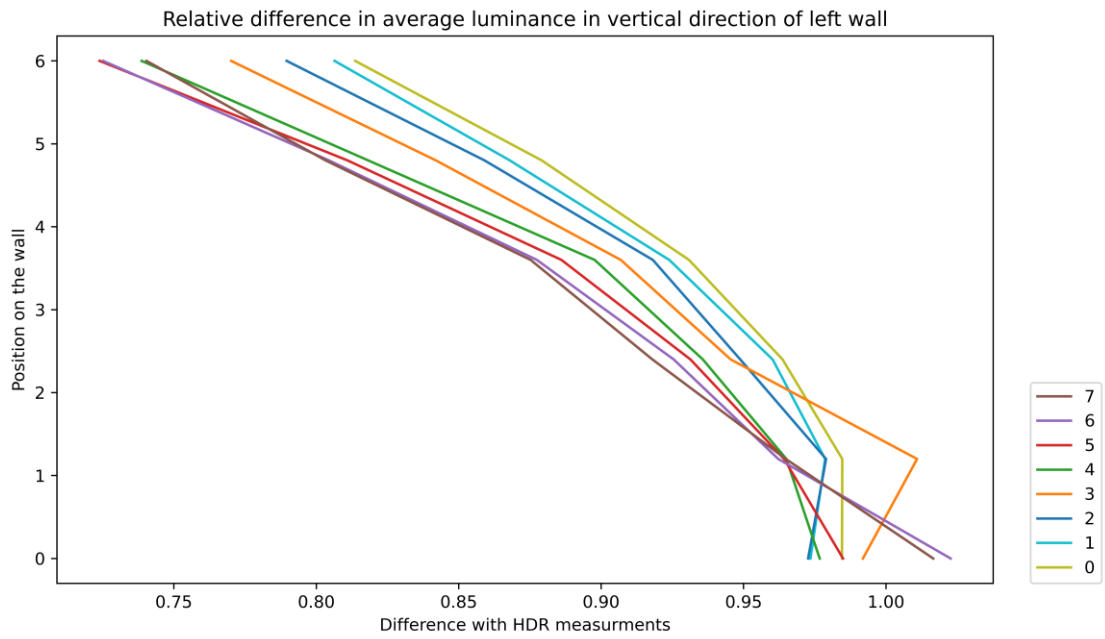


Figure E-24: Relative difference in average luminance in the vertical direction of left wall 228

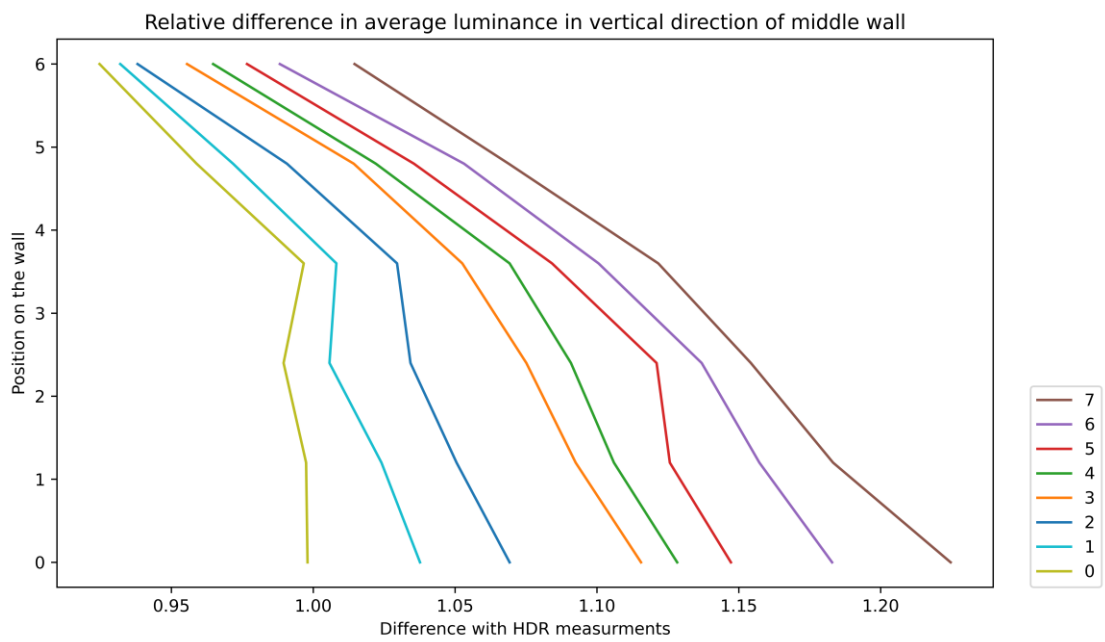


Figure E-25: Relative difference in average luminance in the vertical direction of middle wall 228

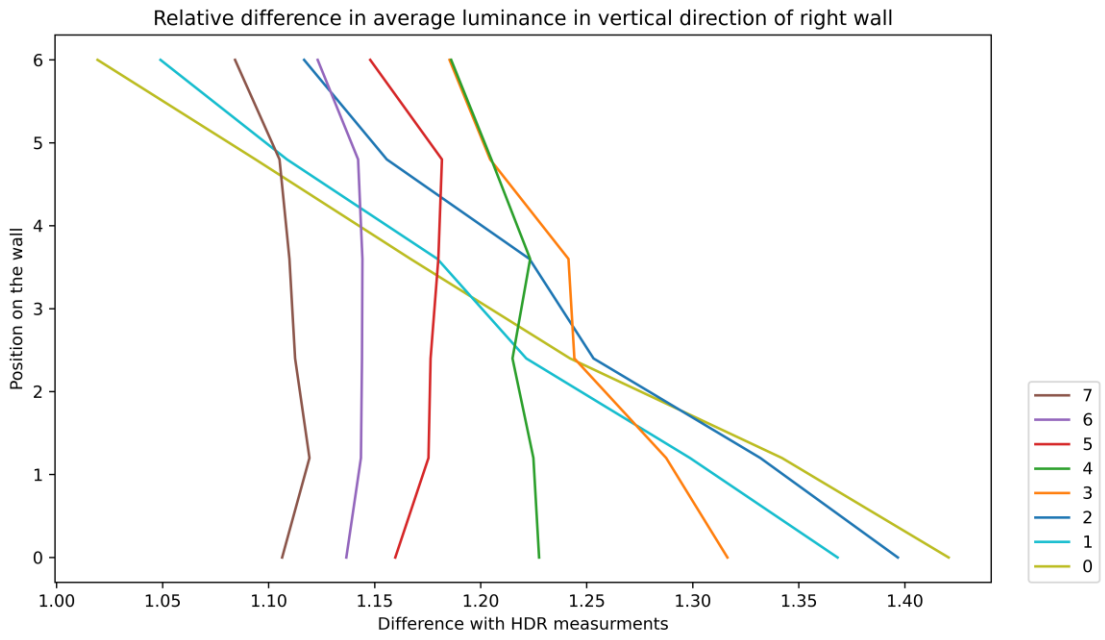


Figure E-26: Relative difference in average luminance in the vertical direction of right wall 228

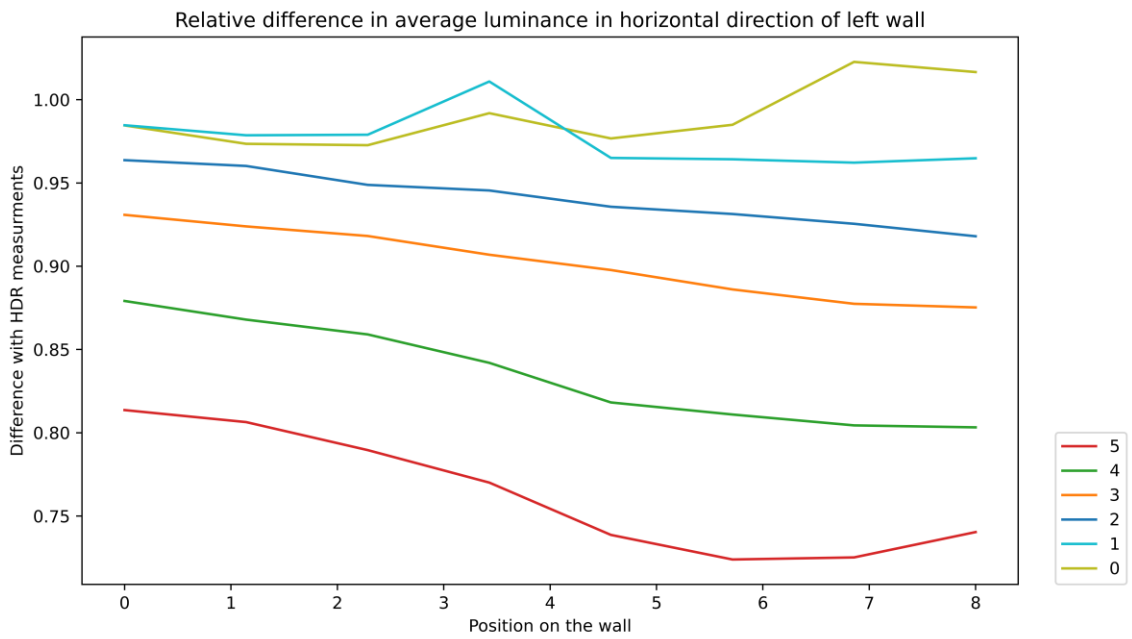


Figure E-27: Relative difference in average luminance in the horizontal direction of left wall 228

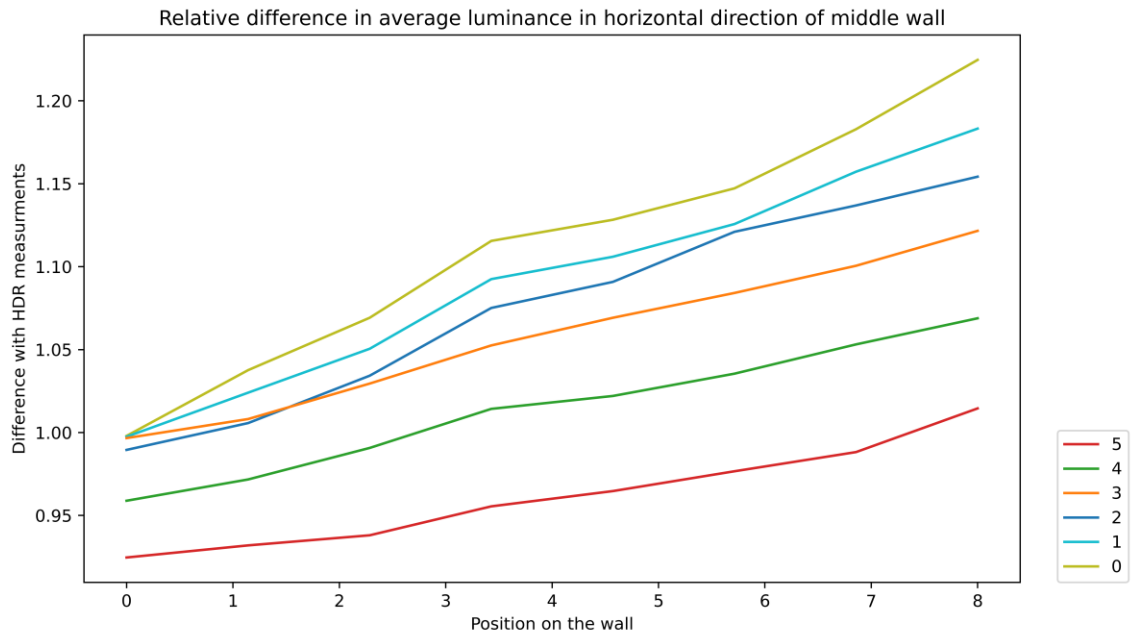


Figure E-28: Relative difference in average luminance in the horizontal direction of middle wall 228

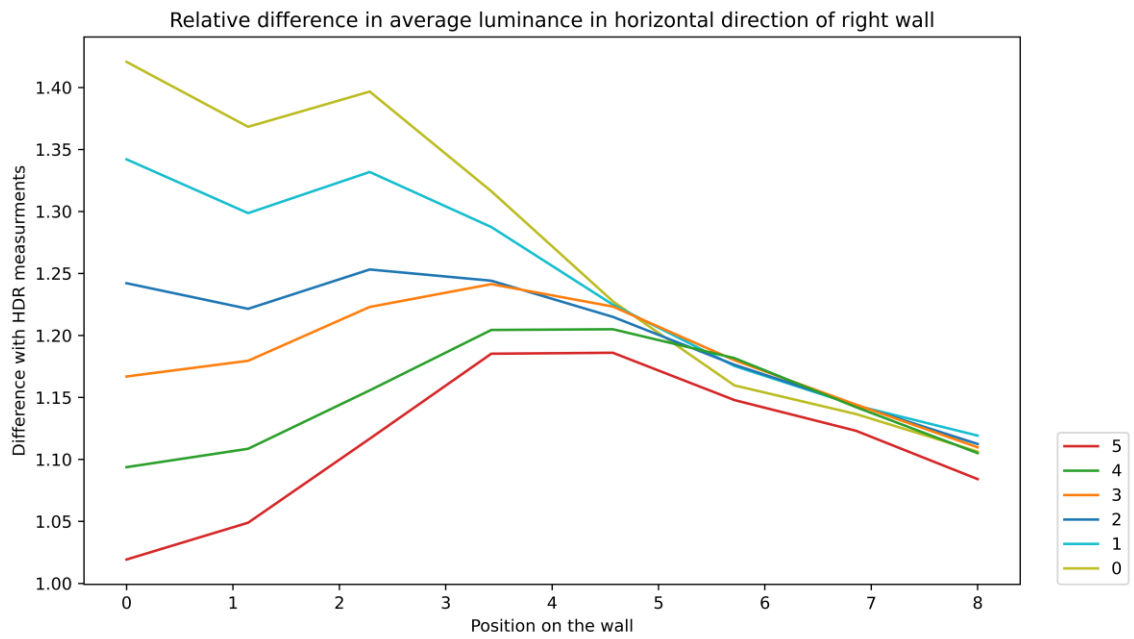


Figure E-29: Relative difference in average luminance in the horizontal direction of right wall 228

## F Sun shading simulation results

### Cabauw 2022

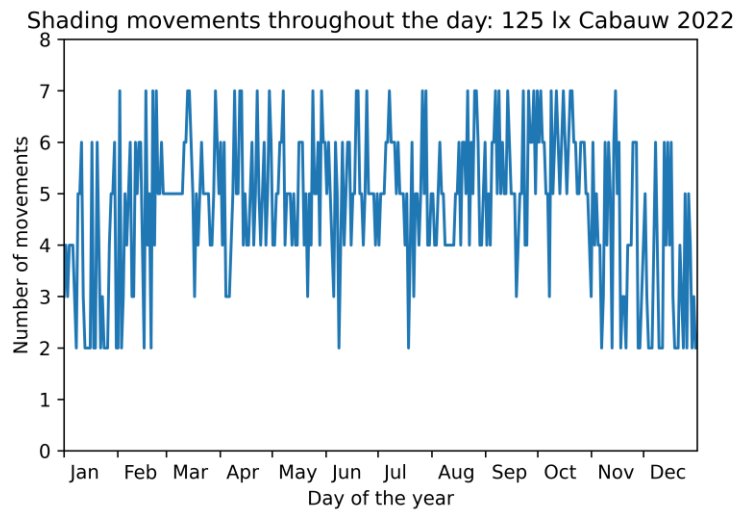


Figure F-30: Shading system movements per day using Cabauw 2022

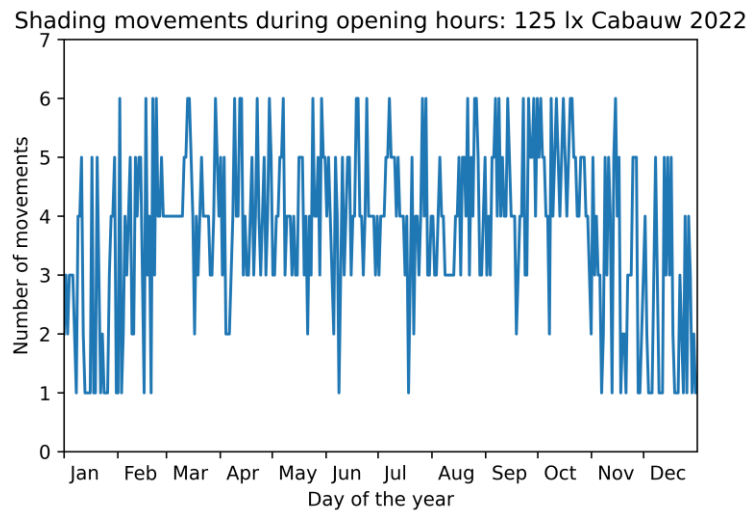


Figure F-31: Shading system movement during opening hours of museum using Cabauw 2022

Maximum and minimum state of system per day: 125 lx Cabauw 2022

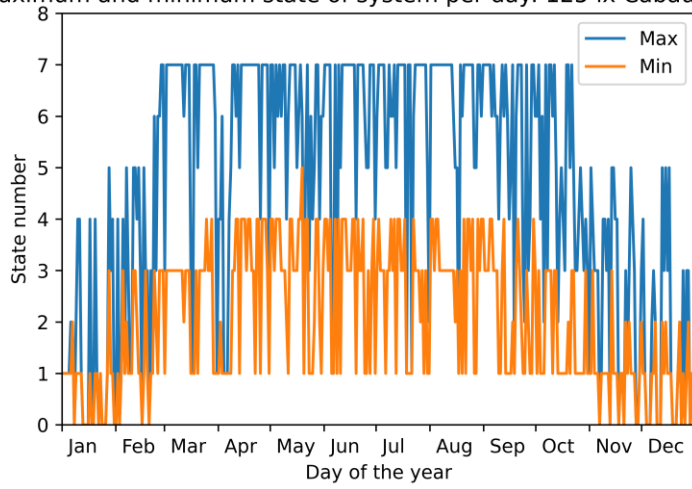


Figure F-32: Maximum and minimum state of shading system per day using Cabauw 2022

Maximum illuminance throughout the day: 125 lx Cabauw 2022

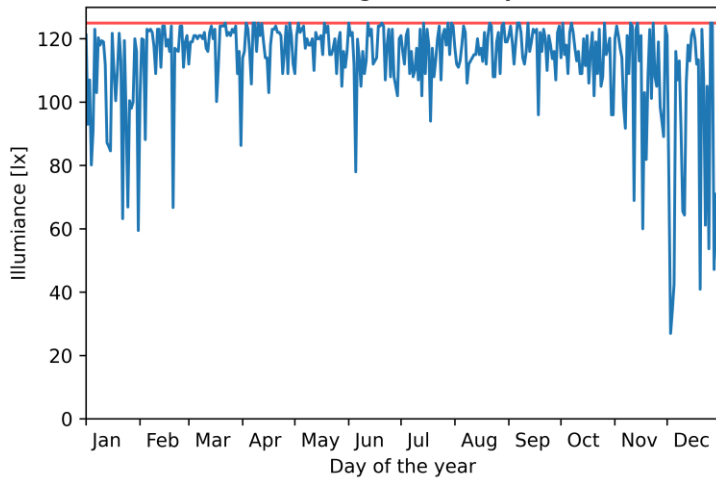


Figure F-33: Maximum illuminance per day in room 228 using Cabauw 2022

Average illuminance throughout the day: 125 lx Cabauw 2022

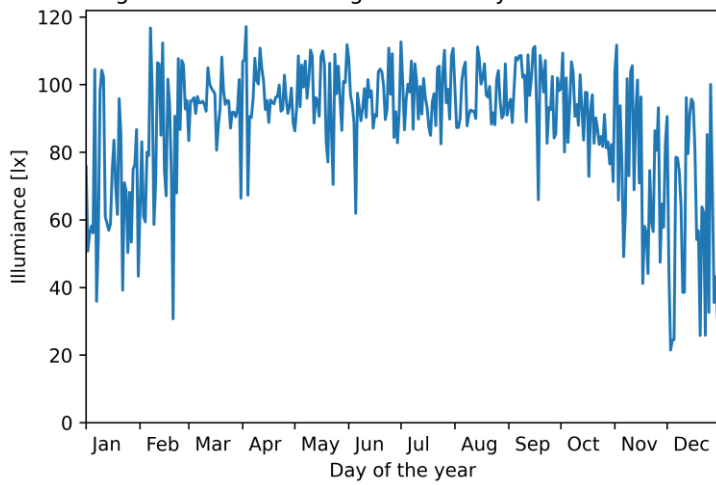


Figure F-34: Average illuminance per day in room 228 using Cabauw 2022

100 lx

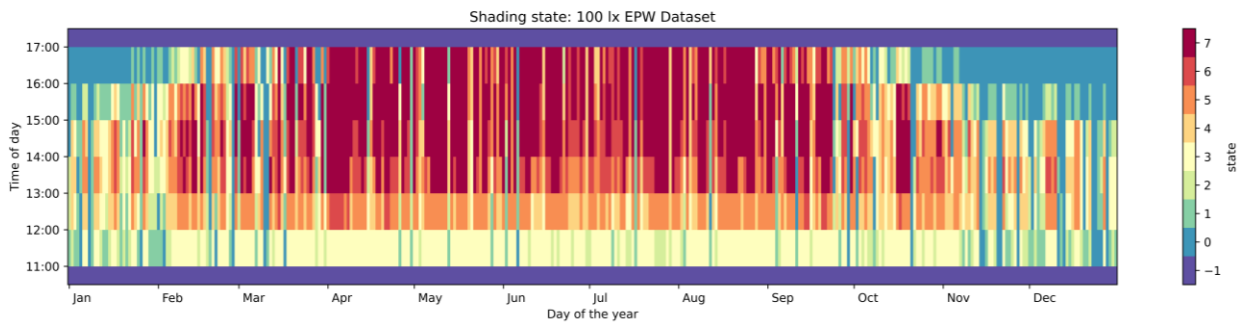


Figure F-35: Shading states room 228 throughout the year using 100 lx

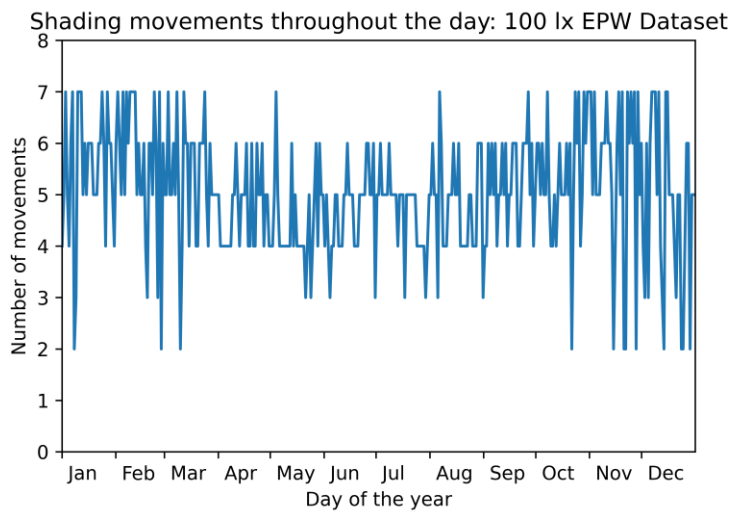


Figure F-36: Shading system movements per day using 100 lx

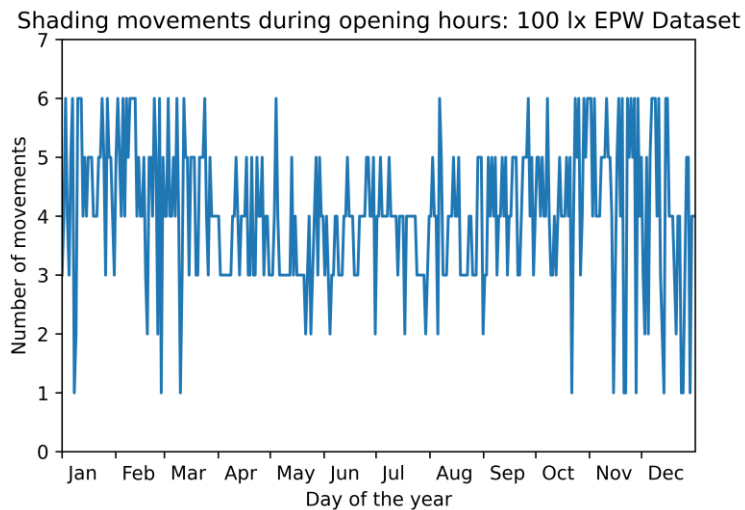


Figure F-37: Shading system movement during opening hours of museum using 100 lx

Maximum and minimum state of system per day: 100 lx EPW Dataset

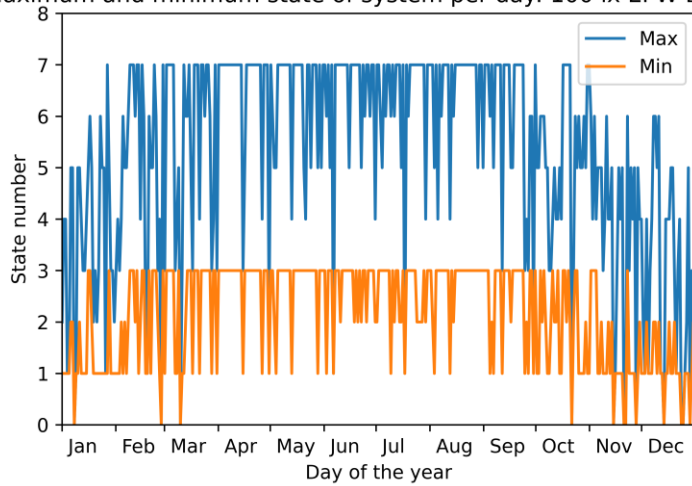


Figure F-38: Maximum and minimum state of shading system per day using 100 lx

Maximum illuminance throughout the day: 100 lx EPW Dataset

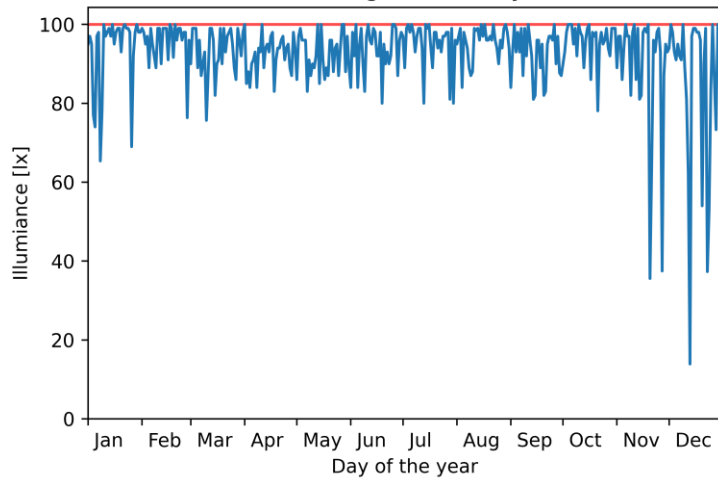


Figure F-39: Maximum illuminance per day in room 228 using 100 lx

Average illuminance throughout the day: 100 lx EPW Dataset

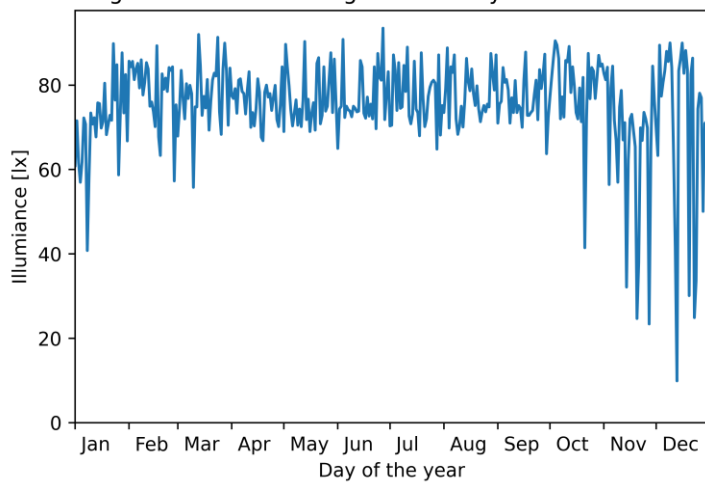


Figure F-40: Average illuminance per day in room 228 using 100 lx

## G Memo to the museumboard

From: Thijs Hamilton  
To: Museum board Boijmans van Beuningen  
Subject: Daylight modelling and control in Van der Steur building  
Date: 25 March 2024

Dear Sirs/Madams,

For my Master's thesis at the faculty of Civil Engineering at the Delft University of Technology, I studied daylight modelling and control for room 228 of the Van der Steur building. The results of this research can be used for the design of sun shading and lighting for this and other rooms in the museum with top lighting.

The calculations show that with the installation of three types of sunscreens above the ceiling, the desired illuminance level of 250 lx can be met. With the installation of a pyranometer on the roof of the museum the control of the sun's shading system can be automatized.

A simulation over the entire year shows that the exposure (during opening hours) stays well below the internationally advised level of 600000 lx·hr.

The total sun shading system can consist of three sunscreen fabrics with a transmission of 0.63, 0.55 and 0.44 plus a separate blackout screen. Reducing the exposure of the art by 82% and expanding the expected lifespan by 5.6 times compared to no sun shading implementation.

For more information, I can send you my Master's thesis and I am willing to supply you with additional information.

Kind regards,  
Thijs Hamilton

Deerns Nederland B.V.  
Anna van Buerenplein 21F  
2595 DA Den Haag  
Nederland  
+31 88 374 0000  
contact@deerns.com  
www.deerns.nl